# Microclimate Effects from Closing Abandoned Mines with Culvert and Bat Gates

Dr. Robert H. King
Professor of Engineering
Colorado School of Mines

**Table of Contents**

1.0 Introduction ..... 4
1.1 The Problem ..... 9
1.2 The Study Area ..... 15
2.0 Data Loggers ..... 18
2.1 Introduction ..... 18
2.2 Data Logger Specifications ..... 21
2.3 Remote Communications ..... 25
3.0 Mines and Measurement Locations ..... 26
3.1 Mine 31 ..... 26
3.2 Mine 59 ..... 30
3.3 Mine 65 ..... 33
4.0 Temperature and Humidity ..... 37
5.0 Modeling ..... 49
5.1 Introduction ..... 49
5.2 Modeling Software ..... 52
5.3 Results ..... 57
6.0 Air Flow ..... 83
6.1 Introduction ..... 83
6.2 Laboratory Tests ..... 90

## Abstract

Threatened bat species inhabit hundreds of thousands of abandoned mines around the world while land managers are closing the mines in an attempt to reduce hazards to the public. Bat gates have been used to reduce hazards to the public while retaining access to mines for bats but they are not appropriate for the common adit-trench type mine portal, so land managers proposed a culvert gate but its effects on the microclimate were unknown. Large microclimate changes may reduce bat fidelity to the habitat, so land managers requested an evaluation of the microclimate effects. We developed a process that integrated a computer model and continuous measurement and applied it for 1-year prior to and 1-year after culvert-gate closure of three Southwestern Colorado abandoned uranium mines. The results showed the culvert-gate closure slightly modified the microclimate by essentially extending the length of the mine, but bats should be able to locate the same climatic conditions a few feet away from original roosting locations. The computer model predictions compared favorably with measurements and the model provided relevant insight regarding the qualitative trends reflected by the field measurements. Therefore, land managers can apply the integrated modeling and measurement method to plan a wide range of abandoned mine closure and habitat conservation actions and assess the results.

# Executive Summary

There are over 300,000 abandoned underground mines in the US and many more internationally that provide important habitat for a variety of bat species, but the mines are being closed to reduce hazards to the general public. About 1,200 of the 33,000 abandoned mines that have been closed with bat gates or pipes to preserve habitat. So, only a small percentage of the mines have been closed and even smaller portions contain habitat preservation structures. Some mines yet to be closed are of the adit trench type where the portal opens at the end of a sloped trench and the trench is too large to cover effectively with the traditional grating and bat gate. Backfilling is a poor solution since maintaining habitat for a diverse set of bat species has important environmental consequences.

In an attempt to preserve habitat, the US Bureau of Land Management (BLM) proposed a culvert gate for adit-trench mines where the bats must enter through a vertical column of 0.6-m wide by 0.15-m high slots welded onto the end of a culvert. The culvert was placed in the trench so it extended part way into the portal, and the space between the portal and culvert was filled and sealed with foam. Finally, part of the trench was backfilled, covering the culvert (with the exception of the gated end) and the trench walls were cut back to a safe slope in the unfilled portion. This process was more expensive (about $3,000 per opening) than conventional gating (about $1500-$2000) and backfilling (about $1000-$1500), which is an important consideration when remediating thousands of mines. Costs could be reduced if small diameter culverts are installed at a higher angle to reduce length; nevertheless if culvert closures reduced bat fidelity to the habitat because microclimate changes, the increased expense for culvert gates would not be warranted.

BLM managers selected three adit-trench mines for study, designated mine 31, 59, and 65 on Calamity Mesa, southwest of the town of Grand Junction, Colorado. The mines were less than 100-ft deep and had been excavated in the Salt-wash Sandstone Member of the Jurassic, Morrison Formation. Biologists from the Colorado Division of Wildlife (CDOW) surveyed the mines and confirmed bat habitation. Researchers at the Colorado School of Mines (CSM) were asked to evaluate the effect of the culvert-gate on the mines' microclimates. After remediation, CDOW surveys indicated reduced bat activity that could be caused by factors such as increased recreational and remediation activity in the area, finding more desirable habitat in other areas, and climatic changes, in addition to microclimate changes.

To get a more comprehensive understanding of the interactions of the complex characteristics of the abandoned mine microclimate, we measured humidity, airflow, and radiation. Microclimate varies temporally and spatially since it depends on complex interactions of surface climate, mine airflow, humidity, and mine geometry. Therefore, we measured characteristics continuously at different locations throughout the mines and on the surface from September 1998 to November 2000, approximately 1-year prior to and 1-year after emplacing culvert gates. Measurement points were located near the

air/rock interface as well as in the center of airways. Abandoned mine microclimate measurements are difficult to make since prior to closure anyone could enter the mines and remove instrumentation. Furthermore, no power lines run through the area, so all instruments had to be battery powered, and batteries had to last for long periods since access was impossible in winter and difficult, expensive, and hazardous at other times. Airflow measurements posed additional problems since instrumentation to measure the small, turbulent flows caused by natural convection was both expensive and delicate.

Surface temperature fluctuations created thermal gradients in the mine resulting in a non-uniform density distribution, which, under the action of gravity, induced a fluid motion called natural convection. Airflow rates were small, around 0.05 m/s, and reasonably priced commercial devices couldn't measure lower than about 0.3 m/s, and they were too fragile to deploy for long periods in a mine. Therefore, we developed a $300 ultrasonic transducer which measured flows ranging from 0 to 0.06 m/s (0 – 12 fpm) range with a small number of readings above 0.122 m/s (24 fps). This compared with smoke tube measurements of 0.05 – 0.25 m/s (10 – 50 fpm), and model predictions of about 0.06 m/s (12 fpm).

The complex microclimate in the abandoned uranium mines contained high levels of radiation. We used an Instant Working Level and Gamma Meter for discrete, manual radiation measurements during two mine visits, and we installed dosimeters that measured accumulated exposure from combined x-ray, $\beta$, and $\gamma$ radiation and alpha cups that measured $\alpha$ radiation at the logger stations.

We used temperature and airflow data to verify a computer model of the natural-convection airflow. We used a commercially available solver, CFD-ACE (CFD Research Corporation, Huntsville AL) to numerically solve coupled, non-linear, second-order partial differential equations that represent the natural convective flows. The physical domain of the mines under study was inherently three dimensional because of the angle between the adit and the acceleration of gravity. We assumed that the irregularity of the mine cross-section and the gross-roughness of the walls were relevant but second-order effects compared to the non-alignment of the mineshaft and the acceleration of gravity. Therefore, we used a 2-dimensional, planar slice of the mine, which reduced the computational effort and captured the salient physical mechanisms.

Microclimate was affected by surface climate, the rock mass, and the mines' geometries. We assumed that the rock temperature was fairly constant and equal to the mean annual surface temperature (MAST), which was about 283 K (50 °F) approximately 1.83 m into the rock mass. Mine air temperatures were affected by conduction from the rock mass since low airflow rates caused the residence time to be longer than the characteristic time. However, the rock mass did not change throughout the study. Neither did mine geometry, even though the slope of the adits contributes to convective flows. Therefore, when we examined temperature and humidity data over the period of the study we had to differentiate between the changes caused by the culvert-gate installation and those caused by surface climate variations.

We tried to locate short periods where the surface climate was approximately the same before and after closure. We identified a 600-sample window from 1252 on 17 July 2000 to 1150 on 28 July 2000 that was similar to the pre-closure surface climate. Mean temperature increased 0.33 to 1.91 K (0.59 to 3.44 ºF) from the pre-closure climate for all but two loggers. The pre- and post-closure windows, while similar, were not exactly the same, since the surface weather temperature was higher at the beginning of the post-closure data window. During July, air movement in the decline mines was minimal, so the mines were strongly affected by pre-window conditions. Therefore, the difference was probably caused by the climate difference, not the culvert-gate installation. Nevertheless, warmer temperatures in July could be beneficial for bat maternity roosts.

Measurements showed that beyond the first few meters, the air is affected more by conduction from the surrounding rock than by convection. Closure reduced variance at every logger, and since variances decline with distance from the portal, this is consistent with the conclusion that culvert-gate closures have the same effect on the microclimate as if the mine were lengthened.

Reduced variance, or attenuation, is caused by thermal inertia, i.e. the effect of the rock mass and the delayed reaction to a change in the surface temperature; therefore, surface climate changes are not immediately felt in the mine, and they have a reduced effect with depth. Consequently, the mine may not react completely to a surface temperature rise before the surface temperature trends downward or vice-versa. Of course, the mine microclimate reacts quicker to the surface climate changes when $\Delta T$ between surface and mine air is largest causing stronger convective flows.

We also separated the surface and closure effects by comparing phase shift and gain with the 30-day running-average surface temperature. Gain is the ratio of mine temperature to surface temperature after the mine temperature is shifted to match the phase of the surface cycle. The result was that phase shift increased and gain decreased at a particular logger location after closure, which is consistent with the premise that adding the culvert-gate had the same effect as lengthening the mine.

The model predicted two convection cells previously unreported in the literature, one near the portal and the other throughout the remaining parts of the mine. Measurements agree with the two cell prediction as T vs x slope is very high in the cell near the portal and much lower over the rest of the mine. Furthermore, variance is much higher in the cell near the portal. The model responded to time varying surface temperatures, reporting that the characteristic time for a change in outside temperature to completely make its effect inside the mine is about 1 hr, dependant on location and $\Delta T$. The model results attenuate with depth into the mine, similar to measured data. The data shows a temperature fluctuation of about 6 K versus a fluctuation of about twice that for the temperatures outside of the mine. The attenuation within the actual mines was more dramatic than in the simulated mine, because we did not simulate all of the complexities inherent to a real mine. The real mine drifts are 3-dimensional, have rough rock surfaces, contain turns and bends, have variable dimensions, and contain abrupt changes in drift perimeters caused by roof falls. Future models should study more extensive mine complexes, evaluate the effect of actual conditions, and analyze detailed features of gate designs.

When we added a 10-m long 4-m diameter culvert to the model, the microclimate the temperature profile did not change in shape and remained close to the portal; however the portal location moved to the end of the culvert. When we reduced the culvert diameter to 2 m the temperature profile shape remained the same, but temperature was approximately 1 K (~2 °F) warmer. When we increased the culvert inclination to 27 °, the temperature profile was similar in shape and magnitude to the 6° culvert model. U (x-direction air velocity) profile shape and magnitude did not vary when a 4-m diameter culvert was added to the mine model. Reducing the diameter of the culvert shortened the first convection cell from 1.7m to 1.3m and reduced the maximum U magnitudes 0.23 to 0.13 m/s (45.3 to 25.6 fpm).

Adit-trench type abandoned mines pose a special challenge for land managers who are trying to preserve ecosystems by maintaining habitat for a diverse set of bat species. Our evaluation of the culvert-gate technique for closing these mines showed only small temperature changes. The changes increased temperatures in the summer maternity roost season, so even though small, they could be beneficial. We also found that if the bats were very sensitive to the temperature change, they could relocate a short distance in the mine to find a temperature equivalent to the pre-closure value. Therefore, we found no reason for managers to discontinue use of culvert gates, especially if the alternative is to backfill the mines and eliminate the habitat.

CDOW bat surveys indicated reduced use of the mines with culvert gates. We recommend that bat surveys continue and that other causes for the reduced bat activity be investigated. It is possible that the frequent visits by researchers and the instrumentation installed in the mines or the closure activity by construction contractors affected the acceptability of the sites for bat habitat. We recommend that new mines be identified for additional modeling and instrumentation with remote data transmission.

Our study developed a model of the flow and heat transfer in the mine, using a CFD code that we can modify for land managers who are planning modifications to caves and mines. Combining the model with our technique to continuously measure and analyze temperature, humidity, and airflow will give land managers a comprehensive procedure to assess the effect of remedial actions on abandoned mine microclimates.

# 1.0 Introduction

## *1.1 The Problem*

This report evaluates the effect of using the culvert bat-gate closure technique on the microclimates of three abandoned underground uranium mines on lands administered by the BLM. This study is important because its findings can be applied to the large number of mines that have been abandoned on private, state, and federal lands in the US as well as mines abandoned internationally where land managers desire to maintain ecological systems by preserving bat habitat. Burghardt estimates 3,200 abandoned mine sites with 10,000 openings in the U. S. National Park System (Burghardt, September 17, 2001). The U. S. Western Governors Conference estimates over 250,000 abandoned mines in 15 western states (Cleaning Up Abandoned Mines: A Western Partnership September 17, 2001). Meier and Garcia estimate over 300,000 abandoned mines in the U.S., and there are hundreds of thousands more around the world (Meier and Garcia, 2000).

Abandoned mines pose hazards to people using private and public lands for activities like hiking, camping, mountain biking, off-road vehicle riding, horseback riding, and hunting. Land users might enter underground workings to explore, camp, seek shelter in a storm, or to collect minerals or mining artifacts. Abandoned mine hazards include falling into open shafts, trenches, or pits; radiation; falling rocks; rodent droppings with Hanta virus; and suffocation.

Many federal and state agencies have developed programs to remediate these sites and warn the public. An example is the Bureau of Land Management (BLM) (BLM's Abandoned Mine Lands Program September 17, 2001; Raschen, 2000). However only 33,000 of the 300,000 abandoned mines in the US have been closed (Meier and Garcia, 2000). Sometimes remediation is as simple as backfilling the mine entrances. However, some mines have become key year-round resources for bats (Tuttle and Taylor, 1994), and backfilling would entrap bats and eliminate future access. Only 1,200 of the 33,000 closed mines preserved bat access with gates or pipes (Meier and Garcia, 2000).

Additional information about these and other species can be found in the literature. (Armstrong et al, 1995) Protecting bat habitat is important since a greater diversity of bat species has a large impact on the environment (Pierson, 1998). Bats save millions of dollars in product damage by preying on agricultural and forest pests. A single bat can consume thousands of insects in one night (Altringham, 1996). Furthermore they reduce our dependence on chemical pesticides. In addition, they are valuable pollinators. Unfortunately, bat populations are in decline and their habitat must be preserved. Six species of bats in North America are considered threatened or endangered. (Navo and Ingersoll, 2001; Tuttle and Taylor, 1994; Burghardt, September 17, 2001)

To preserve bat habitat in abandoned mines and to reduce hazards to people using public and private lands, several special closure techniques have been developed. The most

common is to install a bat gate in openings to underground mines. Bat gates are steel grids with openings large enough for bats, but too small for people to pass through. Burghardt describes several gates installed by the NPS and summarizes the installation technique (Burghardt, September 17, 2001).

Colorado Division of Wildlife (CDOW) is responsible for conservation of bat species, and their surveys show that bats roost in abandoned mines on lands administered by the U. S. Bureau of Land Management (BLM). Consequently the CDOW and BLM, along with other agencies, entered into a Memorandum of Understanding, to help protect bats in Colorado. (Navo and Ingersoll, 2001). CDOW biologists identified the following bats roosting in abandoned mines in the area in Southwestern Colorado studied in this project (Navo and Ingersoll, 2001):

California Myotis - *Myotis californicus (*MyCa)
Western Small-footed Myotis - *Myotis ciliolabrum* (MyCi)
Long-eared Myotis – *Myotis evotis (*MyEv)
Fringed Myotis – *Myotis thysanodes* (MyTh)
Long-legged Myotis - *Myotis volans*(MyVo)
Big Brown Bat – *Eptesicus fuscus* (EpFu)
Townsend's Big-eared Bat - C*orynorhinus townsendii pallescens* (CoTo)

Southwestern Colorado hosts many adit-trench mines where the portals are located at the end of long trenches (Figure 1), and both the mine and the trench pose hazards to the public. Most of the mines in this area are on a decline because the miners where exploiting a strata bound deposit that dips below the surface.

Figure 1. Mine 31 Adit Trench Before Closure.

In attempt to remediate an adit-trench opening, the BLM placed a grate over the entire trench of one mine, but it was too costly to install and maintain to be practical for the thousands of mines that have to be closed. Furthermore, the grated area must be fenced to prevent off-road vehicles or a group of people moving onto the gate. The appearance of the combination fence and gate was conspicuous in the environment, and there has been evidence of some public-land users climbing over or breaking the fence.

Therefore, the BLM developed another approach, the culvert and bat gate where a bat gate was welded onto a culvert (Figure 3). The gate is a vertical column of two-foot wide by six-inch high bat windows. The culvert was placed in the trench so it extended part way into the portal and the space between the portal and culvert was filled and sealed. Finally the culvert was covered with earth to fill the trench, leaving the gated end exposed, where the trench walls were cut to a safe slope (Figure 2). Culvert bat-gate closures cost approximately $3,000/opening, as opposed to about $1500-$2000 for a conventional gate and $1000-$1500 for backfill or bulkhead closures. Following closure, land managers must continually monitor the integrity of both traditional and culvert gates.

Figure 2. Culvert and Bat Gate at Mine 31 Before Trench Remediation

Figure 3. Culvert Bat-gate Closure at Mine 59.

Culvert length and costs can be reduced if culverts are installed at a higher angle than the slope of the original trench. Culvert diameters that are less that the portal dimensions further reduce cost.

While bat gates have been used and studied for many years, the effect of the culvert-gate is unknown (Herder, 2000). Bats are sensitive to temperature. Tuttle and Stevenson report that *Rhinolophus hipposideros* could select the proper temperature of hibernation with accuracy of 0.8 °C (Tuttle and Stevenson, 1978). Bats will abandon even protected roosts if the temperatures vary from those that they prefer (Tuttle and Taylor, 1994). Various species prefer different thermal environments for different activities (hibernation, maternity, bachelor, etc.) (Sherwin et al, 1993). For example hibernation preferences are the lowest non-freezing temperatures available to reduce metabolism. A hibernating *Myotis lucifugus* in a New Jersey mine demonstrated a clear preference for temperatures near 2 °C (35.6 °F) (Tuttle and Taylor, 1994). Bats require warm temperatures (70 ° to 90 °F) for successful maternity roosting (Tuttle and Taylor, 1994).

CDOW researchers suspect that the culvert gate closures are affecting internal microclimates. "Overall, the use of the gated mines this summer was not very encouraging. While bats were documented at most mine sites, the numbers of bats were low, and activity levels appear reduced from earlier documentation pre-gating. The continued use of the gated mines by at least some bats indicates bats can utilize the gate designs, but the overall results suggest some gates may have changed the internal micro-habitat. These remain an issue at the several, most altered entrances, where large trench features were eliminated and culverts were installed." "It is unknown if a reduced bat

population in the area, if real, was in any way related to the closures of mines, and gate design, in the project area." "At this point, pending evidence from the School of Mines study, we would have to believe that culvert gate designs, installed in portals associated with large trench features, and smaller diameter that the original portals, are changing the internal conditions and having an effect on bat use of such sites." (Navo and Ingersoll, 2001)

This report evaluates the effect of using the culvert bat-gate closure technique on the microclimates of three abandoned underground uranium mines on lands administered by the BLM. Table 1 lists the culvert dimensions and closure dates on the three mines studied.

Table 1. Culvert Dimensions and Mine Closure Dates

| Mine | Culvert Length (ft) | Culvert Diameter (ft) | Approximate Dip (°) | Closure Date |
|---|---|---|---|---|
| 31 | 10 | 6 | 24 | 11-09-99 |
| 59 | 30 | 6 | 29 | 11-15-99 |
| 65 | 30 | 8 | 27 | 11-19-99 |

We measured temperature and relative humidity continuously at several points in the three mines for one year before closure and an additional year post closure with inexpensive, commercial data loggers. In addition, we developed a sensor that continuously monitors very low airflows. We also studied models for predicting the effect of culvert and bat-gate closures for future remedial actions at other mines. Data collection covered the period from September 1998 to November 2000 as shown in Figure 4. Monthly reports including interim data analyses were provided to the BLM over this period followed by final data analysis modeling, draft report review, and final reporting.

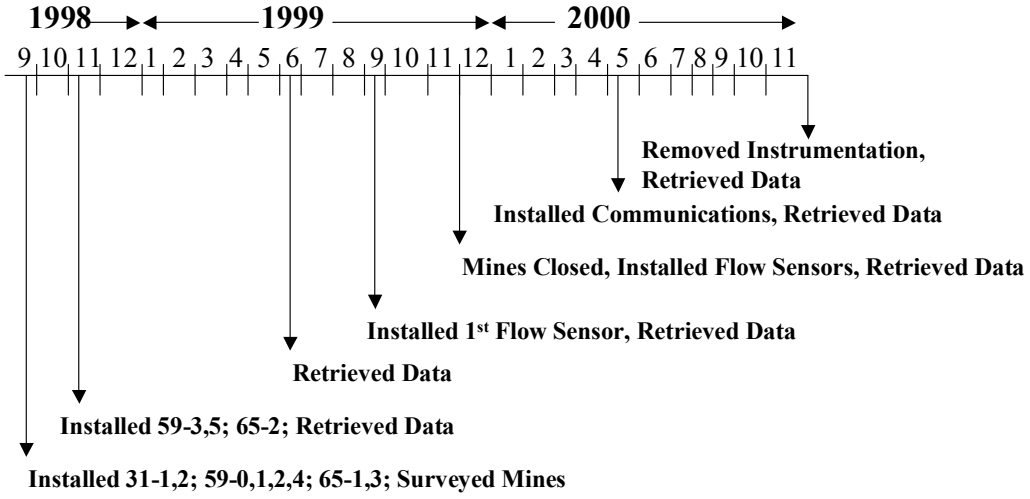


Figure 4. Timeline of mine visit activities.

## *1.2 The Study Area*

The study area is part of the Uravan Mineral Belt in the Uncompraghre Plateau (Figure 5) where many mines have or soon will be closed to human access. Figure 5 shows the geology of the area and the relative locations of the three mines, labeled mine 31, 59, and 65.

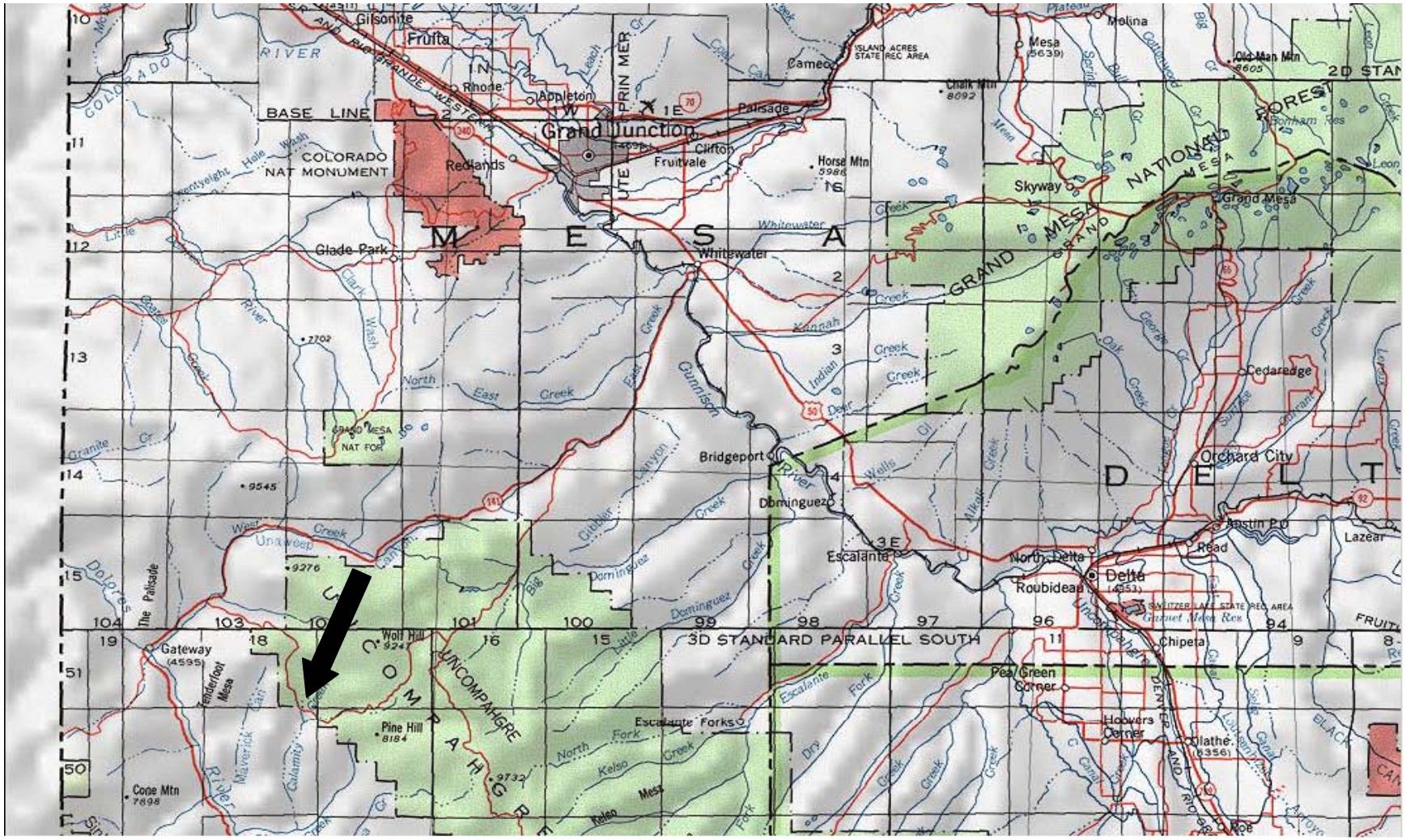


Figure 5. General Location of the Study Area

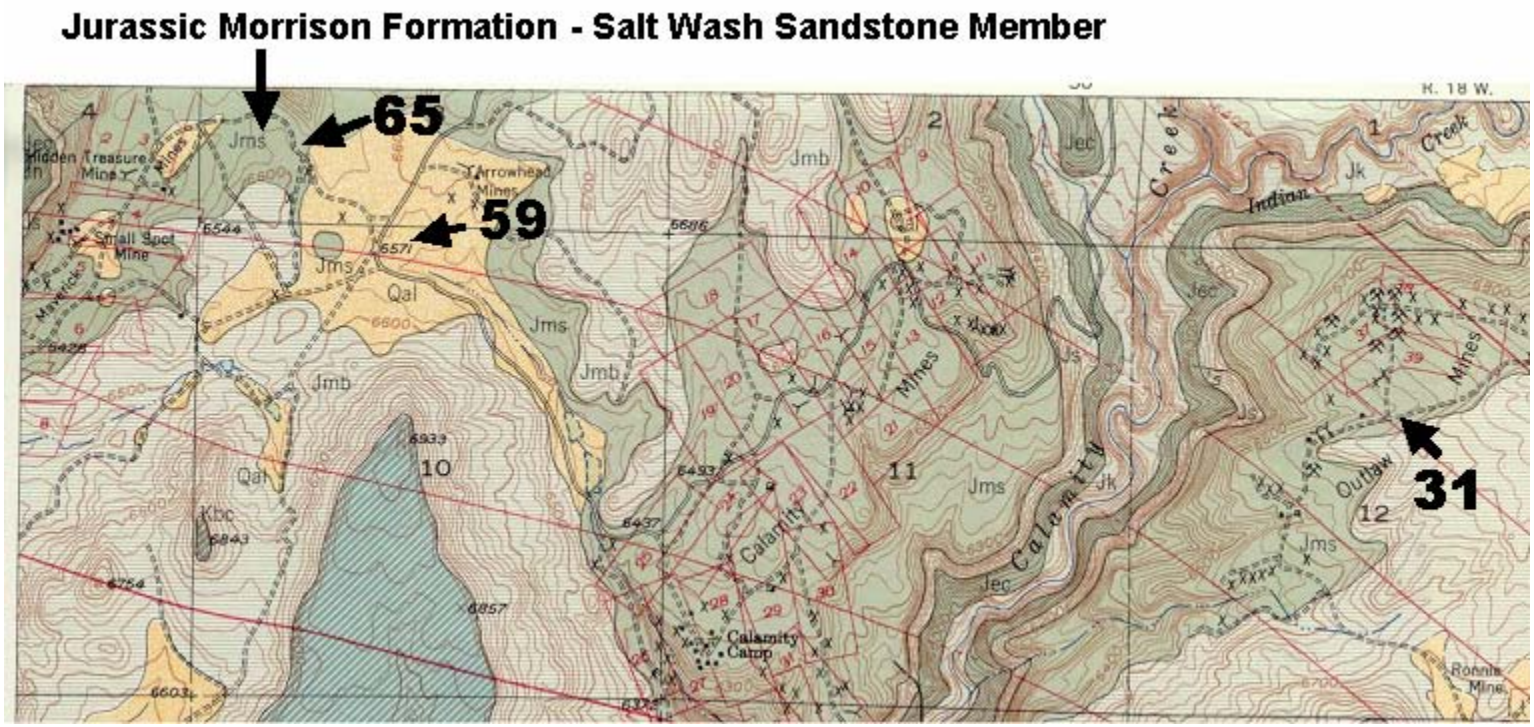


Figure 6. Mine Locations and Geology (U.S. Geological Survey, 1991)

# 2.0 Data Loggers

## *2.1 Introduction*

We installed inexpensive, commercial data loggers with built-in temperature and relative humidity transducers along with instruments to measure radiation and air velocity, in several locations in the three experimental mines. Mine layouts, logger locations and photographs of installations are presented in section 3.

Table 2 summarizes the instrument deployment activities. The first column shows the logger number, and column 2 lists the original installer. Henry Foust was a graduate student at CSM, Kirk Navo is a CDOW biologist, Dr. Tom Grover is a CSM Research Professor, Dr. Robert King is a CSM Professor, and Bruce Fowler is a Geologist with the BLM who participated in all of the installations. Column three identifies the instrument type and serial number, column four describes the location (also shown on maps in Section 3), and the remaining columns briefly describe the activities. The initial plan was to install at least one logger in each mine, but after the mines were surveyed, the need to record microclimates in several additional locations was evident. We replaced a few loggers during the two-year study period, and all instruments were removed during the November-2000 visit.

Table 2. Instrument Deployment Activities

| Number | Original Installer | Instrument Type & S/N | Location Description | 9/24/98 Trip | 11/20/98 Trip | 6/24/99 Trip | 9/10/99 Trip | 12/2/99 Trip | 5/4/00 Trip |
|---|---|---|---|---|---|---|---|---|---|
| 31-1 | Foust | HOBO TEMP+RH 239161, Cup, Dosimeter | End of Left Drift 91 ft from Portal | Install | Retrieved data | Retrieved data | Retrieved data | Set-up error. No Data 9/10 – 12/2 | Retrieved data |
| 31-2 | Navo | HOBO Temp and PRO | End of Portal Incline. 36 ft from Portal | “ | Did not access | Not Found. Replaced by King HOBO PRO 23154 | “ | " | “ |
| 59-0 | Navo | HOBO TEMP 155741 | Near Portal 57 65 ft to Portal 57 493 ft to Portal 59 | “ | Did not access | Retrieved data labeled: Outlaw_ deep A | Dead Battery 6/21 to 9/10/99, mislabeled as 59-03 | “ | “ |
| 59-1 | Foust | HOBO TEMP+RH, 200240 Cup, Dosimeter | Intersection w/ drift to Mine 57, 280 ft from Portal 59. | “ | Retrieved data labeled as 59l | Retrieved data | Retrieved data | “ | “ |
| 59-2 | Foust | HOBO TEMP+RH 200239 Cup, Dosimeter | Back of Mine 59 82 ft from portal. | “ | Retrieved data labeled as 59r | “ | “ | “ | “ |
| 59-3 | King | HOBO PRO 239165, | Right Spur 132 ft from portal | | Install | Retrieved data | No Data | “ | “ |

| | | | | | | | | | |
|---|---|---|---|---|---|---|---|---|---|
| | | Cup, Dosimeter | | | | | | | |
| 59-4 | Navo | HOBO TEMP 155742 | Winze 59 ft from portal | “ | Did not access | Retrieved data labeled as 59no4 Outlaw_portal B | Retrieved data mislabeled as 59-00 | “ | “ |
| 59-5 | King | HOBO PRO 239164 | Surface | | Install | Retrieved data | Retrieved data | “ | “ |
| 65-1 | Navo | HOBO TEMP 155745 | Right Spur 77 ft from portal | Install | Retreived data labeled as Navo65, Outlaw Mine 2 deep D | No Data | No Data | Retrieved data labeled as 65-1-2 | “ |
| 65-2 | King | HOBO PRO 239166, Cup, Dosimeter | Main Drift Opposite Right Spur. 57 ft from portal | | Install | No data. Replaced by King | Retrieved data | No Data 9/10 – 12/2 | “ |
| 65-3 | Foust | HOBO TEMP+RH 200238, Cup, Dosimeter | End of Main Drift 135 ft from portal | Install | Retrieved data labeled Mine 65 | Retrieved data | “ | “ | “ |
| Vel 0 - 6 | Grover | Air-flow Transducers | | | | | Install Prototype | Install Transducers | “ |
| Remote Communication | Grover | Cable | | | | | | | Install |

## 2.2 Data Logger Specifications

We used several different types of loggers that are compared in the following to assist future researchers in choosing loggers for particular applications. We installed the Onset HOBO® H8 Pro RH/ T Logger, shown in Figure 7, at instrument locations 31-2, 59-3, 59-5, and 65-2. Table 3 lists specifications.

Figure 7. HOBO® H8 Pro RH/ T Logger (http://www.onsetcomp.com/)

Table 3. Onset HOBO® H8 Pro RH/ T Logger Specifications Summary

| | Microprocessor & General | Temperature Transducer | Humidity Transducer |
|---|---|---|---|
| Cost | $160 | | |
| Capacity | 65,291 measurements | | |
| Sampling Interval | 0.5 s to 9 hrs | | |
| Time accuracy | ±1 min per wk at +68°F | | |
| Size/Weight | 4 x 3.2 x 2", 3.7 oz. | | |
| Range | | -22°F to +122°F | 0% to 100% RH |
| Accuracy | | ±0.7°F | ±3% |
| Response time | | 34 min | 30 min |
| Operating Environment | | | +32°F to +122°F |
| Drift | | | 1% per year |

We installed the Onset HOBO® H8 RH/ T Logger, shown in Figure 8, at measurement stations 31-1, 59-1, 50-2, and 65-3 . Table 4 lists specifications.

Figure 8. HOBO® H8 RH/ T Logger (: http://www.onsetcomp.com/)

Table 4. Onset HOBO® H8 T/RH Logger Specifications

| | Microprocessor & General | Temperature Transducer | Humidity Transducer |
|---|---|---|---|
| Cost | $85 | | |
| Capacity | 7943 measurements | | |
| Sampling Interval | 0.5 s to 9 hrs | | |
| Time accuracy | ±1 min per wk at +68°F | | |
| Size/Weight | 2.4 x 1.9 x 0.8”, ~ 1 oz | | |
| Range | | -4°F to +158°F | 25% to 95% RH |
| Accuracy | | ±1.27°F | ±5% |
| Response time | | 15 min. | 10 min. |
| Operating Environment | | | +41°F to +122°F |
| Drift | | | 1% per year |

We installed the Onset HOBO® H8 Temp Logger, shown in Figure 9, at instrument stations 59-0, 59-4, and 65-1. Table 5 lists specifications.

Figure 9. HOBO® H8 Temp Logger (http://www.onsetcomp.com/)

Table 5. Onset HOBO® H8 Temp Logger Specifications

| | Microprocessor & General | Temperature Transducer | Humidity Transducer |
|---|---|---|---|
| Cost | $60 | | |
| Capacity | 7943 measurements | | |
| Sampling Interval | 0.5 s to 9 hrs | | |
| Time accuracy | ±1 min per wk at +68°F | | |
| Size/Weight | 2.4 x 1.9 x 0.8”, ~ 1 oz | | |
| Range | | -4°F to +158°F | 0% to 100% RH |
| Accuracy | | ±1.27°F | ±3% |
| Response time | | 15 min. | 15 min. |
| Operating Environment | | | +32°F to +122°F |
| Drift | | | 1% per year |

Table 6 compares the microprocessor and general features of the three data loggers. The H8 Pro RH/T logger can store more measurements, but it is more expensive and larger. The impact of measurement storage was important to our project because we were not able to make visits to the mines frequently. The larger size of the H8 Pro RH/T was not a problem. The H8 Pro RH/ T and H8 T/RH measure relative humidity and temperature,

but the H8 Temp only measures temperature. As will be noted later, the dew point and relative humidity information was important to our study.

Table 6. Microprocessor and General Comparison Between Data Loggers

| | H8 Pro RH/ T | H8 T/RH | H8 Temp |
|---|---|---|---|
| Cost | $160 | $85 | $60 |
| Capacity | 65,291 measurements | 7943 measurements | 7943 measurements |
| Sampling Interval | 0.5 s to 9 hrs | 0.5 s to 9 hrs | 0.5 s to 9 hrs |
| Time accuracy | ±1 min per wk at +68°F | ±1 min per wk at +68°F | ±1 min per wk at +68°F |
| Size | 4 x 3.2 x 2" | 2.4 x 1.9 x 0.8” | 2.4 x 1.9 x 0.8” |
| Weight | 3.7 oz. | ~ 1 oz | ~ 1 oz |

Table 7 compares the temperature measurement capabilities of the three data loggers. The H8 Pro RH/T logger temperature measurement has a larger range and is more accurate, but additional time is required to obtain the accuracy of measurement. The increased range was important for the surface logger, 59-5, but was not important for the mine loggers. The additional accuracy was generally important to our study.

Table 7. Temperature Measurement Comparison Between Data Loggers

| | H8 Pro RH/ T | H8 T/RH | H8 Temp |
|---|---|---|---|
| Range | -22°F to +122°F | -4°F to +158°F | -4°F to +158°F |
| Accuracy | ±0.7°F | ±1.27°F | ±1.27°F |
| Response time | 34 min | 15 min. | 15 min. |

Table 8 compares the humidity measurement capabilities of the two loggers that measure humidity. The H8 Pro RH/ T has a larger range, better accuracy, slower response, and a slightly larger operating range. The better accuracy and larger range were important for our project.

Table 8. Humidity Measurement Comparison Between Data Loggers

| | H8 Pro RH/ T | H8 T/RH |
|---|---|---|
| Range | 0% to 100% RH | 25% to 95% RH |
| Accuracy | ±3% | ±5% |
| Response time | 30 min | 10 min. |
| Operating Environment | +32°F to +122°F | +41°F to +122°F |
| Drift | 1% per year | 1% per year |

## *2.3 Remote Communications*

It was hazardous for researchers to enter the mines to collect data, so we developed a communication link from the portal to the airflow and temperature loggers using a hard-wired system that connected to the RS232 serial port of a laptop computer through a wiring adapter. The RS232 standard is usually limited to 100 feet cable length, but we communicated up to 1000 feet since the 9600 baud rate used by the loggers was much less than the maximum 115,000 baud rate permitted by the RS232 standard. The slower rate transmitted over long distances without errors even tough the waveform was visibly distorted when viewed with an oscilloscope.

Figure 10 shows the wiring schematic for the RS232 connections. The temperature loggers use only the 'transmit' and 'receive' wires, Tx and Rx, with a reference wire, Gnd. The airflow loggers required two additional wires connected to switches S1 and S2. One switch was used to reset the logger and the second was used to select the logger's activity: logging or uploading data. The laptop's RS232 connector had additional wiring to make the system appear to be a telephone modem to the DOS operating system.

The communications system was not implemented until the end of the project, so we report it here only for its usefulness in future projects.

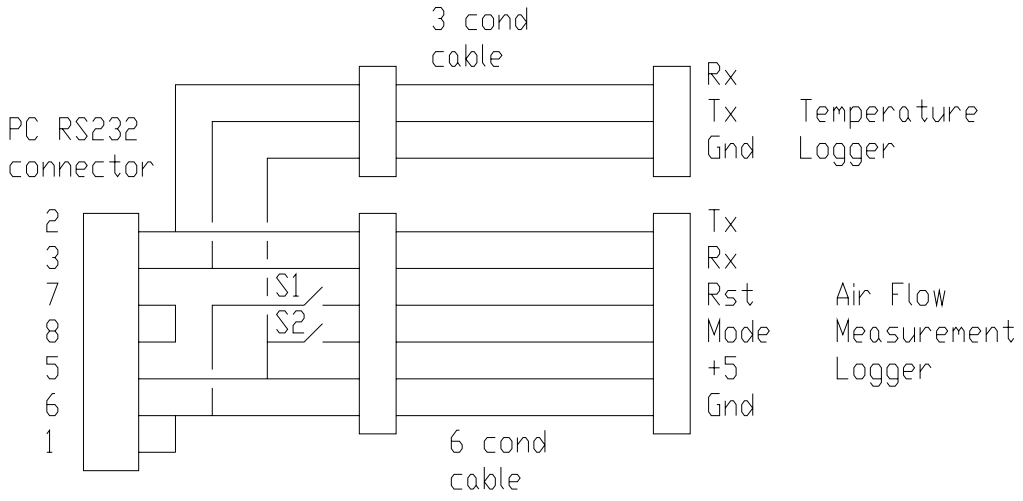


Figure 10. Remote Communications Wiring Schematic

# 3.0 Mines and Measurement Locations

John Burghardt, NPS geologist, surveyed the three mines, estimated the adit slopes, and assessed the safety conditions during the first site visit on September 25, 1998, and subsequently drew the mine maps and adit trenches shown in Figure 11, Figure 15, and Figure 21. The author added the instrument location information.

## *3.1 Mine 31*

Air Flow Transducer 1 was installed about 20 feet into the mine at the entrance to the east drift (Figure 12). Instrument Station 31-1 is 91 ft from the pre-closure portal in the east drift (Figure 13). This station contains a data logger, an alpha cup, a dosimeter, and airflow transducer 6. Data logger 31-2 was installed on a small shelf on the rib, directly below the portal slope (Figure 14).

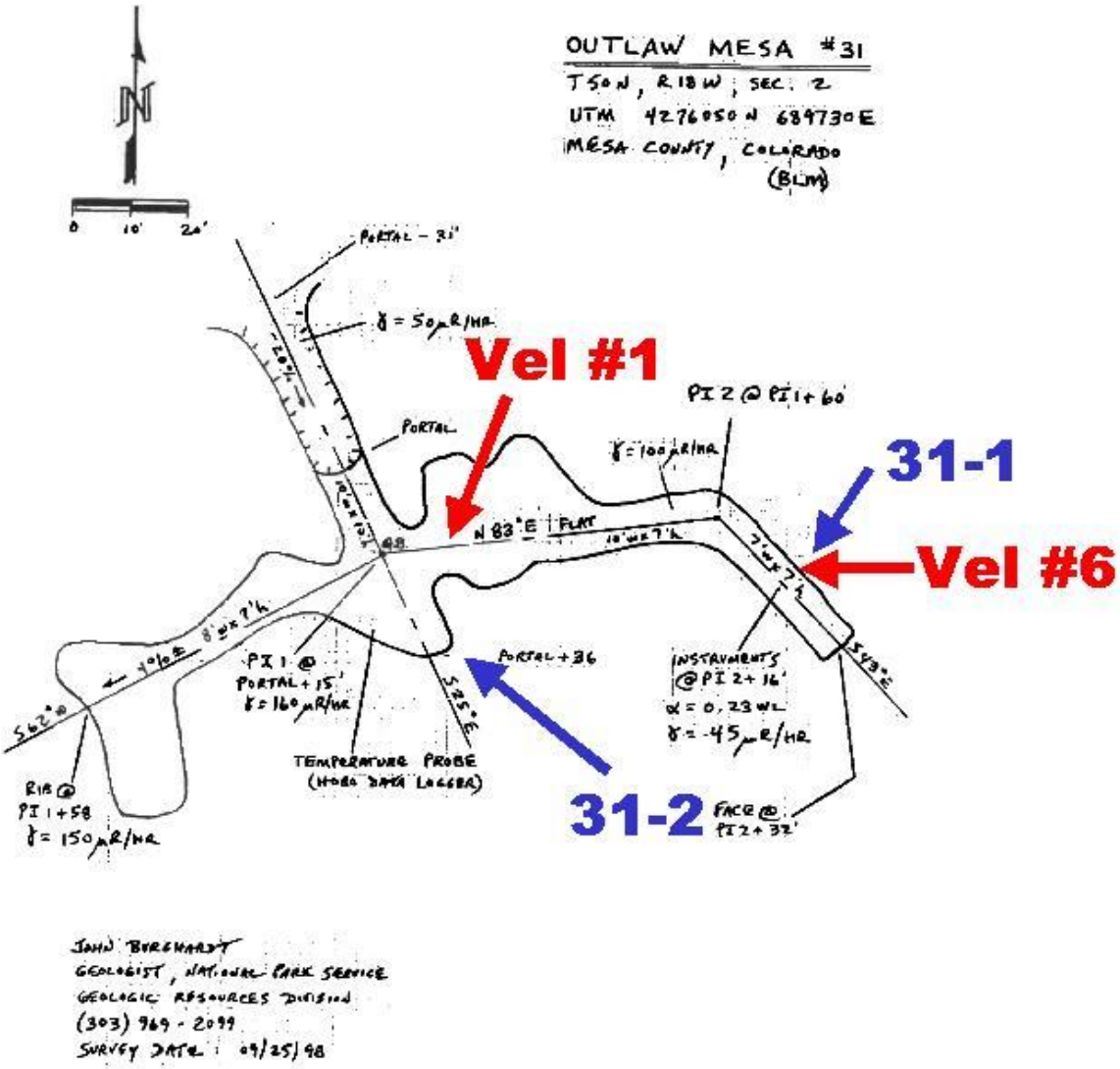


Figure 11. Plan View of Mine 31 Showing Measurement Locations

Figure 12. Photograph of Airflow Transducer 1 in Mine 31

Figure 13. Photograph of Instrument Station 31-1

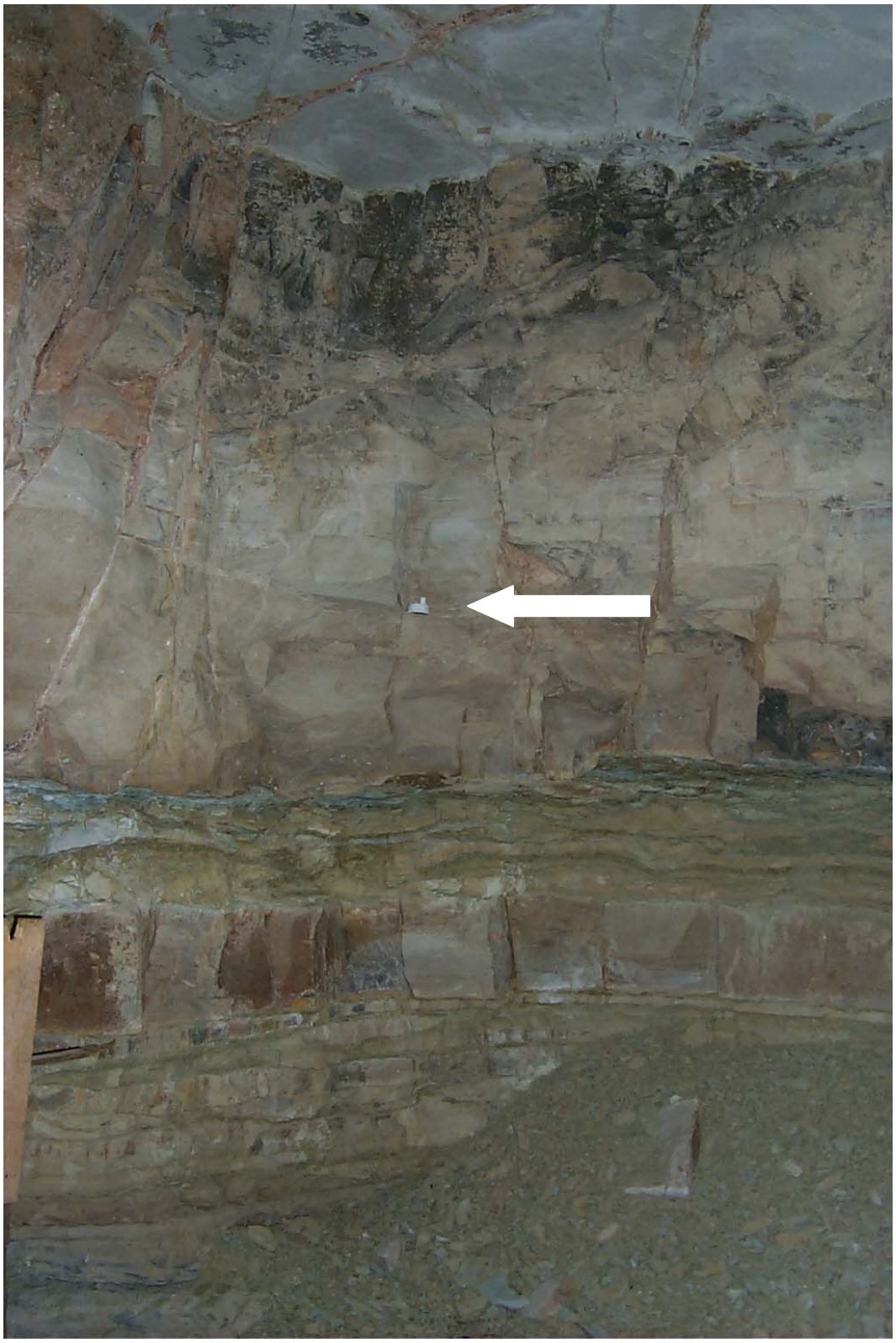

Figure 14. Photograph of Data Logger 31-2

### *3.2 Mine 59*

Mine 59 was larger and more complex than Mine 31, and Mr. Burghardt found a previously unknown connection between two nearby portals

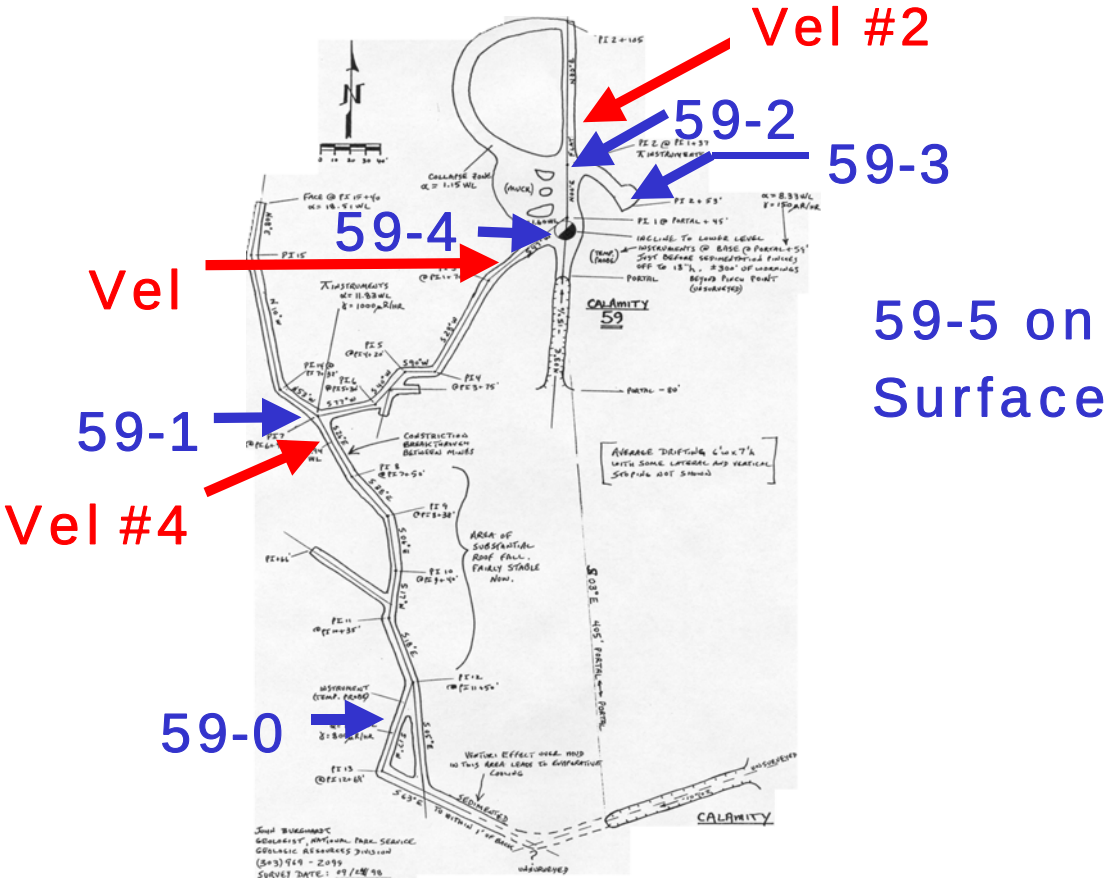


Figure 15. Plan View of Mine 59 showing measurement locations

Figure 3 is a post closure photograph of the north portal of Mine 59. Figure 16 shows instrument station 59-1 with data logger, alpha cup and dosimeter supported by a tripod. Figure 17 shows data logger 59-2 suspended from the back (roof) in mine 59. Figure 18 shows data logger 59-3 sitting on a rock shelf along the rib with the alpha cup and dosimeter supported by a post. Figure 19 shows data logger 59-4 suspended from the back of a winze. Figure 20 shows data logger 59-5 on the surface above mine 59.

Figure 16. Photograph of Instrument Station 59-1.

Figure 17. Photograph of Data Logger 59-2.

Figure 18. Photograph of Instrument Station 59-3.

Figure 19. Photograph of Data Logger 59-4.

Figure 20. Photograph of Data Logger 59-5.

### *3.3 Mine 65*

Mine 65 has a single portal and is small like Mine 31, but its configuration is simpler since there is only one small cutout in the long slope from the portal (Figure 21). At the time of Mr. Burghardt's survey, the mine was flooded at 200 ft from the portal. The photograph in Figure 22 was taken from the bat-gate on the post-closure entrance showing airflow transducer 3 along with Mr. Bruce Fowler and Dr. Tom Grover at the end of the culvert. The photograph in Figure 23 shows instrument station 65-3 and airflow transducer 5.

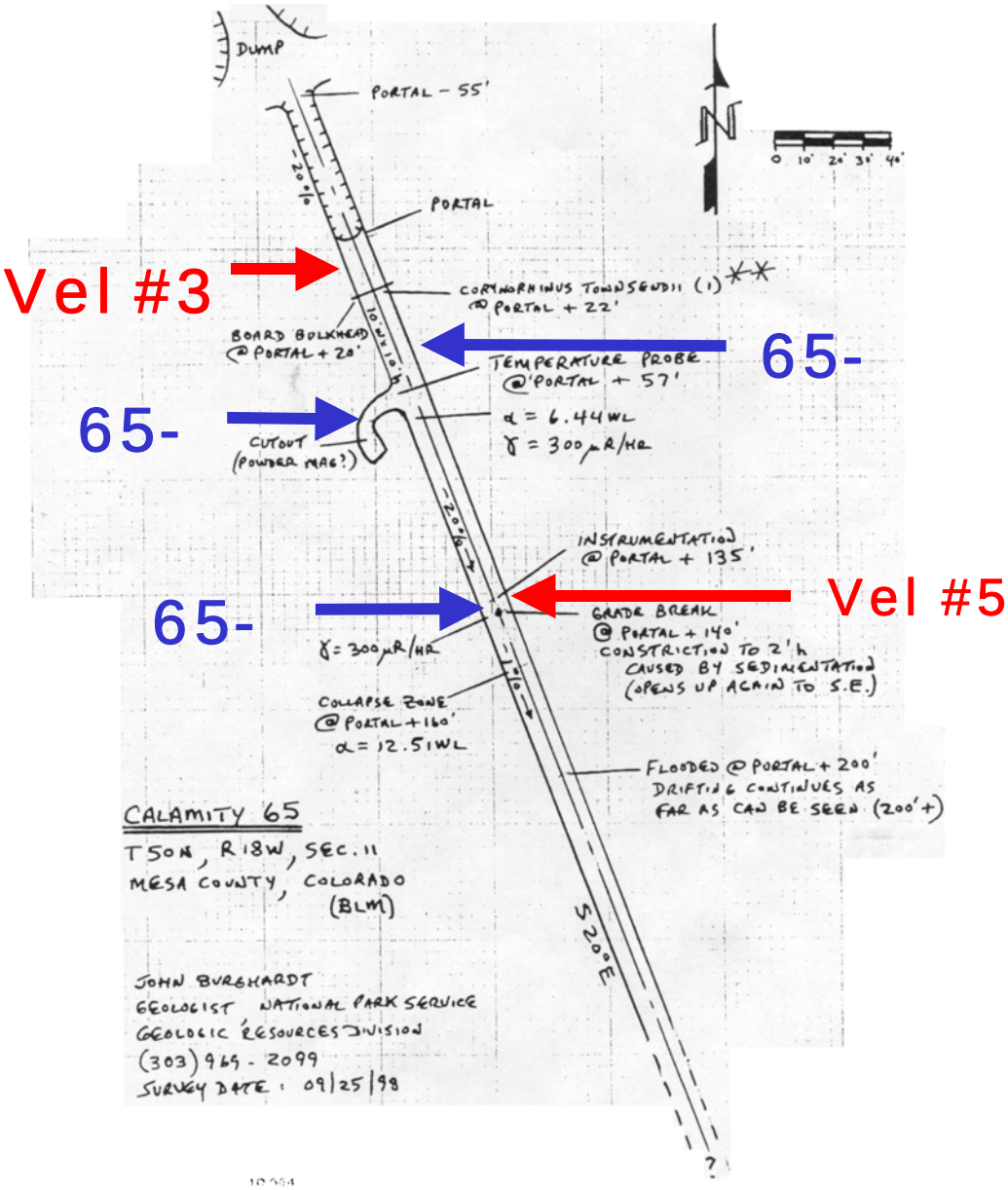


Figure 21. Plan View of Mine 65 Showing Measurement Locations

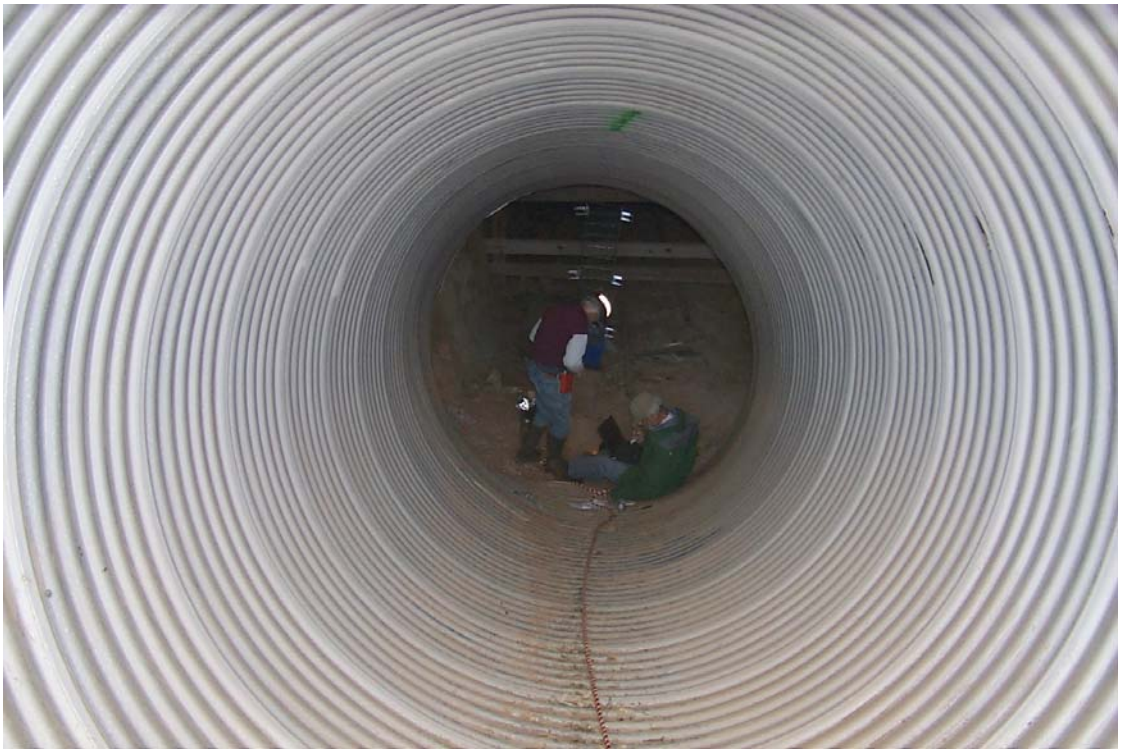

Figure 22. Photograph of Airflow Transducer 3 at Base of Mine-65 Culvert

Figure 23. Photograph of Instrument Station 65-3 and Airflow Transducer 5

Some instruments (31-1, 59-1, 59-2, 59-5, and 65-3) were suspended from tripods in the mine drifts. Others (31-2, 59-0, 59-3, 59-4, 65-1, and 65-2) were installed in close proximity to or actually in contact with the rock surrounding the drifts.

# 4.0 Temperature and Humidity

The graphs in Figure 24 through Figure 34 show the temperature (in black) and relative humidity (in blue) data collected over the study period by each data logger. Researchers downloaded data from each logger during the mine visits indicated in Figure 4. Table 2 listed installation, replacement, and problem actions over the course of the study for each logger. The data was transferred to a spreadsheet program for analysis and graphical display. Section 8 presents the pre- and post-closure analysis.

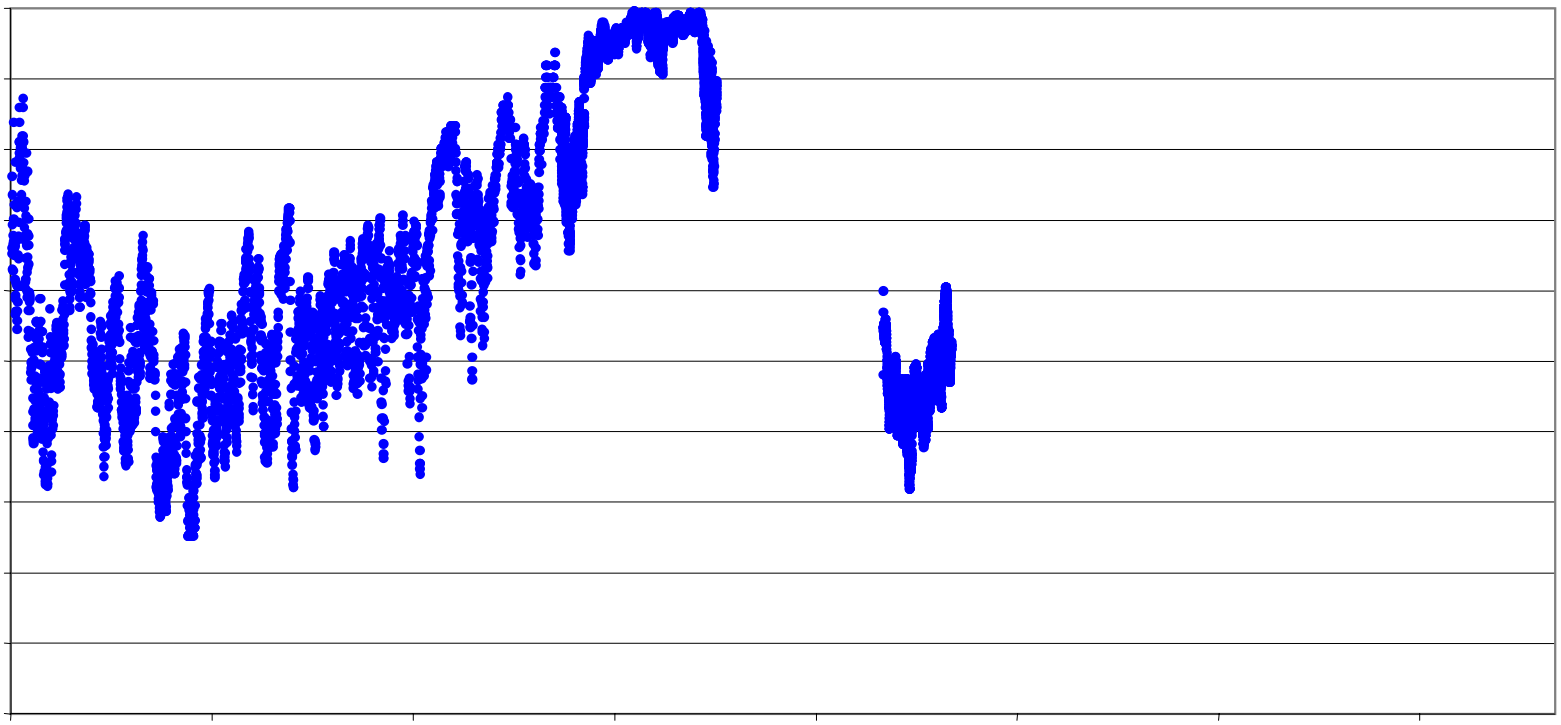

Figure 24. Logger 31-1 Data.

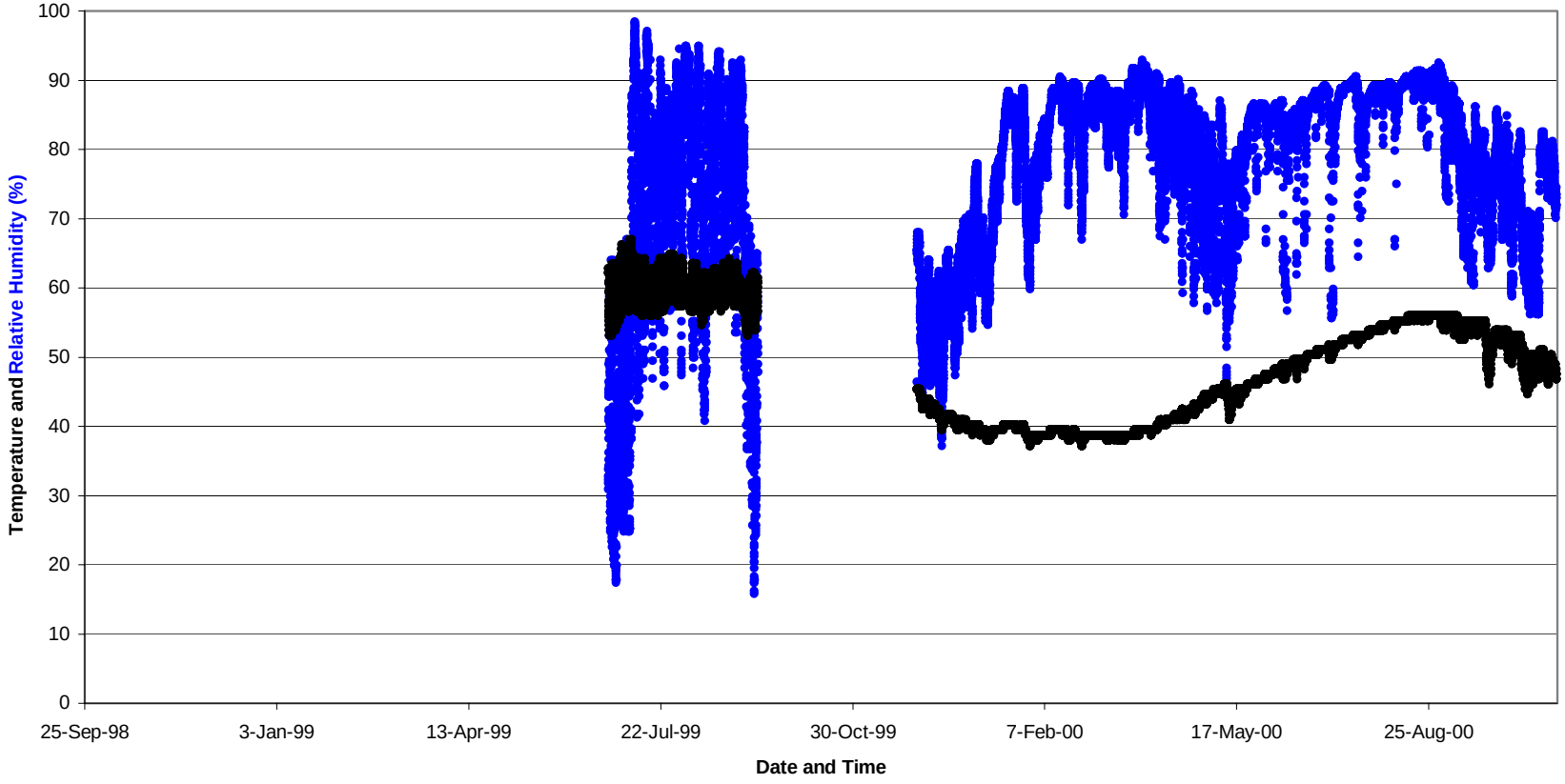


Figure 25. Logger 31-2 Data

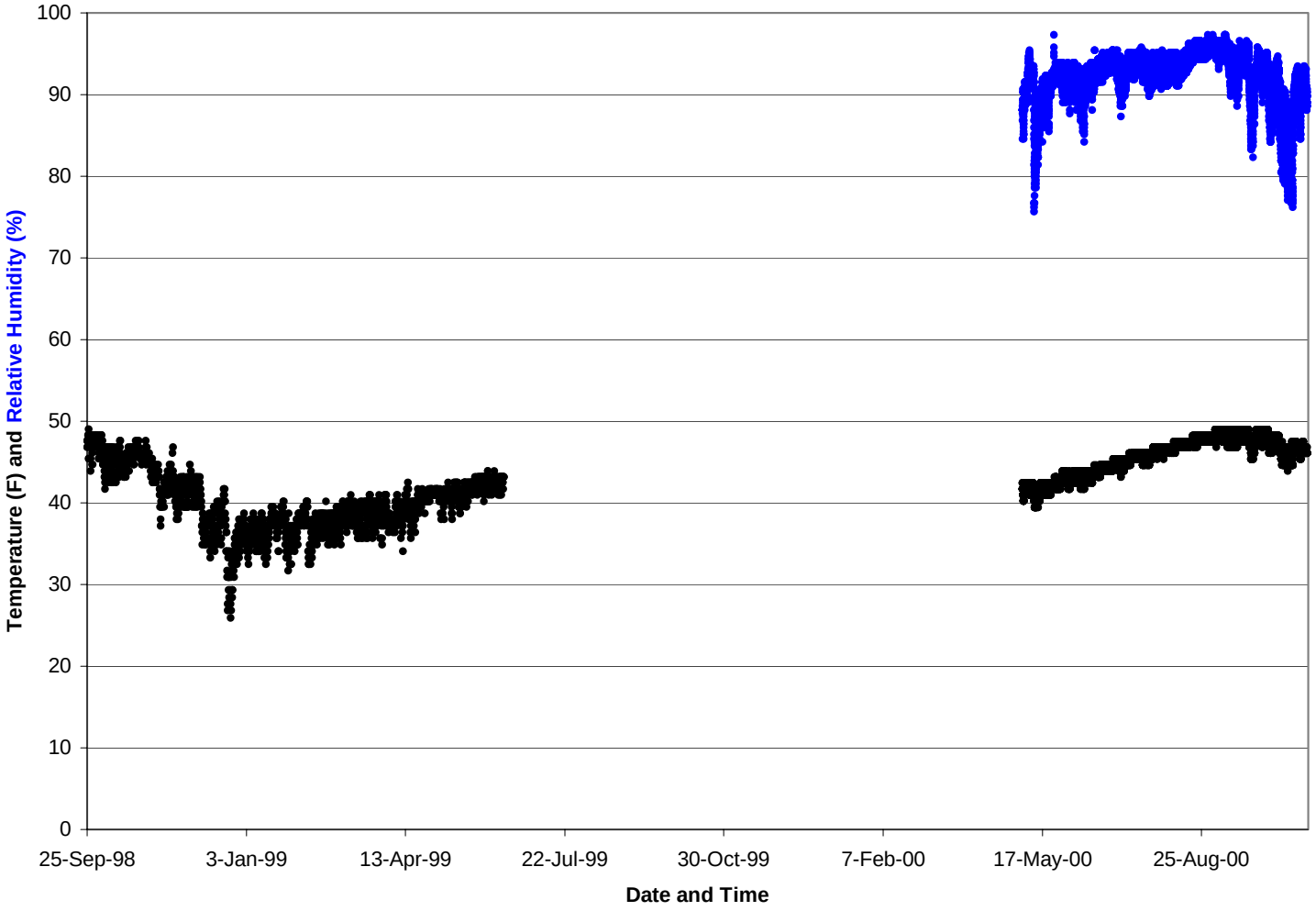


Figure 26. Logger 59-0 Data

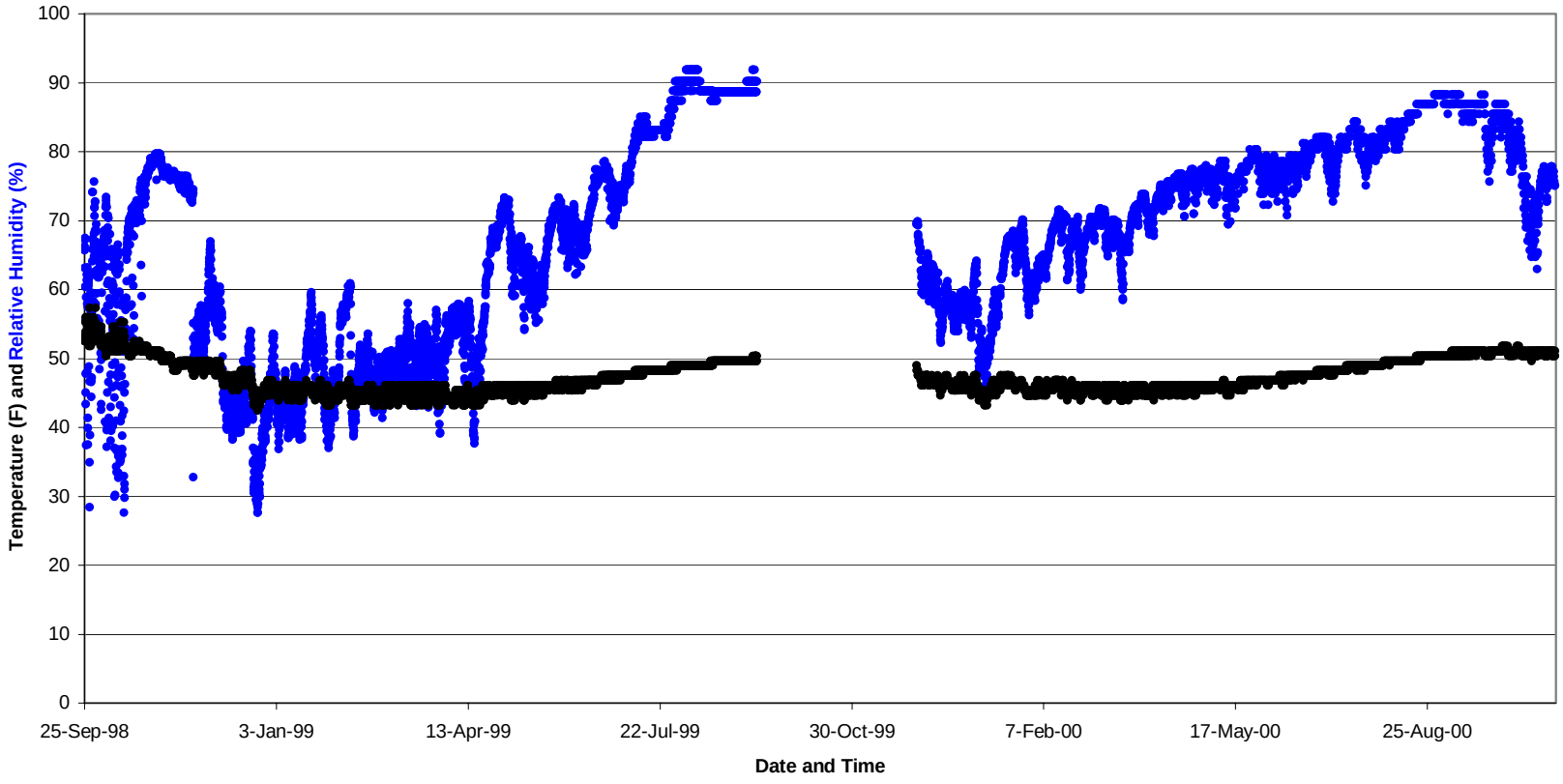


Figure 27. Logger 59-1 Data

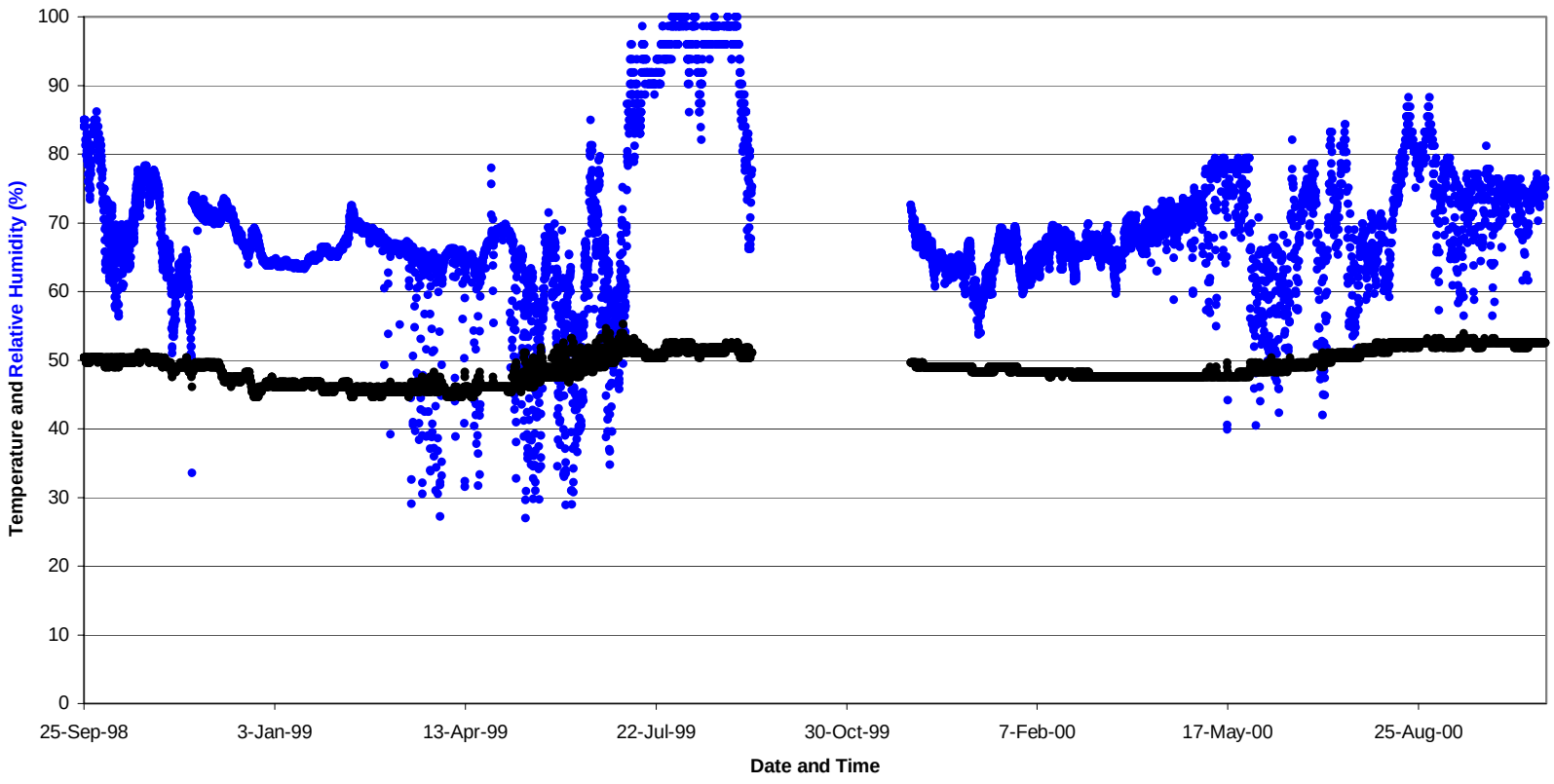


Figure 28. Logger 59-2 Data

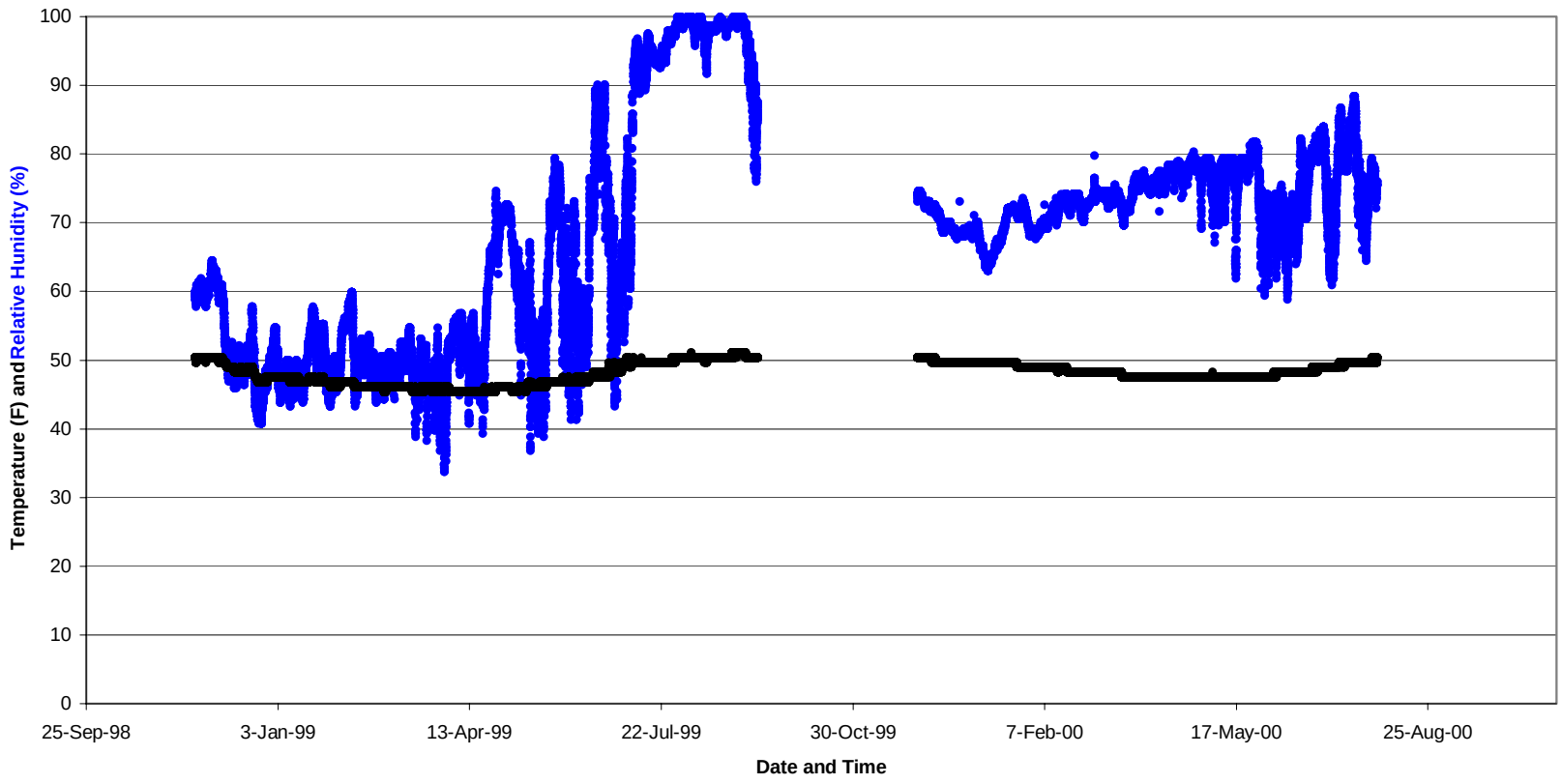


Figure 29. Logger 59-3 Data

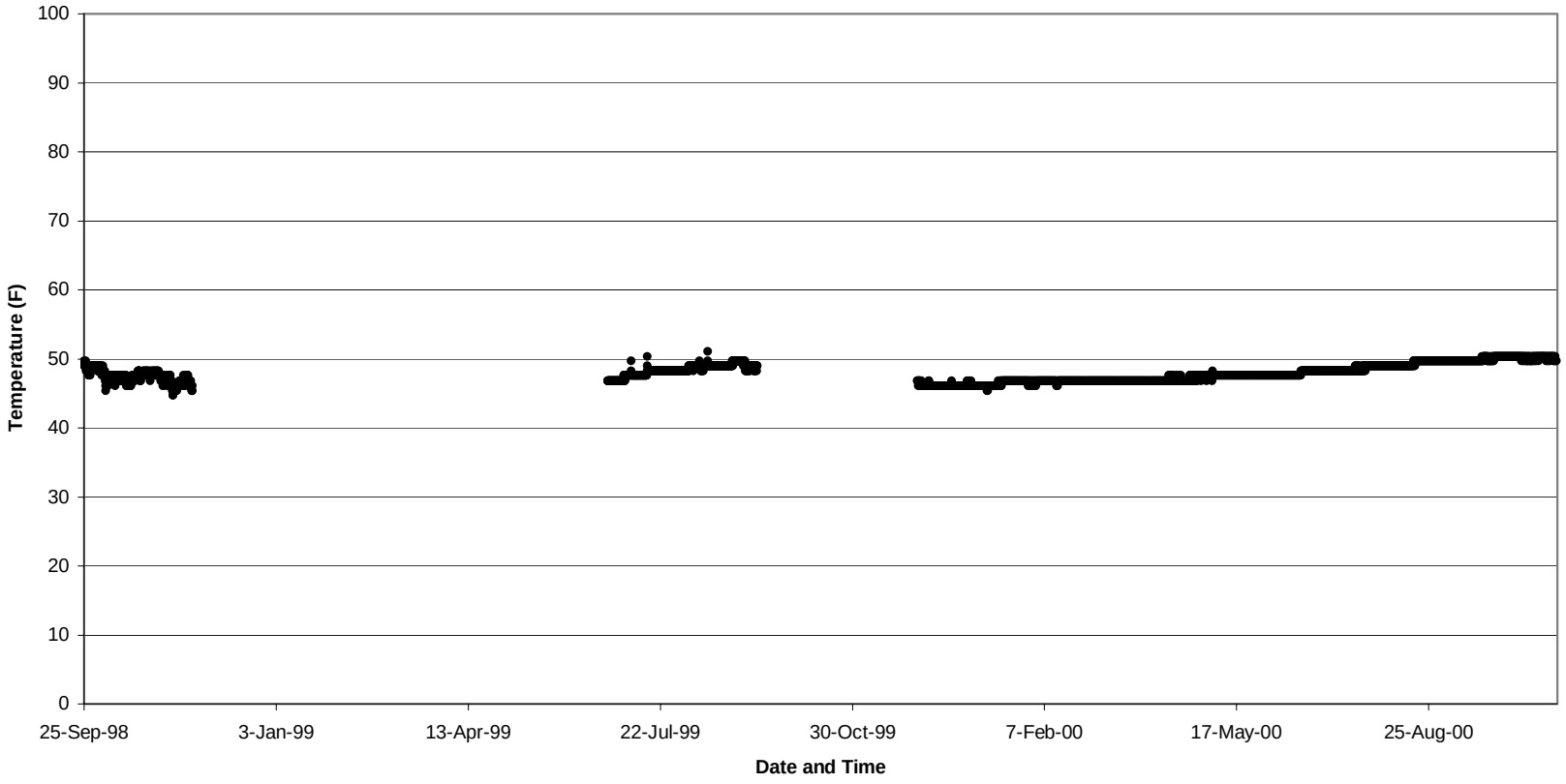


Figure 30. Logger 59-4 Data

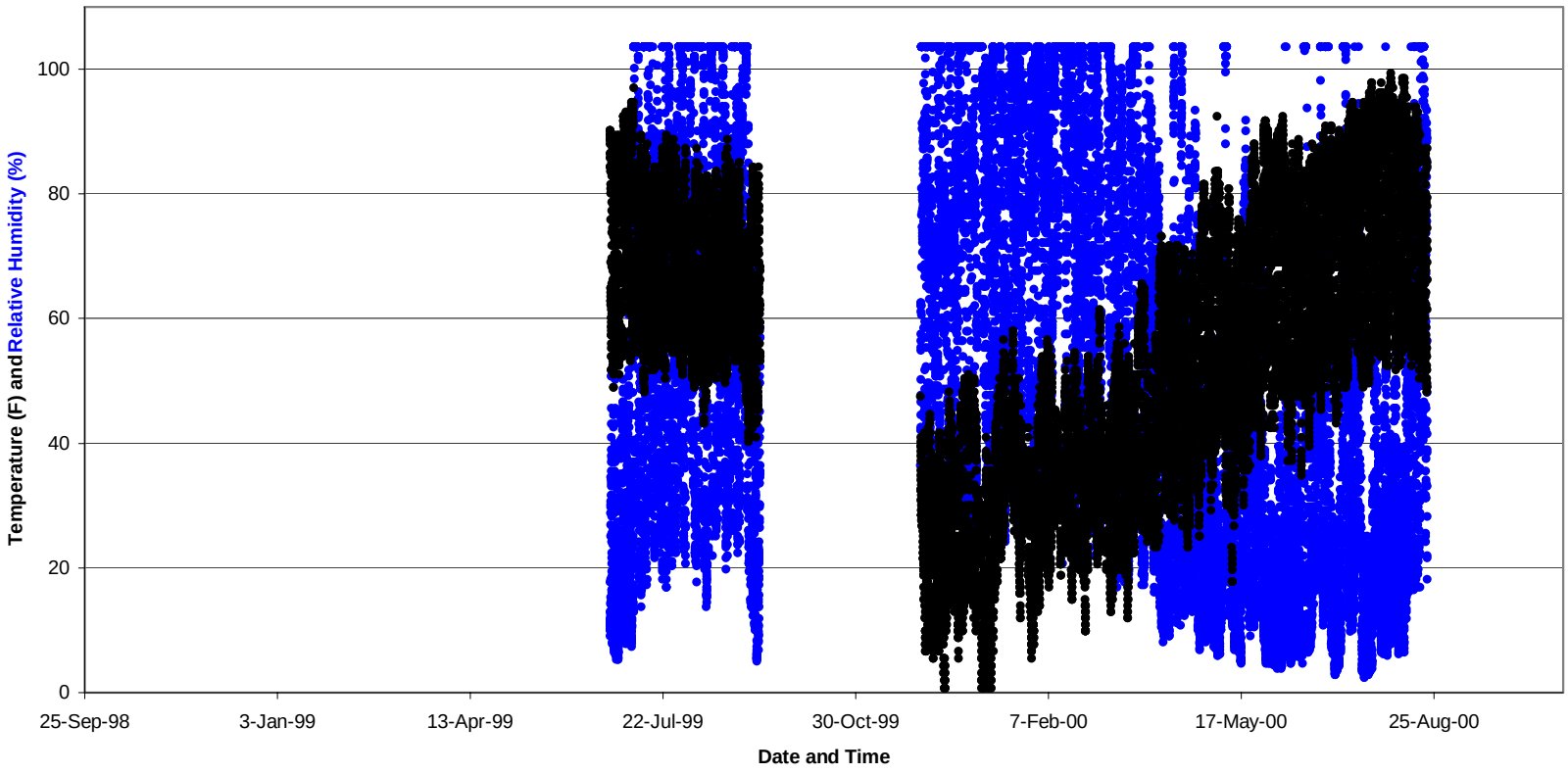


Figure 31. Logger 59-5 Data

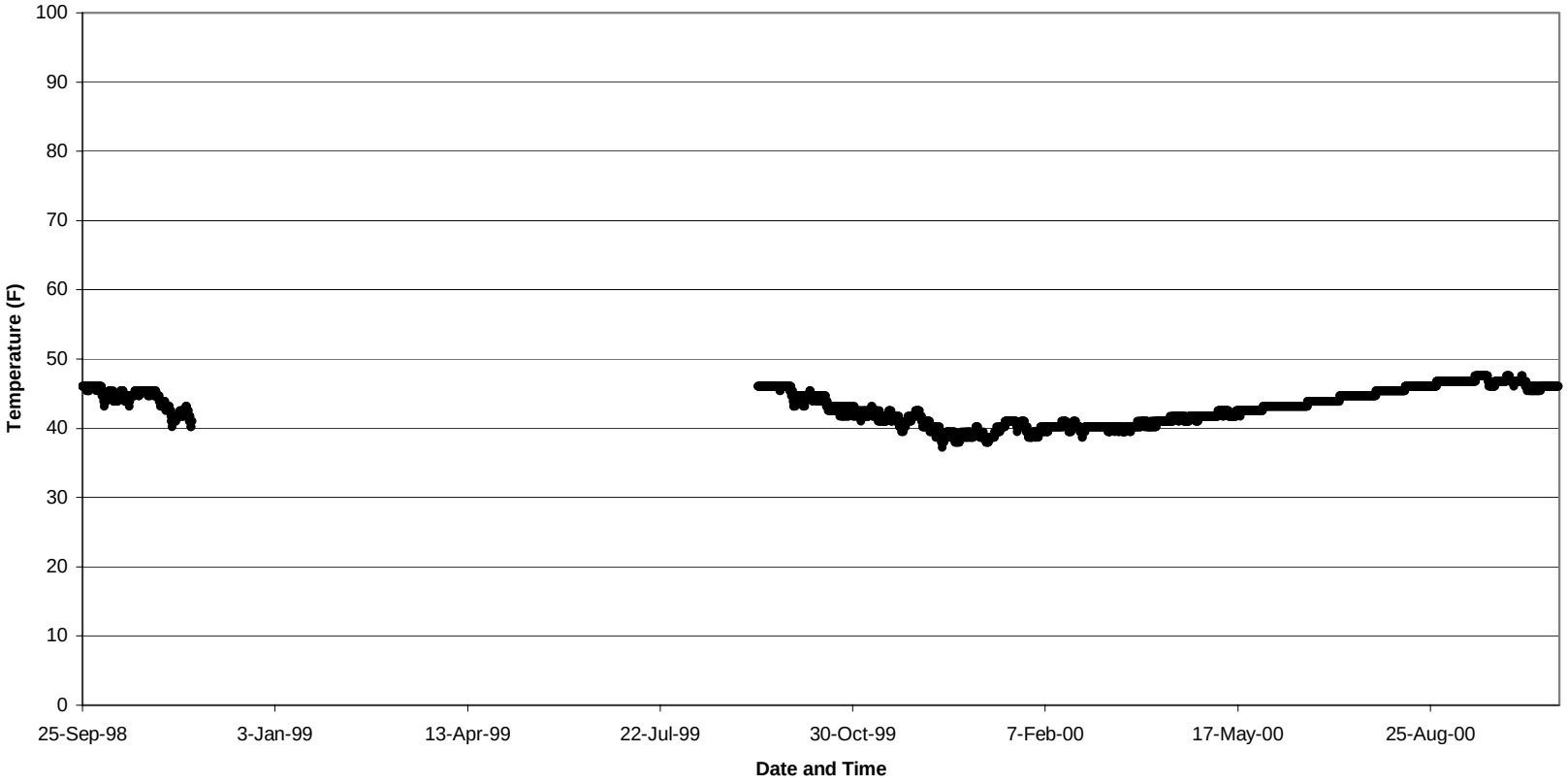


Figure 32. Logger 65-1 Data

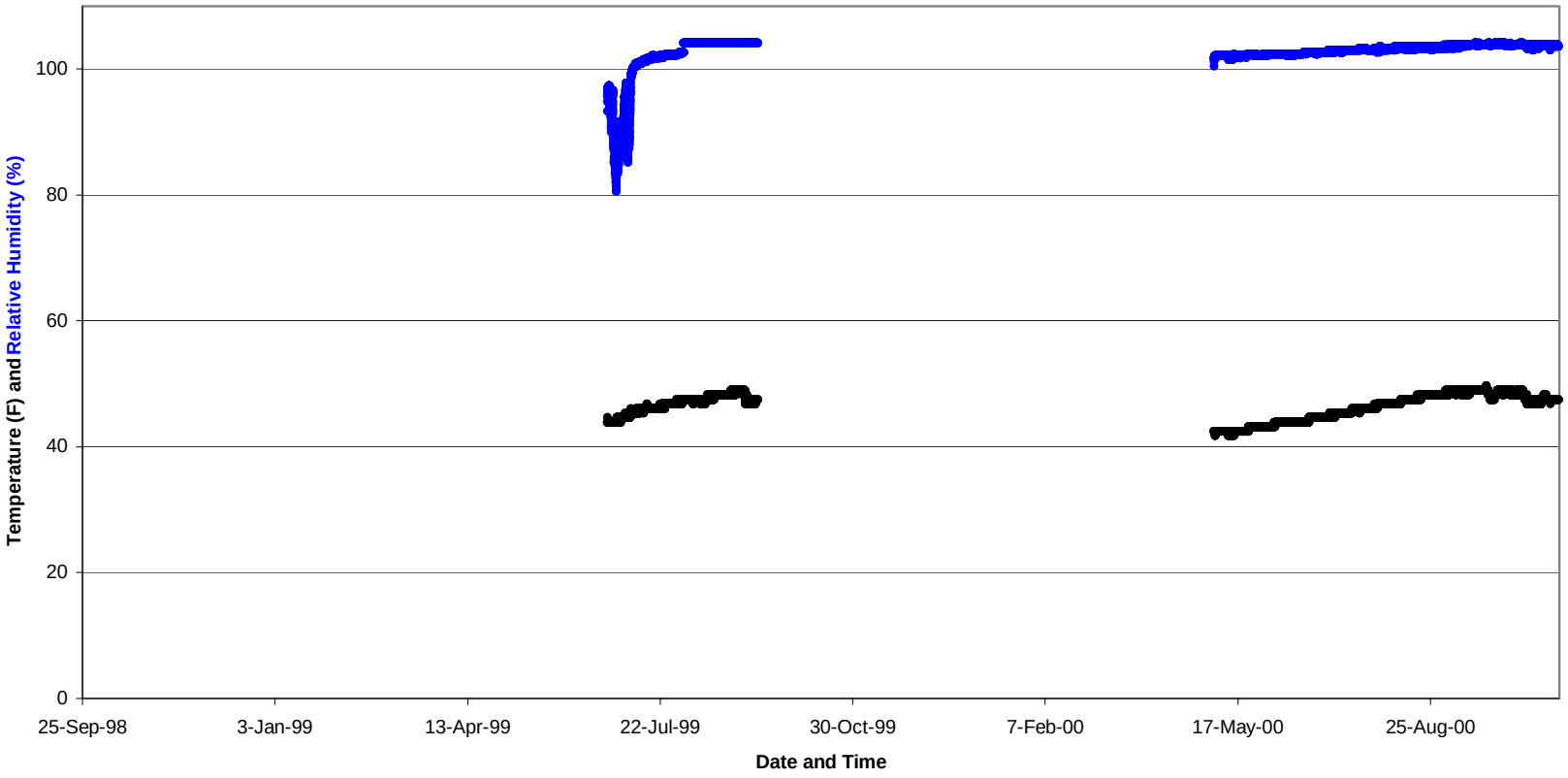


Figure 33. Logger 65-2 Data

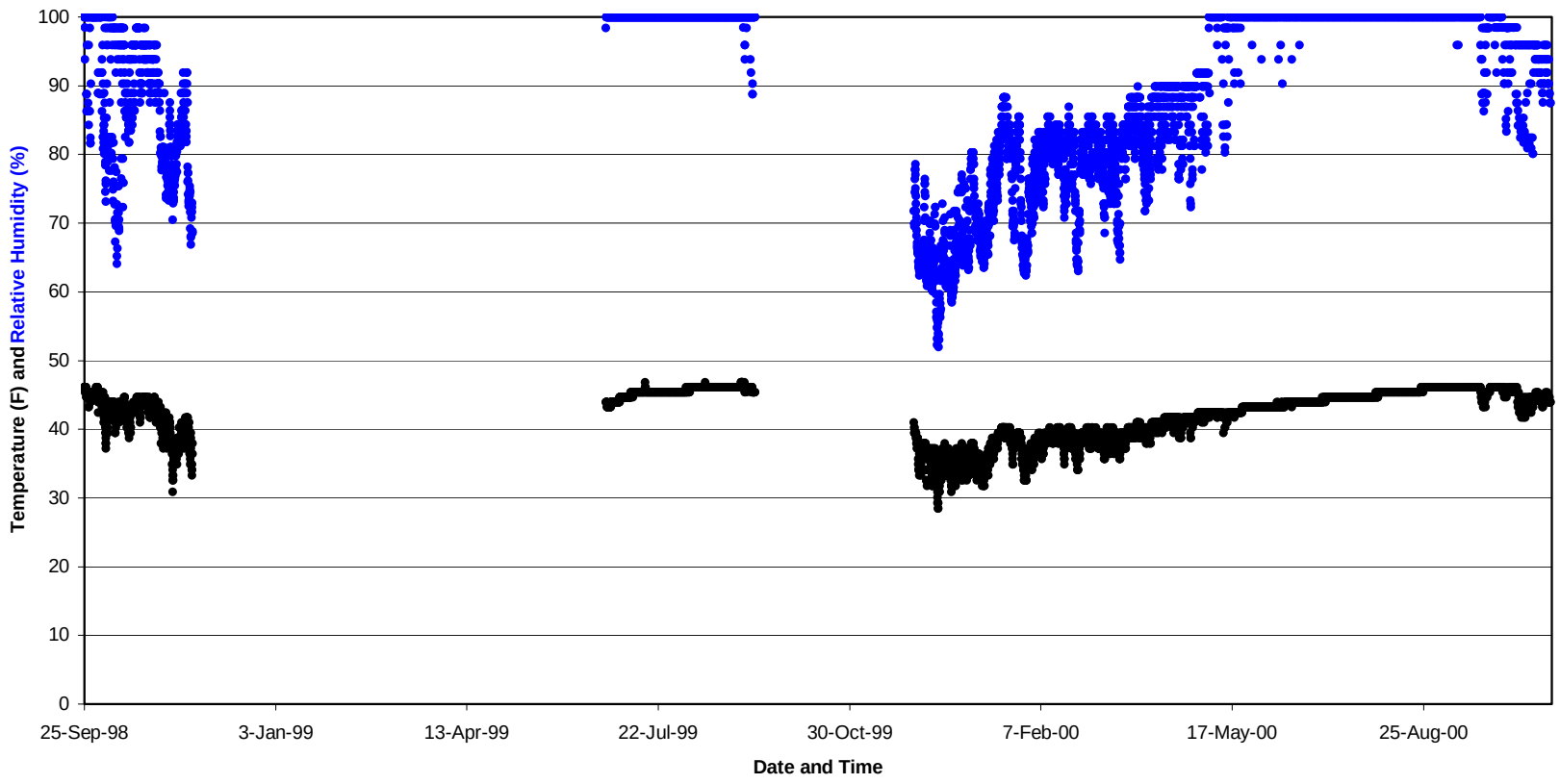


Figure 34. Logger 65-3 Data

# 5.0 Modeling

## *5.1 Introduction*

Tuttle and Stevenson described the effects of conduction, geographic location, water circulation, air circulation, and cave structure on cave microclimate and bat habitat. (Tuttle and Stevenson, 1978) Tuttle and Stevenson agree with the data in the previous section of this report showing that neither temperature nor humidity is constant in a small mine. Both temperature and humidity vary with daily surface temperature cycles, storm events, the seasons, and physical changes. Tuttle and Stevenson report that mine layout and the number of openings affect the microclimate. Two of our study mines have a single opening and the third has two openings, and external influences affect the microclimates differently in these two mine types. However, in both types, the majority of airflow, and consequently temperature and humidity variation, is caused by natural convection created by the difference between the surface temperature and the mine temperature. Tuttle and Stevenson draw a similar conclusion.

Another physical attribute of the mine plays an important part in natural convection. The drifts in the mines in our study slope downward from the portal. Therefore, when the surface air is colder or denser than mine air, the warm air rises out of the mine, buoyed by the colder, denser air that flows in along the floor. Tuttle and Stevenson describe this effect and show different flows for different mine structures.

In addition to convective heat transfer from the surface, heat is conducted to and from the mine air by the mine rock. During periods when cooler airflows into the mine along the floor, heat conducts from the rock to the air. The amount of warming depends on the amount of airflow. If airflow rates are relatively high, the air does not stay long enough to be affected very much by the rock temperature. However, we found that airflows were low, so temperatures were affected by conduction.

Tuttle and Stevenson's general situation suggests a simplistic model with a warmer air layer near the back (roof) where air flows out of the mine and a cold air layer near the floor, where air is flowing into the mine (Figure 35). However, smoke tube tests in the mines did not confirm this condition. We found that air movement within the mine was turbulent. The simple model requires a large temperature differential and a large downward slope. In the mines we studied, the temperature differentials and slopes were small and created weak flows that did not pass very far into the mines before they were damped by the mine air (Figure 36).

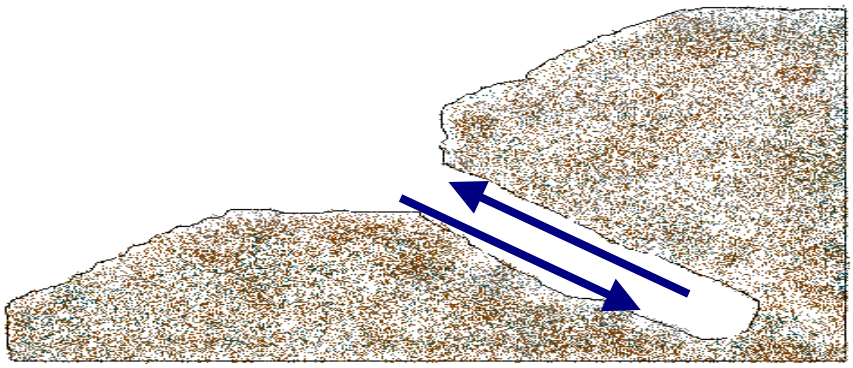

Figure 35. Simple Convection Flow when Surface Air is Much Cooler than Mine Air.

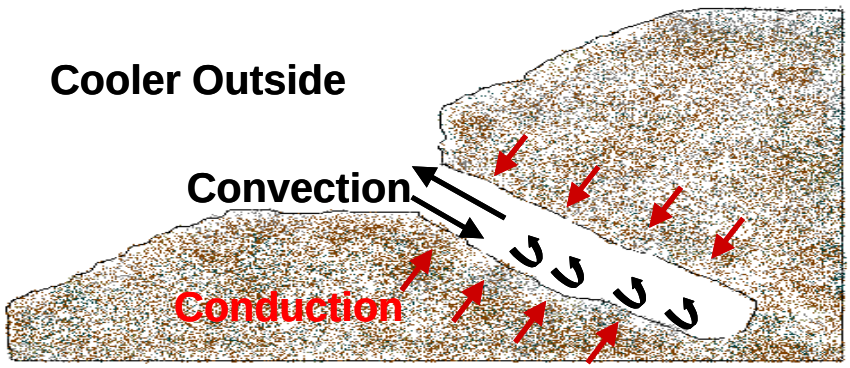


Figure 36. Airflow with Small Temperature Differential, Convection, and Conduction

The rock temperature is fairly constant about 6 ft away from the rock surface where it is approximately equal to the mean annual surface temperature (MAST). The MAST in Grand Junction is about 53 °F (Colorado Climate Center, September 17, 2001). Figure 37 shows the relationship between the Grand Junction Weather Station and the surface temperatures at the mine site (logger 59-5) from 6/24 to 9/10/99. From the relationship, we estimated that MAST at the mine site is 50 °F. This value can be compared with the surface and mine temperatures reported in section 4 of this report.

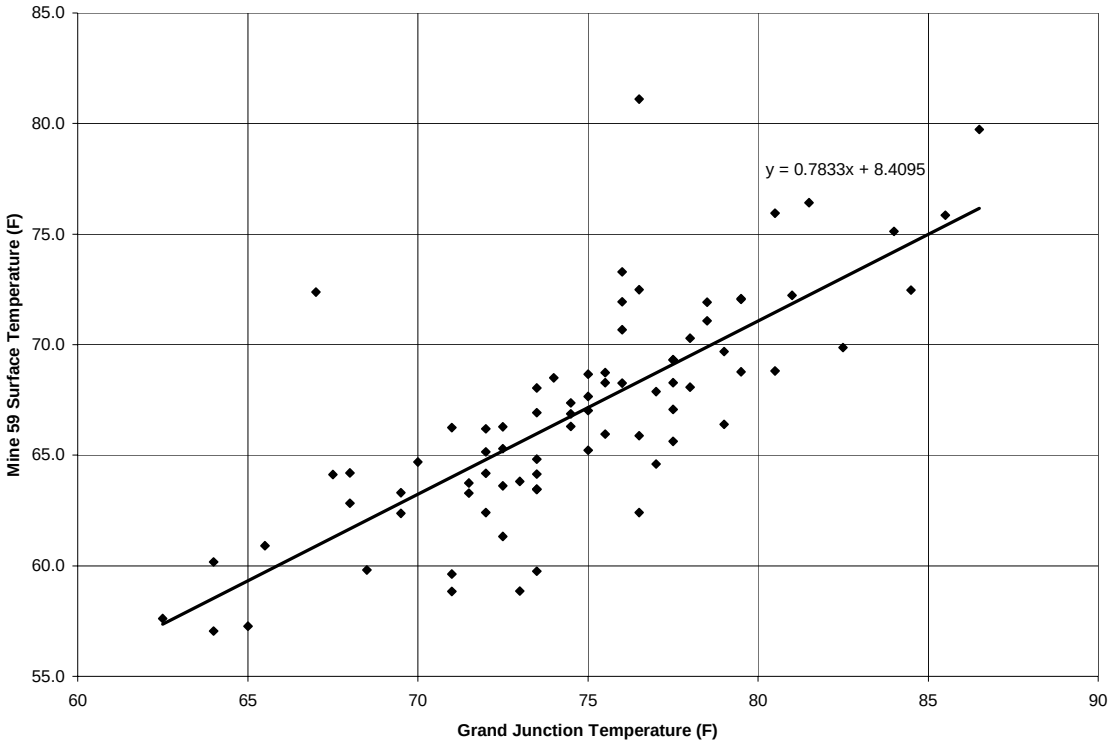


Figure 37. Relation between Grand Junction Weather Station and Mine 59 Surface Temperatures

Seasonal changes affect airflow in these decline mines. In the summer, the surface temperature is above the MAST, so it is warmer than the rock and the air within the mine. As a result, the cooler air is trapped down the decline and there is little mixing between the two systems. If the surface air cools enough during the night or during a storm, warmer air might rise from the mine for a short period.

As the surface air cools in the fall, airflows will increase depending on the transient nature of surface temperature changes. If changes are gradual, the mine air will cool and airflows will be low, but abrupt changes could produce significant air flows for short periods of time. In the winter, the surface temperature continues to drop. The air within the mine is at a higher temperature than the surface air and will rise out of the mine. The mine rock will conduct heat into surface air that flows in to replace the rising mine air.

In the spring, the surface temperature begins to rise. As a result, the winter airflow will decrease as the surface temperature becomes closer to the rock temperature and eventually rises above the rock temperature. In our decline mines, we could expect the colder air to be trapped down the decline. During the night and storms, airflow might occur for short periods.

Of course, unventilated vertical features in the mine, such as cavities remaining after a roof fall, may trap warmer air. These features were minimal in the mines studied.

## 5.2 Modeling Software

Traditional software that simulates mine airflows is designed to model active mines with large fans and large pressure differentials could not calculate the weak natural convective flows characteristic of our problem. We also attempted to develop our own model with limited success, since the mathematical representation of convective flow is very complex.

An example of natural convection is when a horizontal fluid layer heated from below becomes thermally unstable because the fluid near the heated boundary is hotter and therefore lighter than the fluid above. This type of instability, known as the Rayleigh-Bénard instability, causes fluid motion from competition between buoyancy, which tends to destabilize the fluid layer, and viscous friction, which has a stabilizing effect (Drazin and Reid 1981 and Chandrasekhar 1961). The Rayleigh number classically quantifies the relative magnitude of these two mechanisms, so if the Rayleigh number is larger than a critical value, the configuration is unstable.

In order to simulate the seasonal and daily variations in natural convection and conduction in the mine, our model had to solve the Navier-Stokes equations governing fluid flow:

$$\frac{\partial \rho}{\partial t} + \nabla \cdot (\rho \mathbf{V}) = 0$$

$$\rho \frac{\partial \mathbf{V}}{\partial t} + \rho(\mathbf{V} \cdot \nabla)\mathbf{V} = -\nabla p + [\nabla \cdot \boldsymbol{\tau}] + \rho \mathbf{g}$$

and the heat transfer or energy equation:

$$\rho \frac{\partial h}{\partial t} + \rho(\mathbf{V} \cdot \nabla h) = -\nabla \cdot \mathbf{q} + \frac{Dp}{Dt} + [\boldsymbol{\tau} : \nabla \mathbf{V}]$$

where $\rho$ was the fluid density, $\mathbf{V}$ the velocity vector, $p$ the pressure, $\boldsymbol{\tau}$ the viscous stress tensor, $\mathbf{g}$ the acceleration of gravity, $h$ the enthalpy per unit mass, and $\mathbf{q}$ the heat flux vector. Since the fluid density drove the flow and was a function of temperature, the momentum and energy equations were coupled and had to be solved simultaneously. The density variation was small compared to the average density $\overline{\rho}$, so we assumed that $\rho \approx \overline{\rho}$ everywhere except in the buoyancy term. The model combined the hydrostatic part of the pressure field with the buoyancy term, assuming the ideal gas law applied, to develop the momentum equation with the Boussinesq approximation:

$$\bar{\rho}\frac{\partial \mathbf{V}}{\partial t} + \bar{\rho}(\mathbf{V}\cdot\nabla)\mathbf{V} = -\nabla p + [\nabla\cdot\boldsymbol{\tau}] + \bar{\rho}\,\bar{\beta}\left(T - \bar{T}\right)\mathbf{g}$$

where $p$ was evaluated relative to the hydrostatic pressure and $\bar{\beta}$ was the volumetric thermal expansion coefficient. As expected in systems of such size, the flow was turbulent which affected momentum and heat transfer, so our work used the $k-\varepsilon$ model where k was the turbulent kinetic energy and $\varepsilon$ was the turbulence dissipation (Jones and Launder 1972).

We used a commercially available solver, CFD-ACE (CFD Research Corporation, Huntsville AL) to numerically solve these coupled, non-linear, second-order partial differential equations. It has been thoroughly tested in a variety of applications including aerospace, combustion, semi-conductors, microelectronics, bio-medical, automotive, multi-disciplinary and air-turbo rocket models. CFD-ACE used a finite-volume approach to discretize the flow and energy equation and solved the resulting algebraic equations iteratively. A CSM graduate student, Joe Dodds, investigated whether the CFD software could model the convection and conduction induced flows in abandoned mines. He developed the model as a two dimensional representation of a cylindrical airshaft with 4-m diameter and 30-m length with 2 m of surrounding rock. (Dodds, 2001) CFD ACE required boundary conditions, initial conditions, and materials properties (Figure 38 and Table 9). The iterative solver stopped after 2000 iterations or when it converged and all residuals were less than $10^{-7}$ or any residual less than $10^{-18}$. Increasing the number of iterations beyond 2000 did not significantly improve the results.

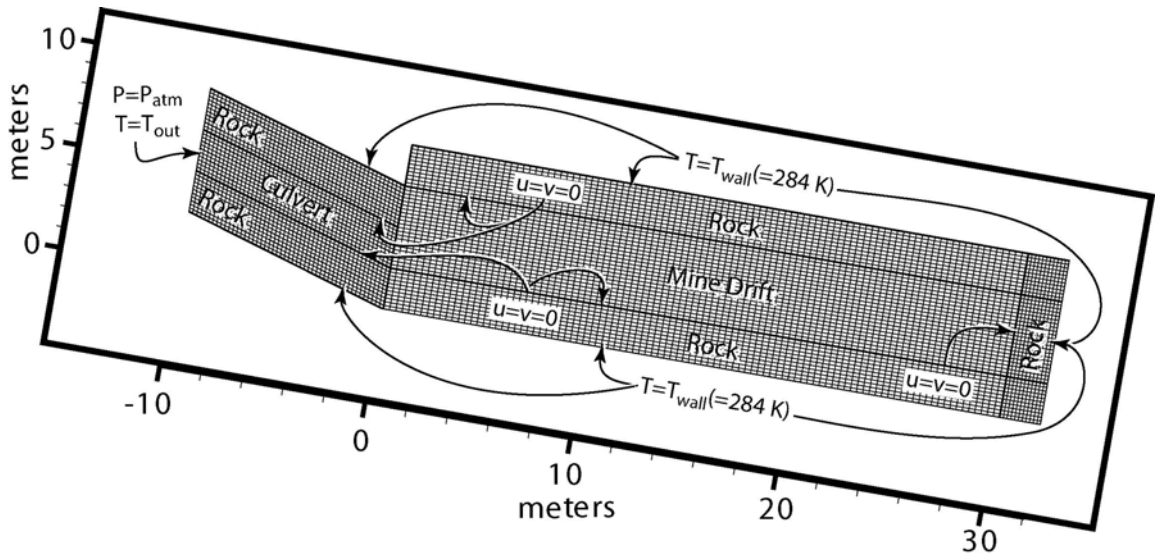


Figure 38. Vertical Cross Section of a Remediated Mine with a Small-diameter Inclined Culvert showing the CFD Model Mesh and Typical Boundary Conditions.

Table 9. Material Properties Used in the CFD Model

| Symbol | Property | Value |
|---|---|---|
| $\rho_{rock}$ | Rock Density | 2150 kg/m$^3$ |
| $Cp_{rock}$ | Rock Specific heat | 745 J/kg-K |
| $K_{rock}$ | Rock Thermal Conductivity | 2.9 W/m-K |
| $\mu$ | Dynamic Viscosity | 1.71 E-5 kg/m-s |
| | Air Molecular Weight | 29 |
| $Cp_{air}$ | Air Specific Heat | 1000 J/kg-K |
| $K_{air}$ | Air Thermal Conductivity | 0.024 W/m-K. |

The domain over which the governing equations are solved numerically is a representation of the physical domain studied, but it must also satisfy constraints such as allowing a reasonable computation time to permit the investigation of various configurations. The physical domain of the mines under study was inherently three dimensional because of the angle between the adit and the acceleration of gravity. We assumed that the irregularity of the mine cross-section and the gross-roughness of the walls were relevant but second-order effects compared to the non-alignment of the mineshaft and the acceleration of gravity. Therefore, we used a 2-dimensional, planar slice of the mine, which reduced the computational effort and captured the salient physical mechanisms.

CFD ACE uses three different software modules to build a simulation; the first is CFD GEOM, which captures the 3D geometry of the process to be simulated, in this case the structure of the mine. GEOM consists of four sub-modules: the geometry module, the structured grid generation module, the unstructured grid generation module, and the editing module. The user identifies the basic structure and then determines how to divide the structure into elements described by a three-dimensional grid or mesh. The geometry module uses Non-Uniform Rational B-Splines (NURBS) geometric primitives and transfinite interpolation (TFI) methodology to automatically generate meshes to any user-specified precision. Figure 38 is an example of one of the meshes used in our study. The large upper area and the two smaller areas to the right are the rock surrounding the mine; the large lower area is the drift. Our study used a very simple grid to evaluate the capability of the software with our limited time resources. Researchers with greater resources can generate more sophisticated structures and grids in GEOM.

The number of cells in the mesh affects the accuracy of the results. The finer the mesh, the more accurate the results, if the algorithm converges. However, computer run time increases as more grids are added to a mesh. To justify the number of cells used for the simulations in this project, Mr. Dodds executed a mesh sensitivity study. As will be explained later, our results identified two adjacent, circulating air masses, or convection cells, in the simulated mine, one near the portal and another extending to the end of the mine. The point where these two cells meet is an important output result. The location of the interface is determined by the change of direction of the u (x-direction velocity) vector, i.e. where the u vector switches from negative to positive. Mr. Dodds graphed the location of the interface between two convection cells, versus fineness of mesh. First, he defined a number of grids for the base mesh and then tested meshes that were coarser and finer than the base by 20 and 40%. The various meshes had 36, 64, 144, and 196 % of the number of grids in the base mesh. Figure 39 is a plot of the interface location versus the number of cells used in the mesh. The result was that increasing the resolution beyond that chosen for the base mesh did not significantly change the interface location.

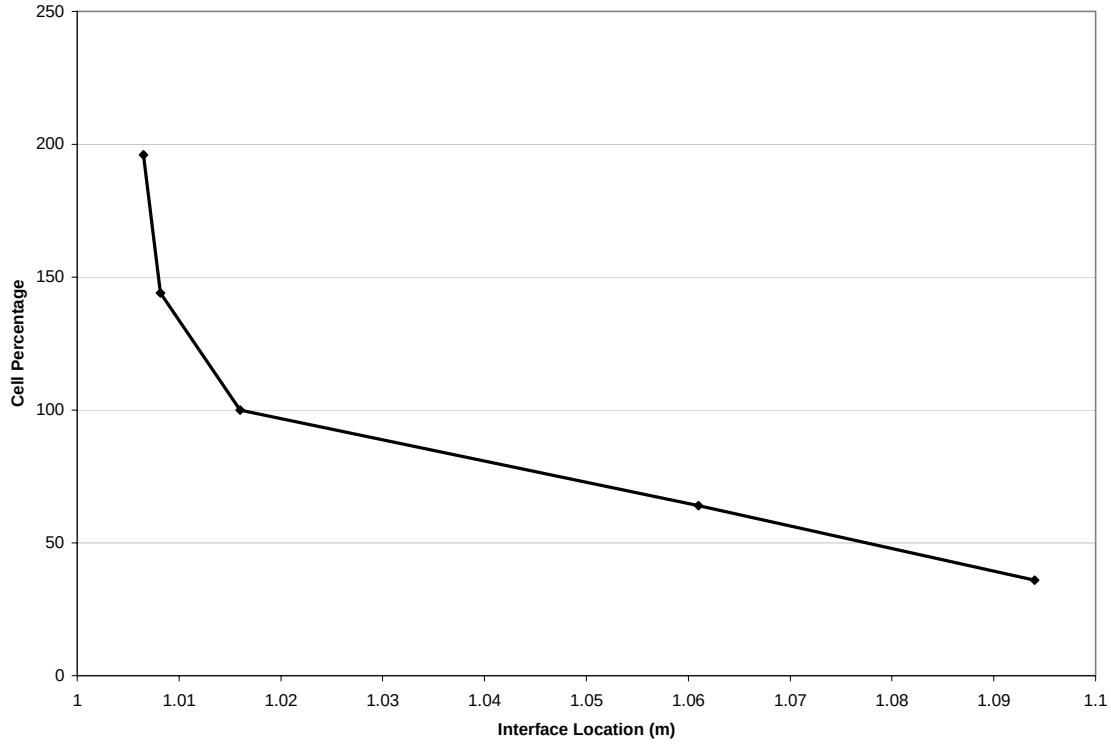


Figure 39. Interface Location versus Number of Cells in the Mesh

The mesh generated by GEOM becomes an input to the second module, ACE, that solves for quantities such as heat transfer and fluid flow. The user also inputs boundary conditions, volume conditions, and initial conditions. The flow module solves the Navier-Stokes equations, which express the conservation of mass and the conservation of momentum in the flow field.

ACE uses finite difference calculations to solve these equations. This entails reducing the differential equations to sets of algebraic equations by discretization. These algebraic equations are solved simultaneously at each node with relation to its neighboring nodes within the mesh. While ACE is solving the Navier Stokes equations, the user can view the residuals, or errors, which represent the difference between the numeric solution and the estimated true solution (Figure 40). Falling residuals indicate the iteration is converging on a solution (Figure 40).

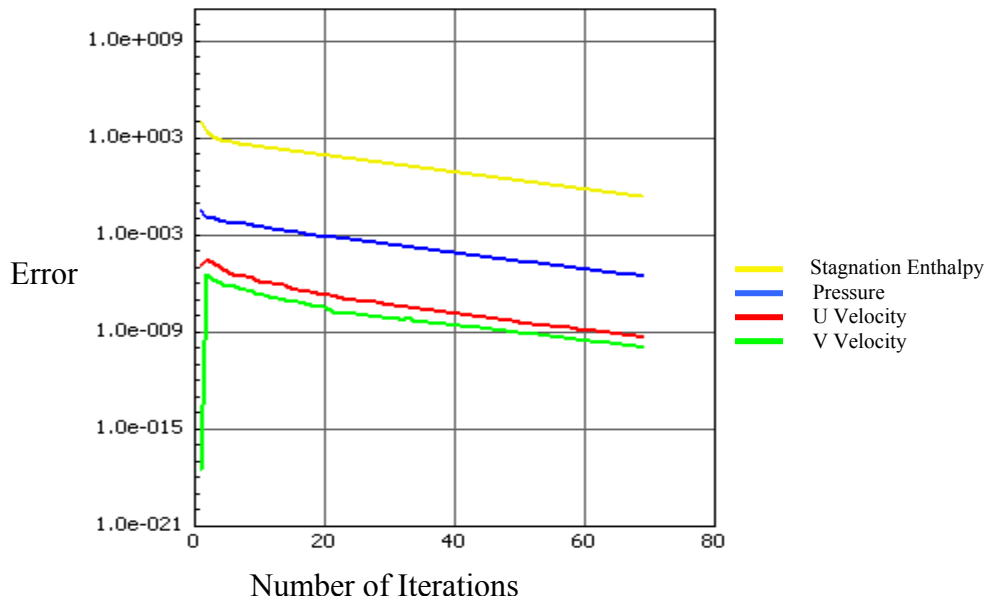


Figure 40. Example of a Residuals Plot.

The user can specify the criteria for termination, as an error value or the number of iterations.

Another module in the software, CFD VIEW, graphically presents the output from ACE including temperature and velocity profiles, stream functions and other variables specified by the user as point plots, line plots, or planar plots. Output data can be saved to file for use by other programs like spreadsheets.

## *5.3 Results*

Mr. Dodds divided the problem into five cases that gradually grew in complexity (Dodds, 2001). The first three cases are axi-symmetrical and the last two are planar representations of a cylinder shape chosen to represent a simulated mine.

The first case was steady state without heat transfer or gravity. Mr. Dodds specified a constant velocity, laminar flow, for half of the entrance and constant pressure over the other half. This case produced a steady flow field contained in the immediate entrance of the mine. The flow was quickly damped by viscous forces as distance into the mine increased.

The second case added heat transfer by means of forced convection. Half of the entrance still had a constant velocity and the other half had constant pressure. The introduction of convection entails making the walls of the model mine isothermal at a temperature of 284 K (51.5 °F). The air within the mine is initially 284 K (51.5 °F) as well. The air

being introduced from outside, however, was slightly cooler. The results of the second case differed little from the first.

The third case introduced heat transfer by means of conduction through the rock surrounding the mine. This entailed setting the boundary condition at the outer edge of the rock in Figure 5-2 to a constant temperature (isothermal at 284 K). Heat is conducted through the rock when the mine air is at a different temperature.

The fourth case added a gravity vector to simulate the sloped drift from the portal. Consequently, Mr. Dodds removed the constant velocity. The x-direction gravity vector was determined by:

$g_x = -9.81*\text{Sin}\phi$ and $g_y = -9.81 * \text{Cos}\phi$, where $\phi = 6°$ = the angle of inclination of the mine drift.

This essentially tilts the mine so its axis is no longer perpendicular to the gravity vector. Therefore, the model is no longer axi-symmetric, and it was changed to a two-dimensional type.

The boundary condition of constant pressure was applied across the entire portal area.

The velocity profile of the steady solution was estimated to exceed the Reynolds number for laminar flow. Therefore, a turbulent model was used. Furthermore, the mesh was modified to provide finer meshing in the near wall region where the velocities and the velocity gradients were higher than in previous models. These modifications increased the iterations required for convergence.

Figure 41 shows the mesh created for Case 6a, which simulated the mine with a 10-m long, large-diameter (4 m) culvert closure. The mesh for Cases 4 and 5 is similar, but without the culvert. The mine air is surrounded on three sides by a 2-m thick layer of rock. Beyond 2 m, the rock temperature was assumed to be constant, 283 K (49.7 °F).

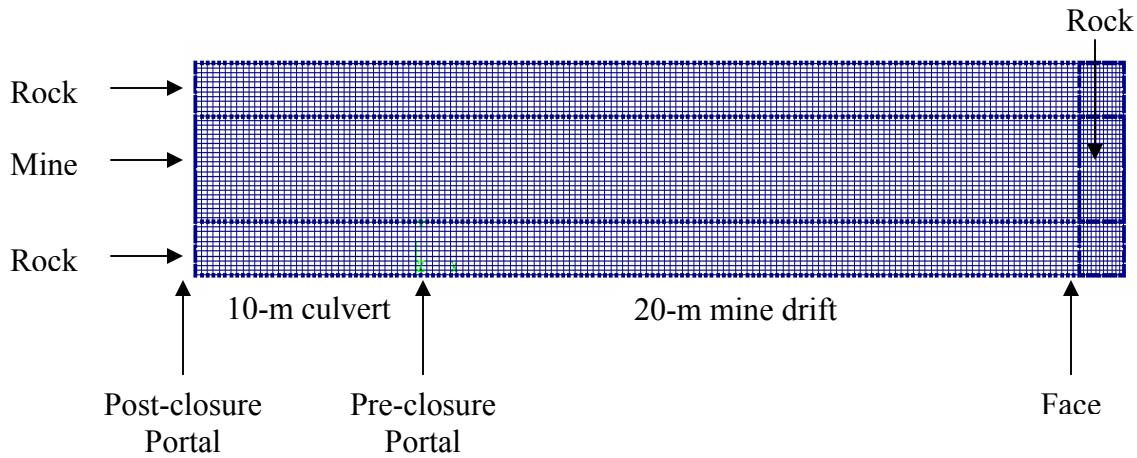


Figure 41. Mesh Created with CFD GEOM for Case 6a.

Figure 42 shows the temperature profile for the inclined, simulated mine in Case 4 where the surface air is 275 K (35.3 °F) and the mine rock temperature is 283 K (49.7 °F). The figure is skewed to depict the six degree incline. The model was not actually skewed, but was inclined with lines intersecting perpendicularly.

When this case runs to an equilibrium state, convection from the surface cools the mine air from its initial value of 283 K (49.7 °F) to 275 K (35.3 °F) near the portal and 279 K (42.5 °F) near the face. As a result, heat is conducted from the rock into the mine air and the rock temperature varies from 283 K (49.7 °F), 2 m into the rock, to 278 K (40.7 °F) near the portal and 281 K (46.1 °F) near the face.

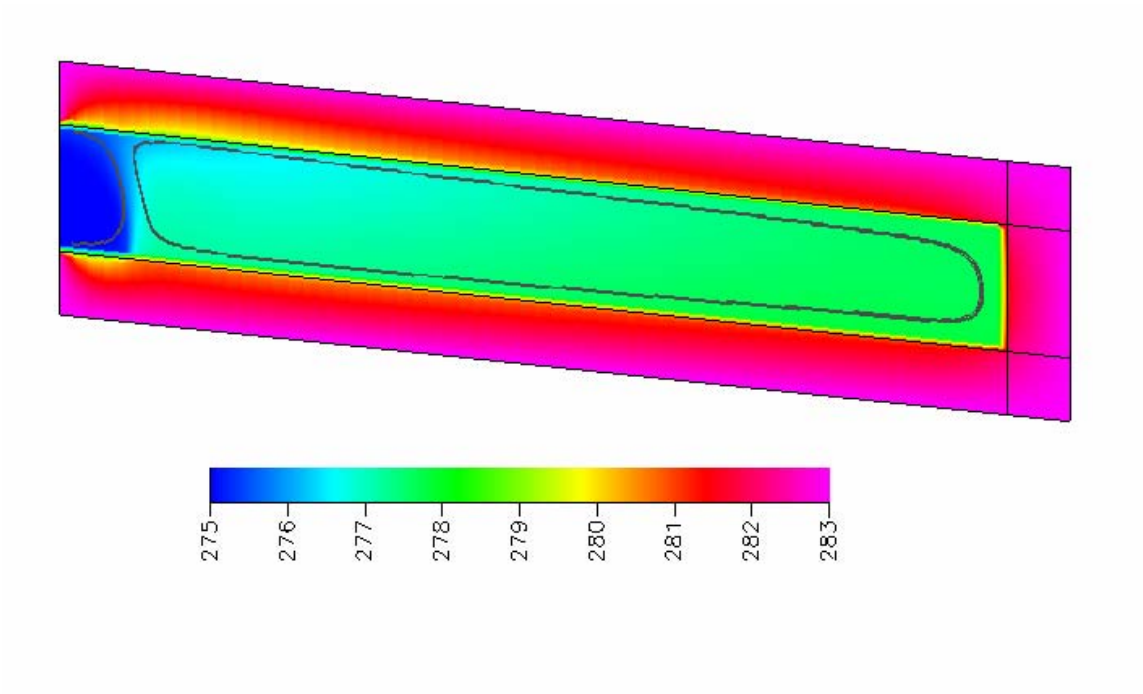


Figure 42. Simulated Mine Temperature (K) Profile for Case 4.

The temperature variations caused by convection and conduction create airflow as the warmer air rises and flows out of the upper portion of the inclined portal.

Figure 43 shows the resulting U profile, the air velocity in the x direction, and velocities are highest near the floor (0.6 m/s, 120 fpm) and roof (- 1.1 m/s, 220 fpm) at the portal. Black streamlines in the figure show two cells. A streamline is tangent to the direction of flow at every point in the flow field. In a steady flow field, a streamline is the path taken by a particle or smoke.

The first cell, in the region near the portal, results from warmer, less-dense air rising and exiting the mine near the roof. In order to satisfy mass conservation, the incoming air causes an equal mass of cooler, denser air to enter along the floor causing a circular current flowing counter-clockwise near the portal. The temperature difference doesn't create enough energy and force to completely overcome the viscous forces deeper into the mine, so the counter-clockwise motion does not extend to the end of the mine. It decreases with depth into the mine until the stream function is zero. At this point, the counter-clockwise circular current induces a clockwise flow and forms a second cell through the remainder of the mine from friction between the two air masses. Note that the velocities in the second cell range from – 0.2 m/s (- 40 fpm) to 0.2 m/s, and are much lower than those in the first cell, which range from - 0.6 m/s (120 fpm) to 1.1 m/s (220 fpm). The mine-air cell velocities are higher (0.2 m/s) near the interface between the two cells and lower (~0 m/s) near the face.

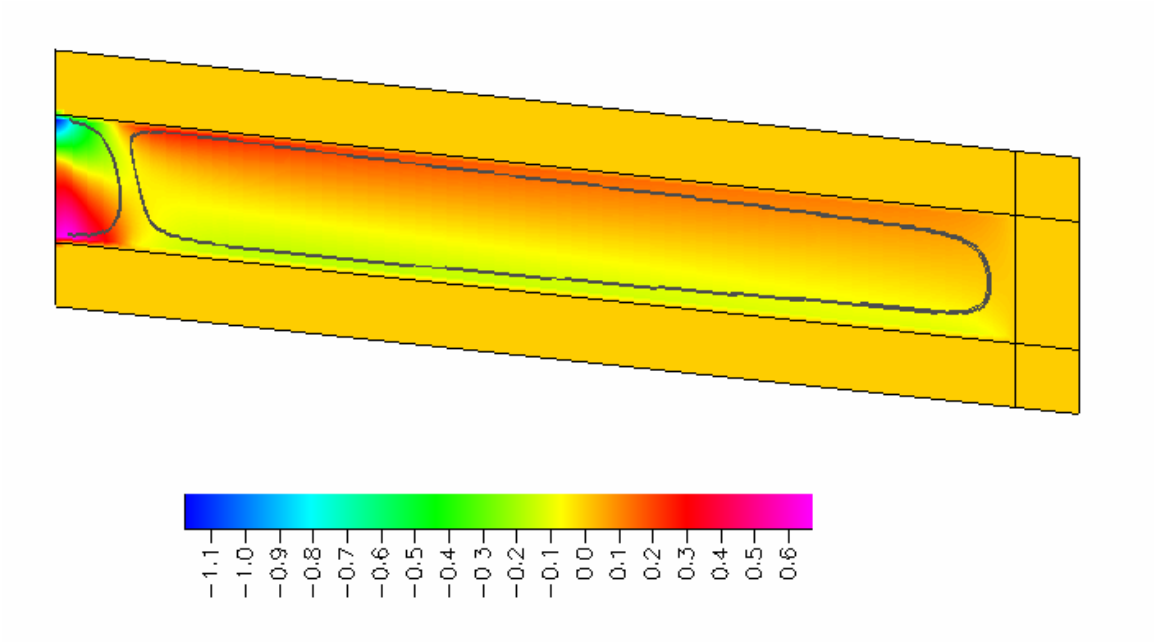


Figure 43. U (x-direction air velocity, m/s) Profile for Case 4.

Surface and mine temperatures vary with time. The software does not support time-varying simulations in a single run. For example, case four models the mine at a given point in time. Therefore Mr. Dodds ran the model twice with different temperature gradients, 3 K (5.4 °F) and 11 K (19.8 °F) lower than the 284-K mine-rock temperature. Figure 44 plots U (the x-direction component of the air movement) along the central axis of the mine (y = 4m) versus X (the distance into the mine from the portal). The two lines intersect zero at different values of X. When U is zero, the air velocity changes from positive to negative at the interface between the two convection cells. The interface point shifts farther into the mine with higher temperature differentials.

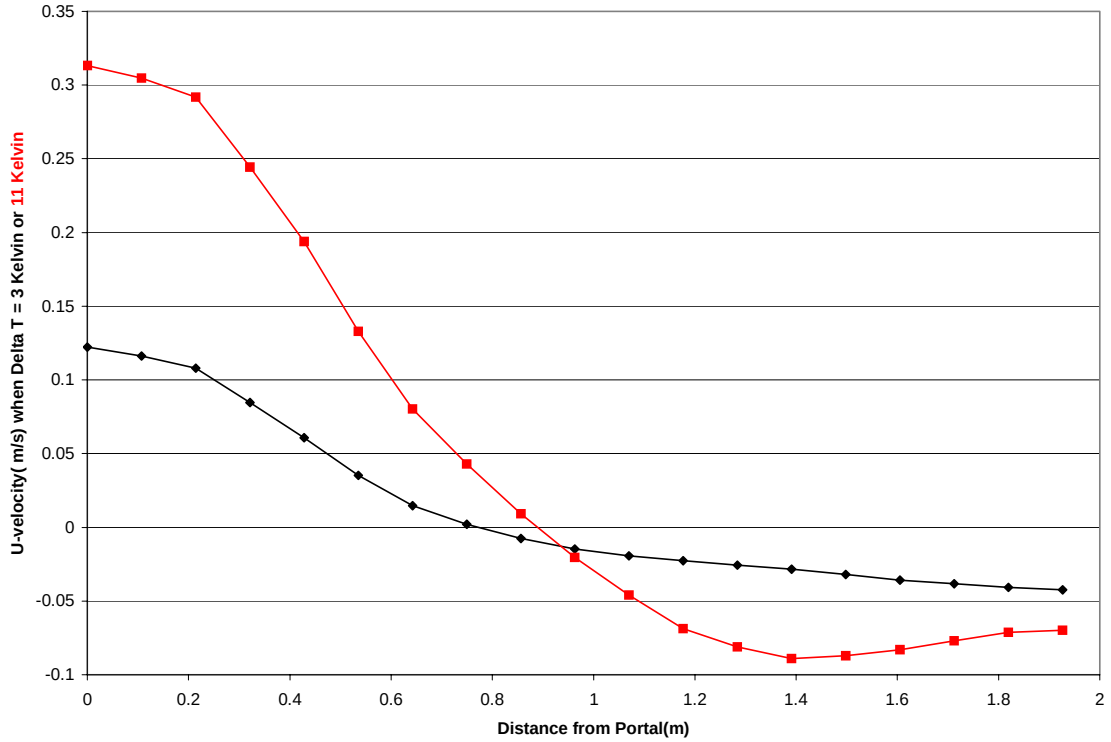


Figure 44. U (x-direction air velocity) where Surface Temperatures are 3 and 11 K Lower than Mine Rock Temperature (284 K).

If there were no gravitational gradient and hence no driving force to initiate airflow, conduction would be the only mode of heat transfer. If so, the temperature profile along the axis of the mine would show a linear change from temperature of the outside air to the temperature of the surrounding rock at the end of the mine. There is evidence of this mechanism in both the model and the logger data, but convection is the main mode of heat transfer.

Careful inspection of Figure 42 shows that the roof rock near the portal is slightly cooler than the floor. One might expect that the floor would be cooler since cool surface air is flowing into the portal along the floor. However, Figure 45 and Figure 46 show that the air velocity near the roof (0.3 m/s) is higher than that near the floor (–0.12 m/s). Perhaps the higher values near the roof are due to less dense, warmer air near the roof expanding to a larger volume, or air near the floor occupying a larger cross section. Higher velocity causes a little more heat transfer via convection and slightly cooler temperatures in the immediate roof rock.

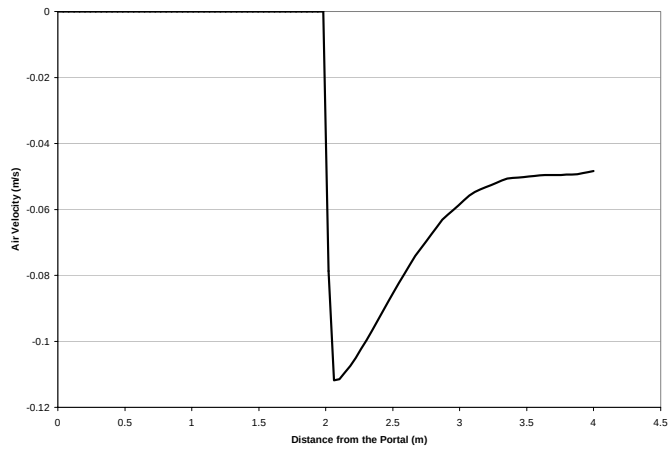


Figure 45. Air-velocity Near the Floor.

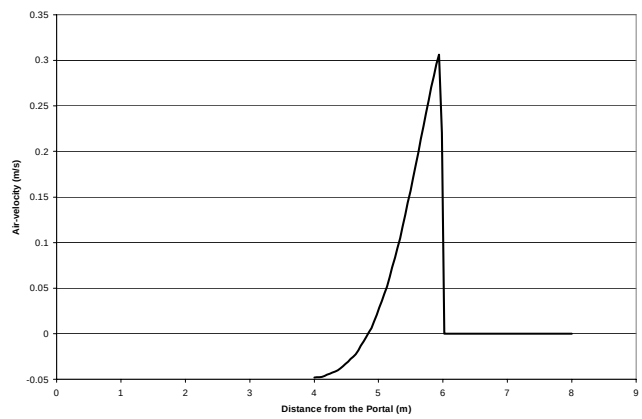


Figure 46. Air-velocity Near the Roof.

Figure 45 and Figure 46 show the no-slip boundary condition at the rock-air interface. The velocities reach a maximum near the interface and are zero at the interface to meet this condition. The mesh has finer resolution near the interface.

Figure 47 shows the temperature at various heights and locations when the surface-air temperature is lower than the mine-temperature. At the portal (x = 0), the isothermal boundary condition at the rock-air interface does not allow the temperature to vary with height except within 2 m of the interface. At 15 m from the portal, the temperature varies linearly with height from warm rock-air interface to the cooler center of the mine. This is the expected result of a steady-state heat-transfer problem with conduction as the exclusive heat-transfer mechanism.

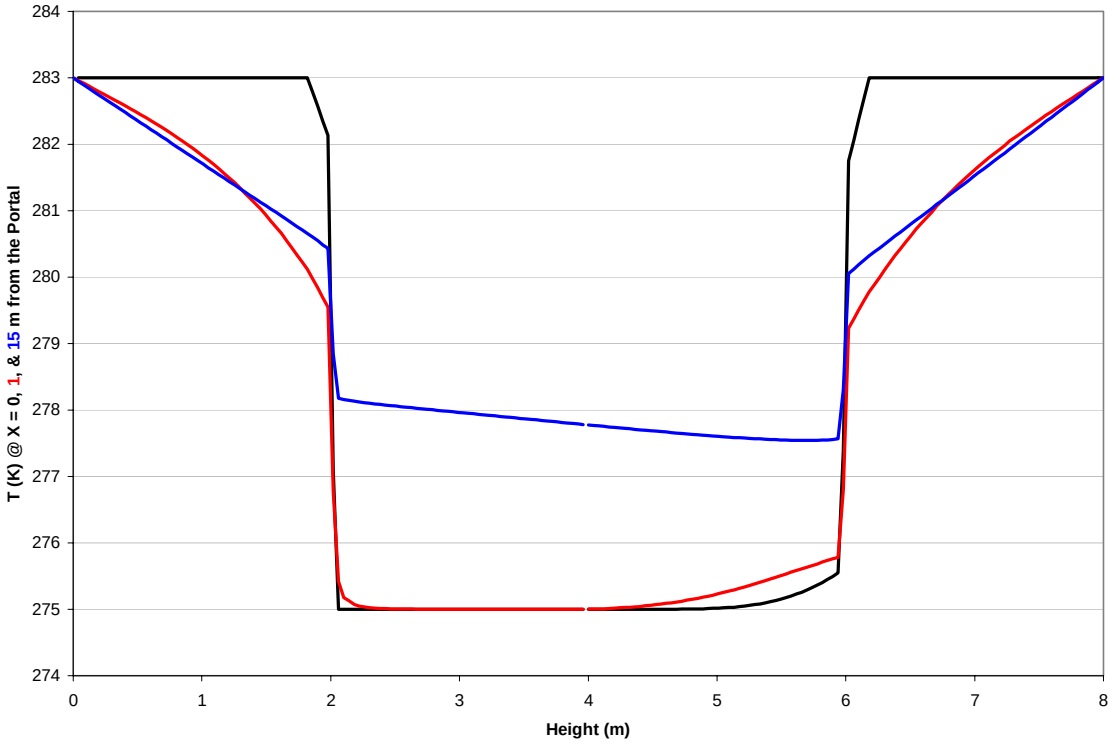


Figure 47. Temperature (K) Versus Height at x = 0, 1, and 15 m from the Portal.

The fifth case compares temperatures calculated using CFD-ACE to the measured temperatures inside the mine. A measured surface cycle was input to the model in a sequence of runs. Figure 48 shows the 24-hr data segment. The temperature cycle was centered close to the MAST (mean average surface temperature).

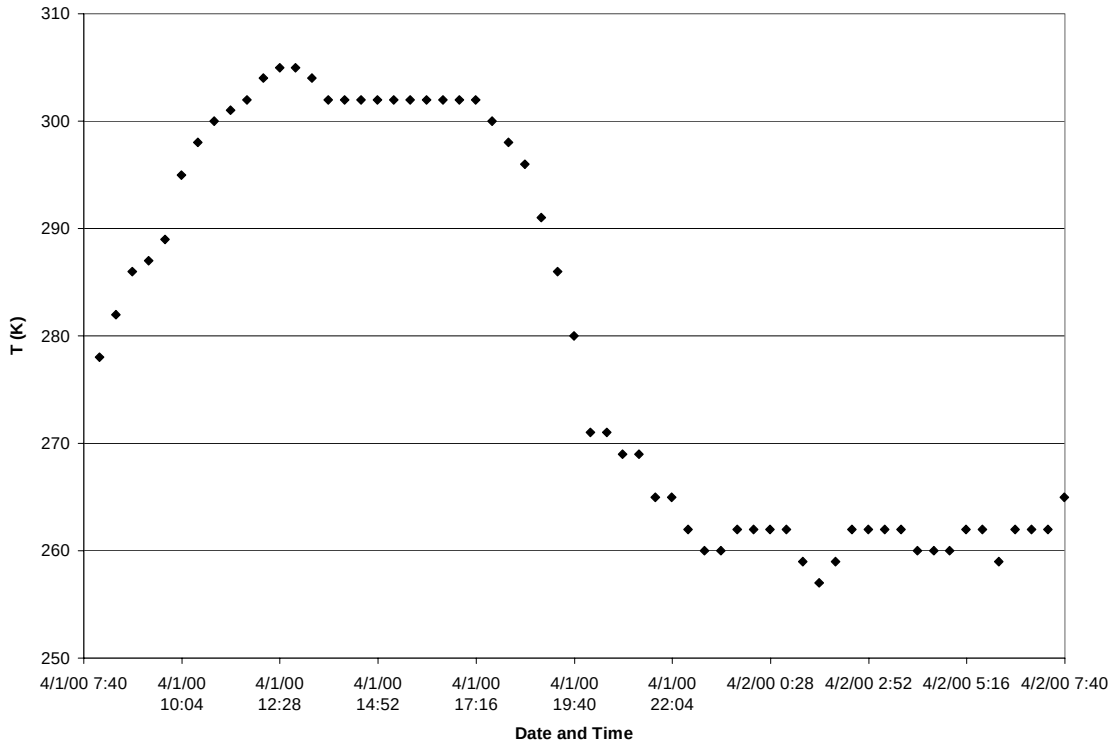


Figure 48. Surface (Logger 59-5) Data, 4/1/00 and 4/2/00.

In case 5a, the model again solves for turbulent flow and heat transfer. The model is two-dimensional and non-axisymmetric. The time dependence is, however, transient using an Euler or first order approximation. The gravity vector and the slope of the model are the same as in Case 4 and the Boussinesq approximation is used for the buoyancy force with a reference temperature of 284 K (51.5 °F) and a thermal expansion coefficient of 1/284 or 0.0035 $K^{-1}$. For the turbulence solver, the K-ε model was used with a turbulent Prandtl number of 0.9. The rock and the air have the same properties as those assigned in the fourth case. The boundary conditions are the same as those for the fourth case (the x and y direction velocities are set to zero at the walls with a constant temperature of 284 K and a pressure of zero at the outlet) except there is a temperature profile in time imposed on the opening of the mine as shown in Figure 48, and the kinetic energy and the dissipation rate are set to zero at the outlet. For the initial conditions, the x and y direction velocities and the pressure equal zero, temperature equals 284 K (51.5 °F), and the kinetic energy and dissipation rate equal zero. Each step of the simulation runs for a maximum of two thousand iterations with a convergence criterion of all residuals being less than $10^{-7}$ or with any residual reaching the minimum of $10^{-18}$. The first simulation used 24 hrs of data, with 1-hr intervals (the logger sampling interval was 24 min).

This simulation produced a flow field similar to that predicted by the model of the fourth case when the surface temperature is lower than the mine temperature. A weak, localized, reversed flow occurs when the temperature outside is greater than the

temperature inside the mine. The interface is nearly vertical and there is a small amount of air in the mine that is higher than a small amount of the air outside the mine as shown in Figure 49. The CFD program had difficulty converging in this situation.

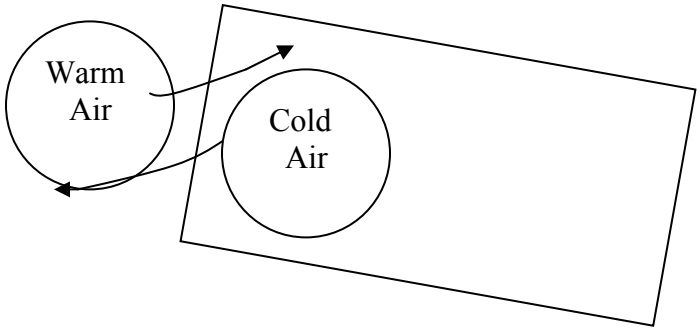


Figure 49. Airflow When Surface Air is Warmer than Mine Air.

In case 5b, the time interval was changed to 24 min to match that of the logger, and the data set length was reduced to 6 hr. A 6-hr data set captures the important features and saves computation time. The outside facing wall above the opening to the mine has the same temperature profile in time as the opening to better simulate the actual mine. This simulation produced two convection cells. The flow direction in the cells reversed when the surface temperature cycled from cooler to warmer than the mine temperature.

Figure 50 through Figure 56 show the stream functions and the velocity and temperature profiles for the first four time steps, respectively, and the last time step of the simulation. The airflow near the entrance of the mine is counter-clockwise during the first two time steps and clockwise in the subsequent time steps as the surface air temperature rises above that of the inside air temperature.

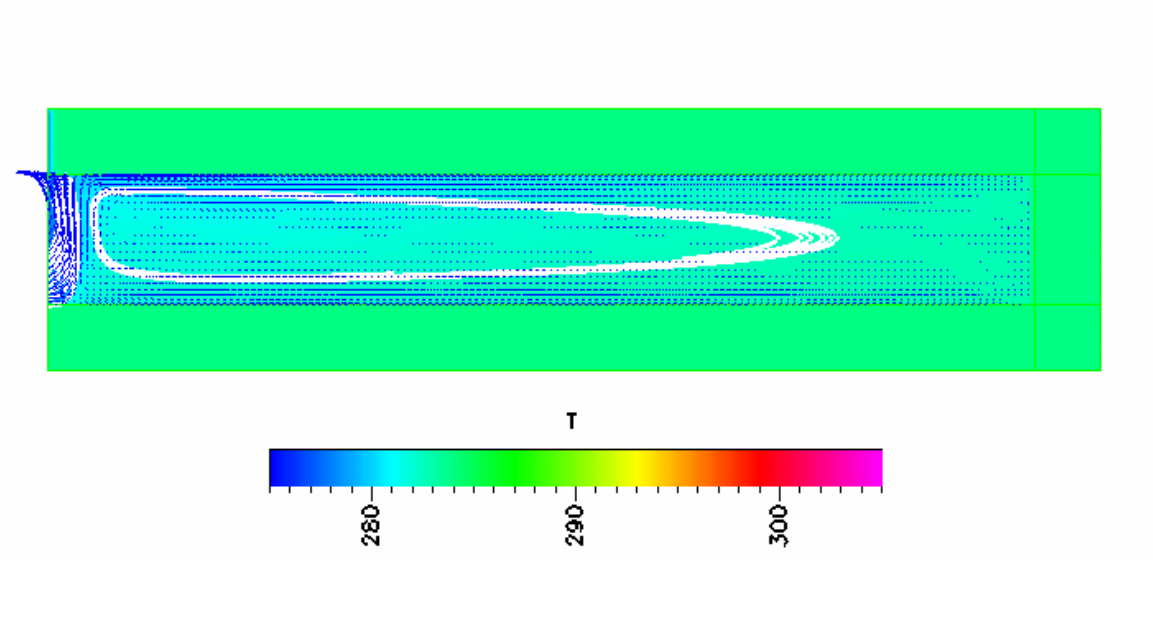


Figure 50. Profile of the Stream Function ($m^3/s/m$) and Temperature (K) for Case 5b at t = 20 min. Height = 4 m. Length = 30 m.

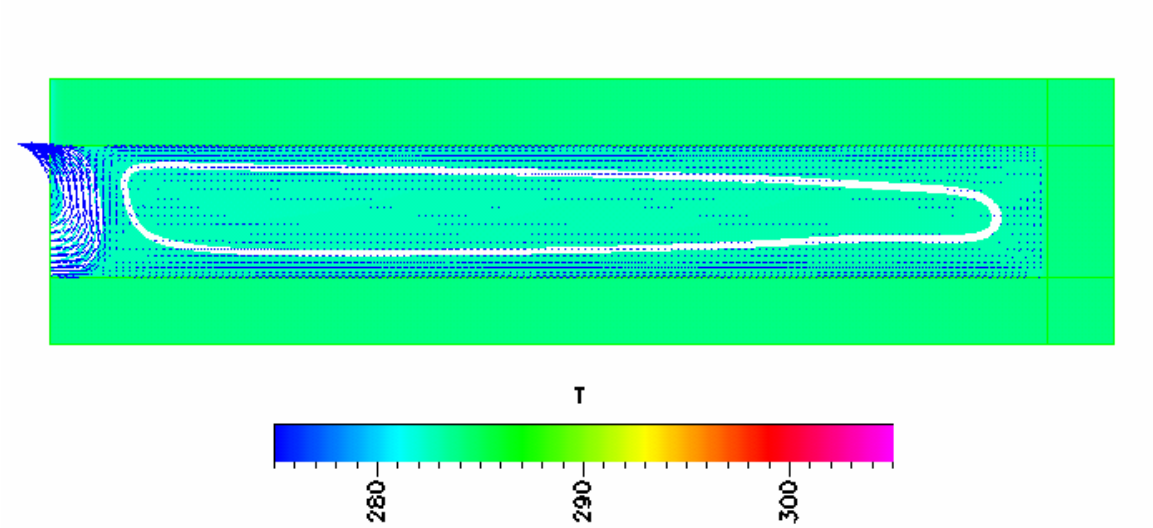


Figure 51. Profile of the Stream Function ($m^3/s/m$) and Temperature (K) for Case 5b at t = 40 min. Height = 4 m. Length = 30 m.

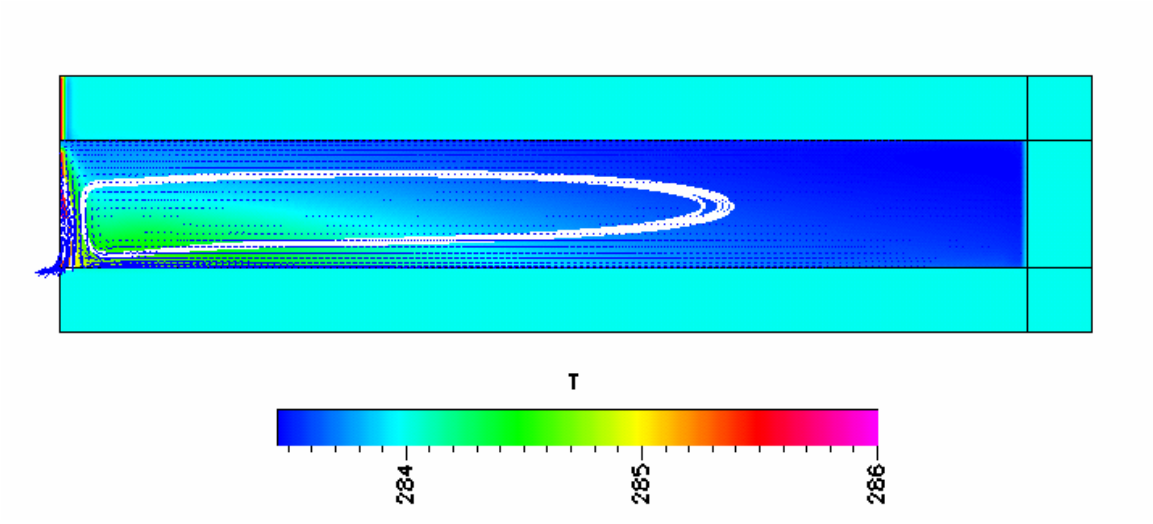


Figure 52. Profile of the Stream Function ($m^3/s/m$) and Temperature (K) for Case 5b at t = 1 hr. Height = 4 m. Length = 30 m.

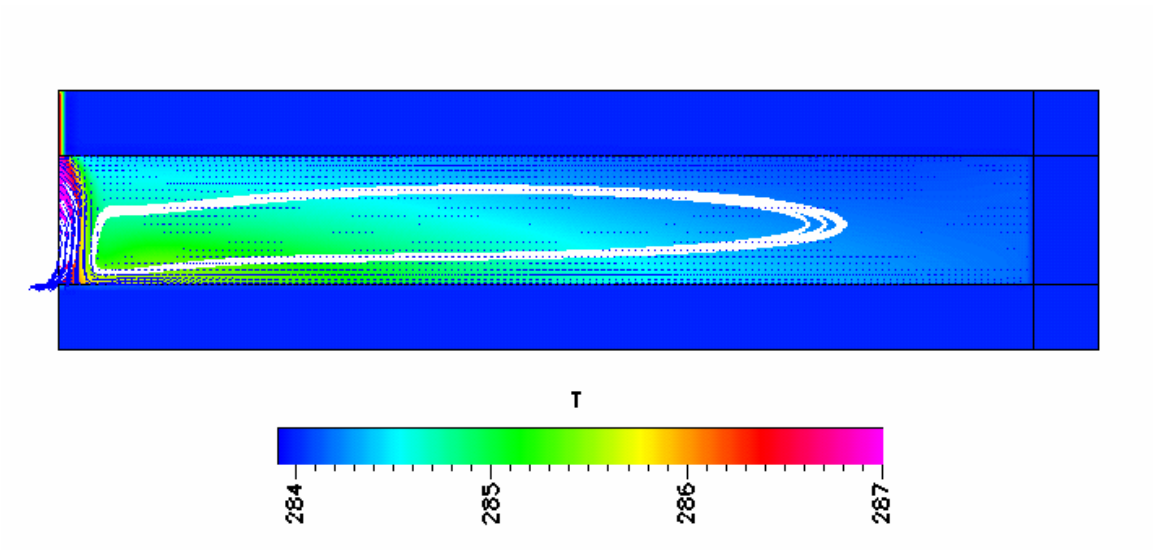


Figure 53. Profile of the Stream Function ($m^3/s/m$ ) and Temperature (K) for Case 5b, at t = 1 hr 20 min.

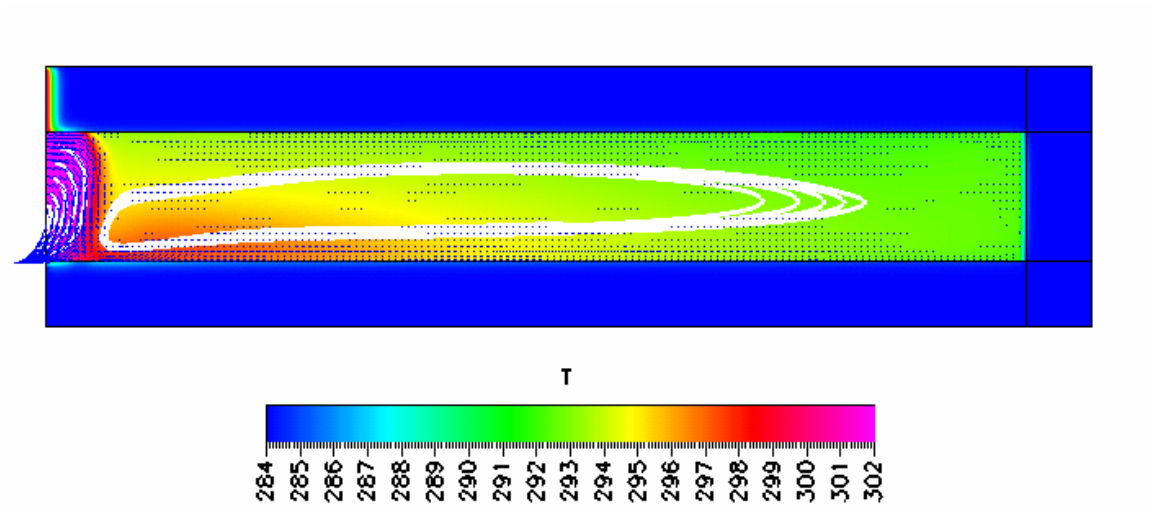


Figure 54. Profile of the Stream Function ($m^3/s/m$) and Temperature (K) for Case 5b, at t = 3 hr 20 min.

Residual values showed that the solver does not converge as the surface air transitions to a temperature warmer than that of the air inside the mine because the flow is too weak.

Figure 55 shows the mine temperature at x = 2 m at different heights in the mine as time increases over the first four and the last time steps. 0-2 m is the rock below the mine, 2-6 m is the mine opening and 6-8 m is the rock above the mine. Note the effect of the isothermal boundary condition set for the rock-air interface.

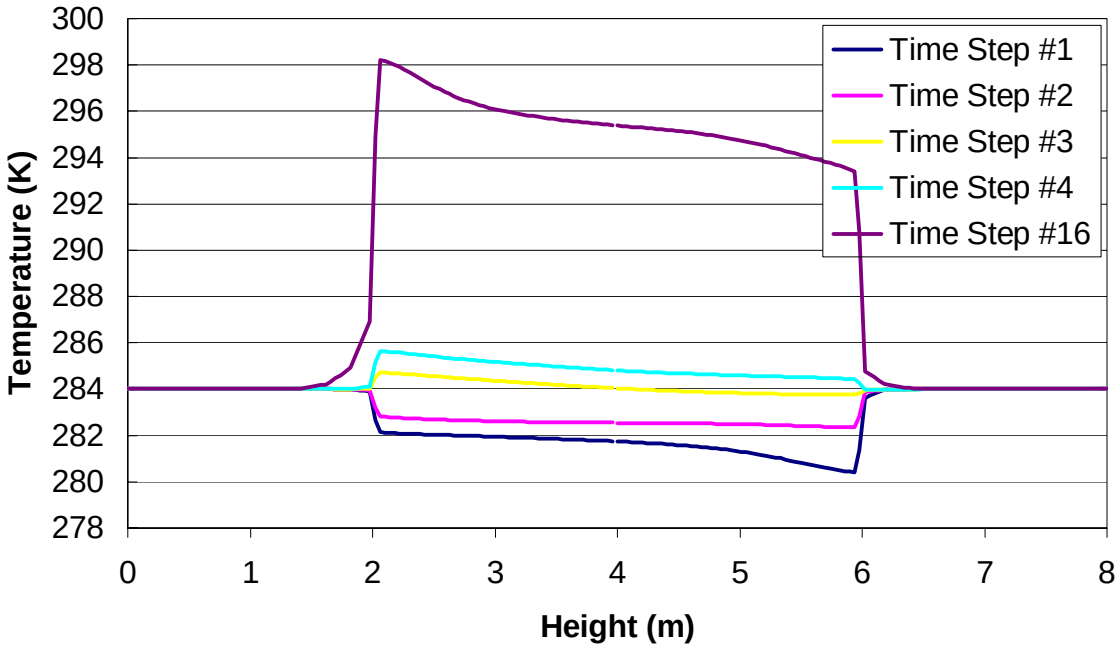


Figure 55. Line Plots of Temperature at Various Heights and Increasing Time Intervals at x = 2 m for Case 5b.

Figure 56 shows the same information as Figure 55, but deeper in the mine at x = 15 m where the airflows are smaller.

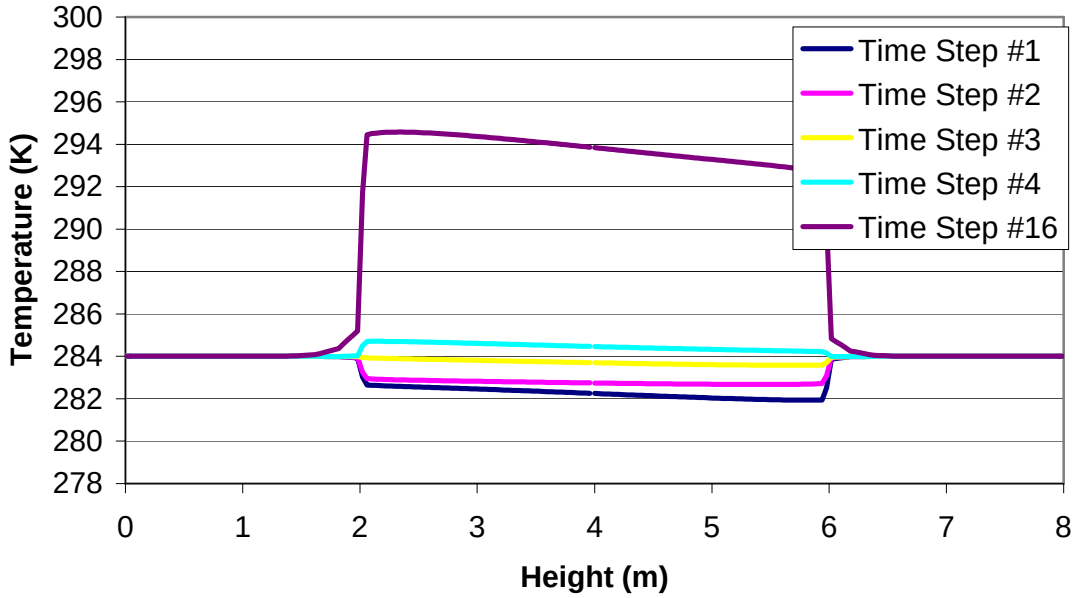


Figure 56. Line Plots of Temperature at Various Heights and Increasing Time Intervals at x = 15 m for Case 5b.

Next, we investigated whether the CFD model could accurately predict the temperatures within the mines given the temperatures outside of the mines. Figure 57 plots temperatures from five different data loggers during the same period as Figure 48. Table 10 presents measurement distances from the portals. Temperatures produced by the CFD model are plotted at x = 8 m and x = 28 m. The model and mine temperatures cover similar ranges, but the mine 31 and 59 temperatures are attenuated more that those predicted by the model because the model had a simpler structure than mines 31 and 59. The simulated mine most closely resembles mine 65. Logger 65-3 data shows a sinusoid that is attenuated more than the prediction because logger 65-3 is 42 m from the portal. The model data shows more attenuation at X = 28 m than at X = 8m.

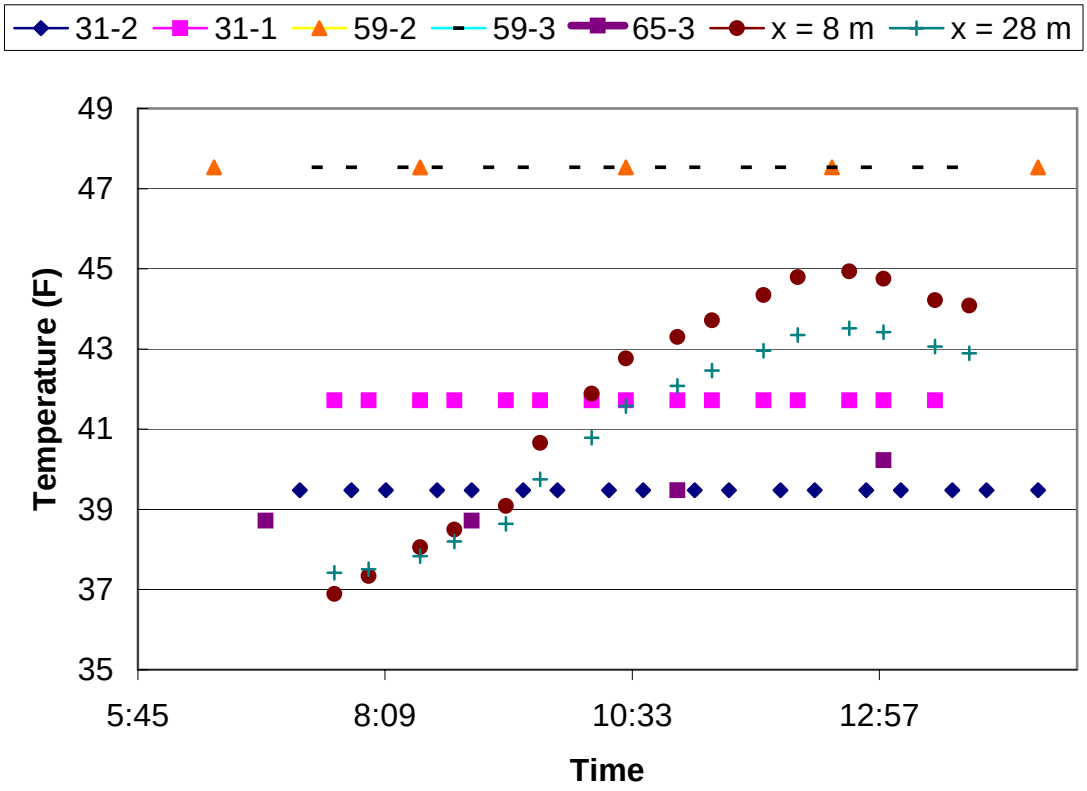


Figure 57. Comparison between Temperatures Predicted by CFD and Measured Temperatures.

Table 10. Distance from Measurement Locations to Portal

| Logger | Dist from Portal (m) |
|---|---|
| 31-1 | 28 |
| 31-2 | 11 |
| 59-1 | 86 |
| 59-2 | 25 |
| 59-3 | 41 |
| 59-4 | 18 |
| 65-2 | 17 |
| 65-3 | 42 |

Next, we investigated the time step for the heat transfer processes. Figure 58 through Figure 61 present the results. The figures display only time steps 1, 2, 3, and 8 as the changes in the output are insignificant after the third time step. The figures show that one hour is required for surface effects to be completely realized in this particular instance of temperature gradient. Velocities did not change significantly. Although the temperature profile of the air in the mine becomes relatively constant with time, the surrounding rock is still at a higher temperature than the air in and outside of the mine. Thus, the cooler outside air enters the mine, is warmed by the rock and a counter-clockwise current is produced as the air warms, rises, and exits the mine.

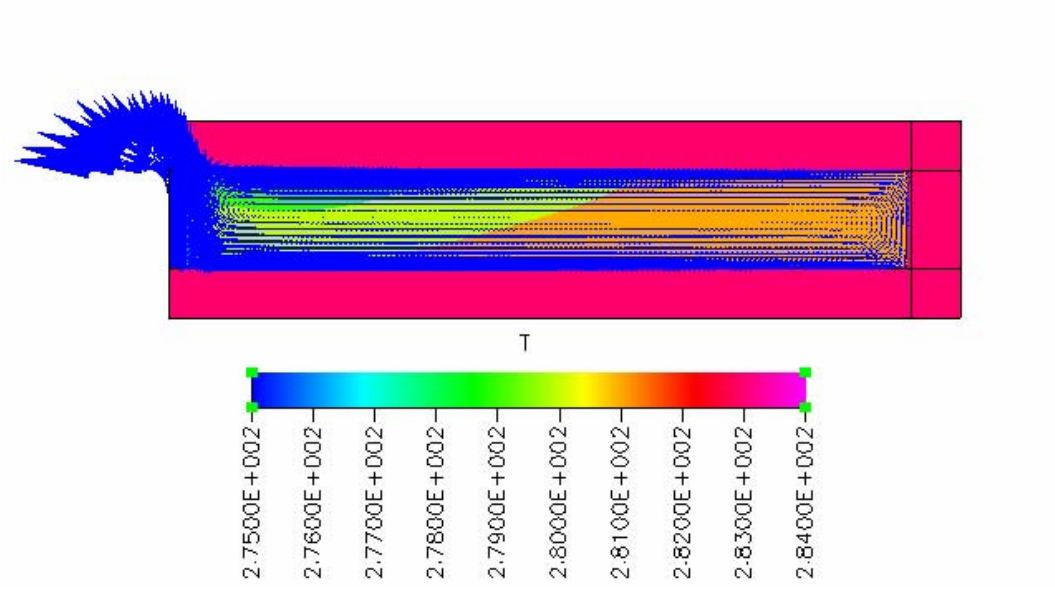


Figure 58. Profile of the Stream Function ($m^3/s/m$) and Temperature (K) for Time-Lag Analysis, Time step #1.

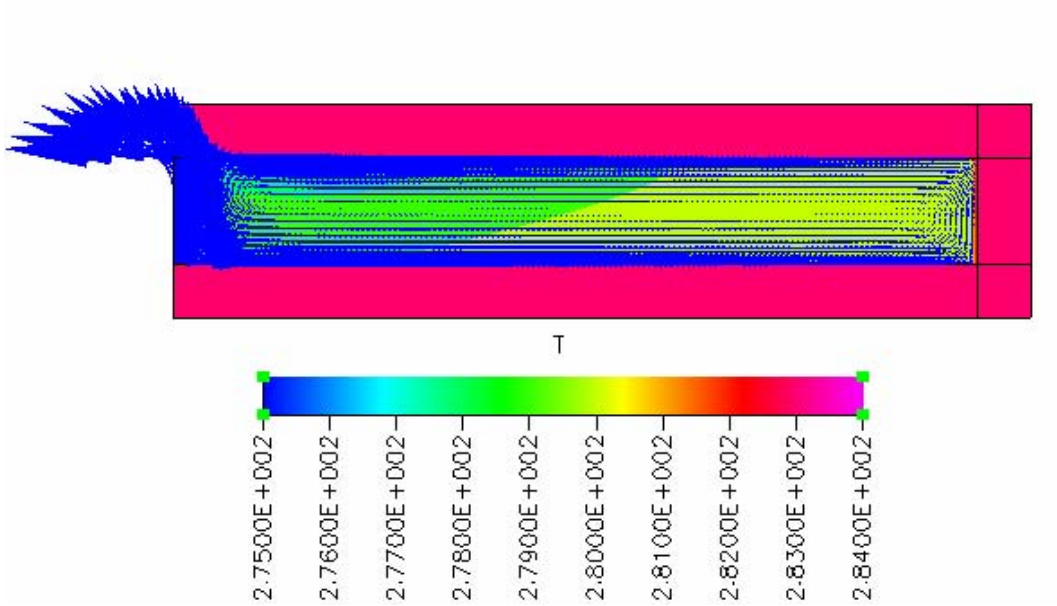


Figure 59. Profile of the Stream Function ($m^3/s/m$) and Temperature (K) for Time-Lag Analysis, Time step #2.

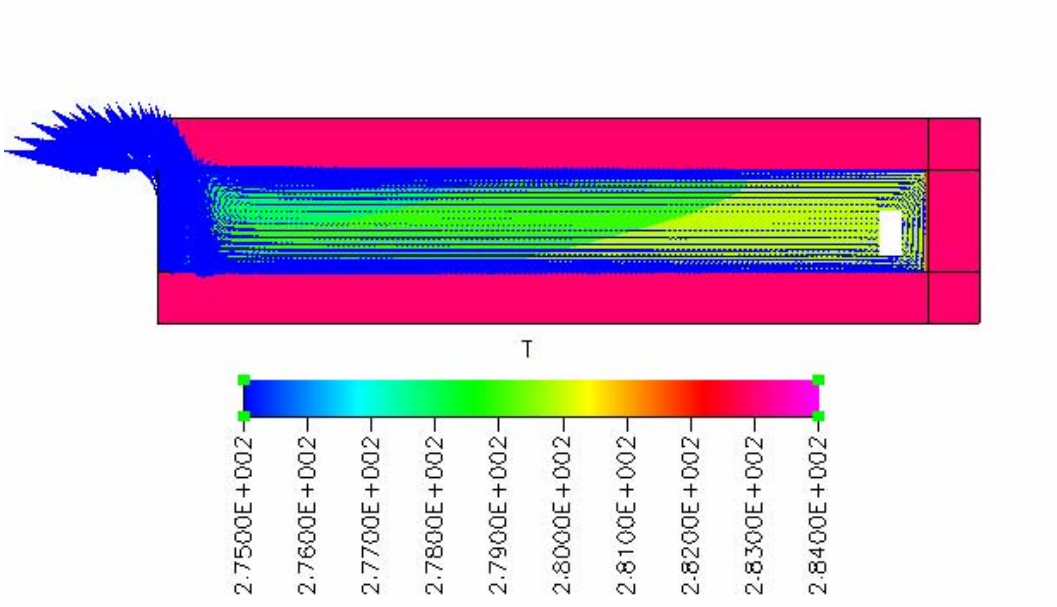


Figure 60. Profile of the Stream Function ($m^3/s/m$) and Temperature (K) for Time-Lag Analysis, Time step #3.

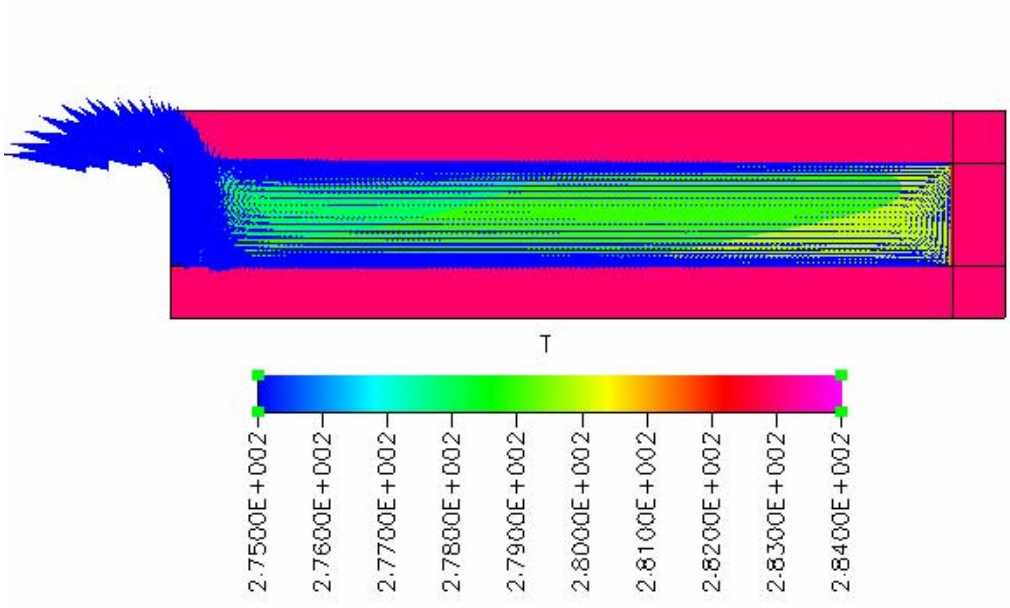


Figure 61. Profile of the Stream Function ($m^3/s/m$) and Temperature (K) for Time-Lag Analysis, Time step #8.

Case 6 analyzed the effect of remediation via a backfilled culvert and bat gate. First, a 10-m long culvert was added to Case 6a. This culvert was the same diameter (4m) and slope (six degrees) as the mine. Figure 62 shows a plot of the values of stream function and U (x-direction velocity) along the center of the mine (at y = 4 m) before and after adding the backfilled culvert to the model. The interface between the two cells occurs where the stream function is zero. The zero point on the pre-closure line occurs at about 2 m from the origin at the pre-closure portal. The zero point on the post-closure line occurs at about –8 m from the pre-closure portal, which is 2 m from the post-closure portal. Therefore the 10-m long culvert shifted the interface 10 m from the end of the mine. Consequently the microclimate in the first 20 m of the mine remained the same, but it is shifted by 10 m.

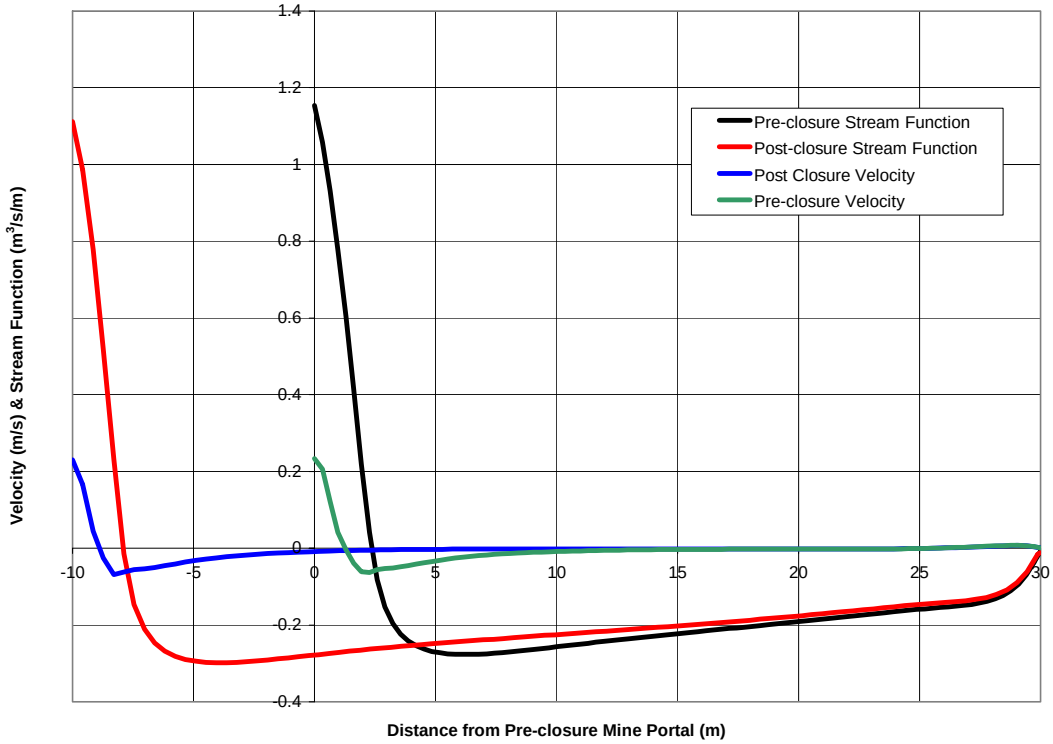


Figure 62. Comparison of U (x-direction air velocity) and Streamline Function values Pre- and Post-closure at y = 4 m.

Next, we investigated the effects of reducing mine closure costs by using a smaller diameter culvert. We reduced the diameter of the culvert by 50% to 2 m in Case 6b.

Figure 63 shows the temperature profile for Case 6b where the surface air is 275 K (35.3 °F) and the mine rock temperature is 283 K (49.7 °F). When this case runs to an equilibrium state, convection from the surface cools the mine air from its initial value of 283 K (49.7 °F) to 275 K (35.3 °F) near the portal and 280.2 K (44.7 °F) near the face. As a result, heat is conducted from the rock into the mine air and the rock temperature varies from 283 K (49.7 °F), 2 m into the rock, to 280 K (44.3 °F) near the portal and 282 K (47.9 °F) near the face.

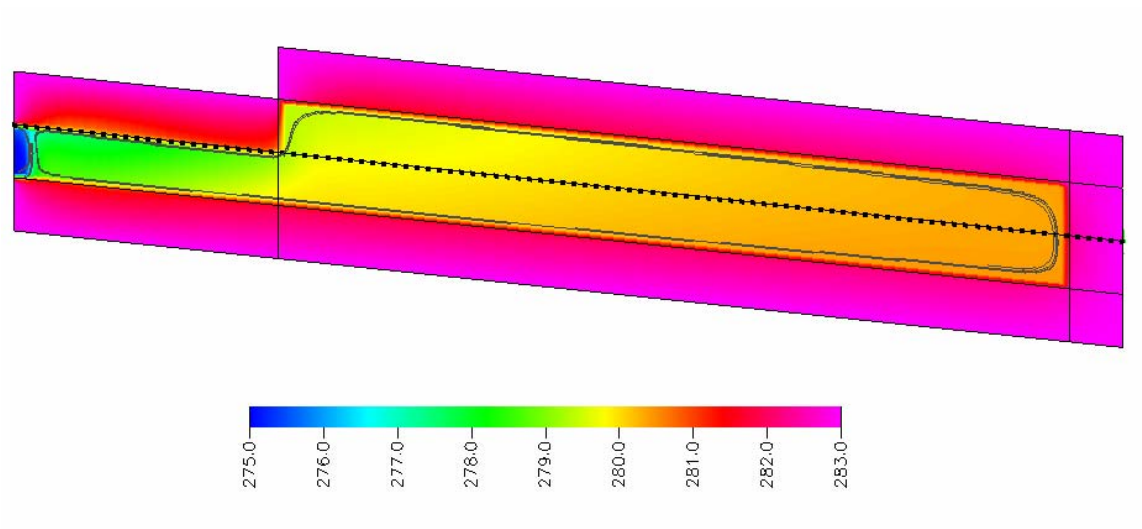


Figure 63. Temperature (K) Profile for Case 6b (Small-diameter Culvert).

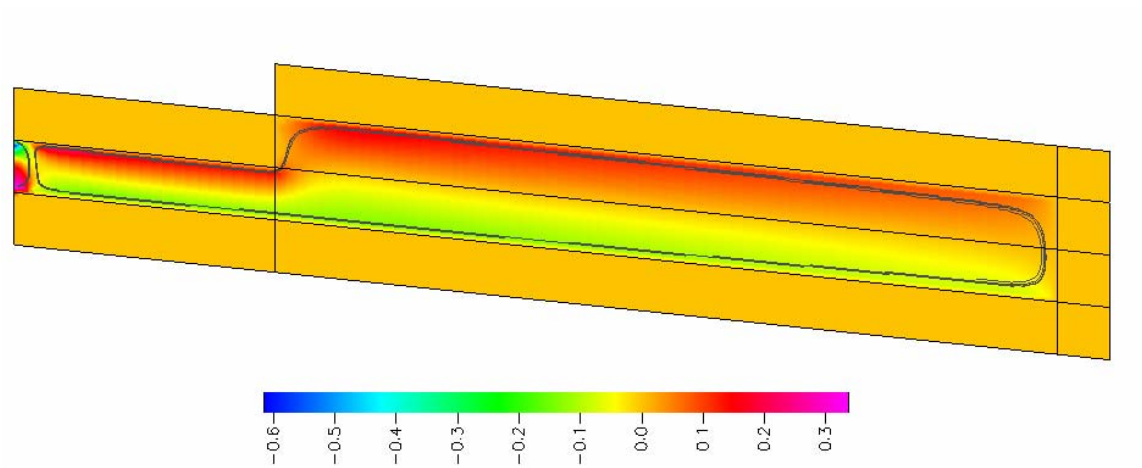


Figure 64. U (x-direction air velocity, m/s) Profile for Case 6b (Small-diameter Culvert).

Case 6c investigated the effects of installing the culvert at a steeper angle, to shorten its length and further reduce closure costs. Figure 65 shows the temperature profile for Case 6c where the surface air is 275 K (35.3 °F) and the mine rock temperature is 283 K (49.7 °F). When this case runs to an equilibrium state, convection from the surface cools the mine air from its initial value of 283 K (49.7 °F) to 275 K (35.3 °F) near the portal and 280.5 K (45.2 °F) near the face. As a result, heat is conducted from the rock into the mine air and the rock temperature varies from 283 K (49.7 °F), 2 m into the rock, to 281 K (46.1 °F) near the portal and 282 K (47.9 °F) near the face.

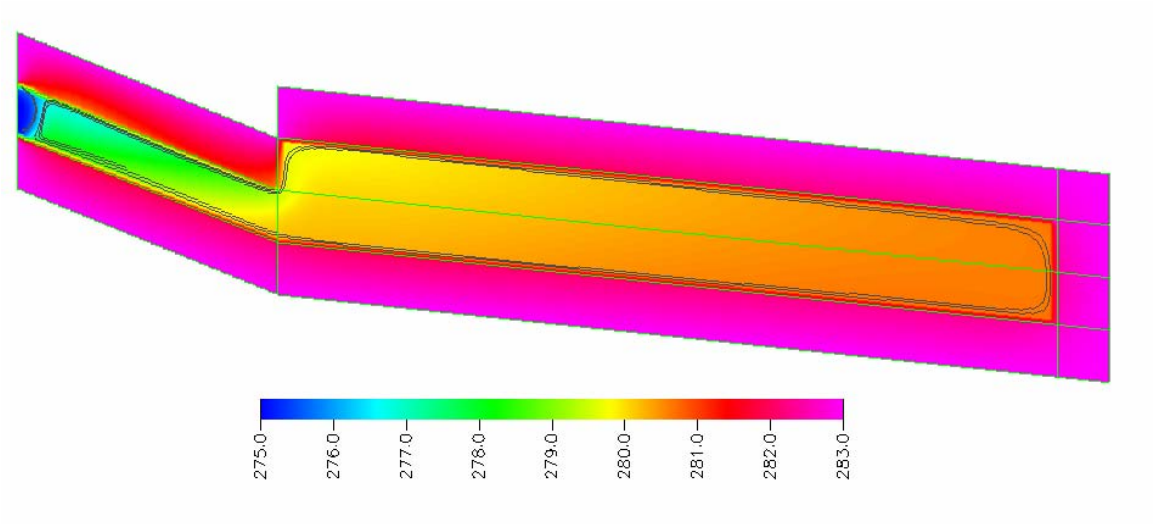


Figure 65. Temperature (K) Profile for Case 6c (Small-diameter, Inclined Culvert).

Figure 66 shows the U profile, the air velocity in the x direction, for Case 6b. Velocities are highest near the floor (0.3 m/s, 59 fpm) and roof (- 0.6 m/s, 120 fpm) at the portal. Black streamlines in the figure show that there are two cells. The velocities in the second cell range from – 0.2 m/s (- 40 fpm) to 0.2 m/s, and are much lower than those in the first cell. The second cell velocities are higher (0.2 m/s) near the interface between the two cells and lower (~0 m/s) near the face.

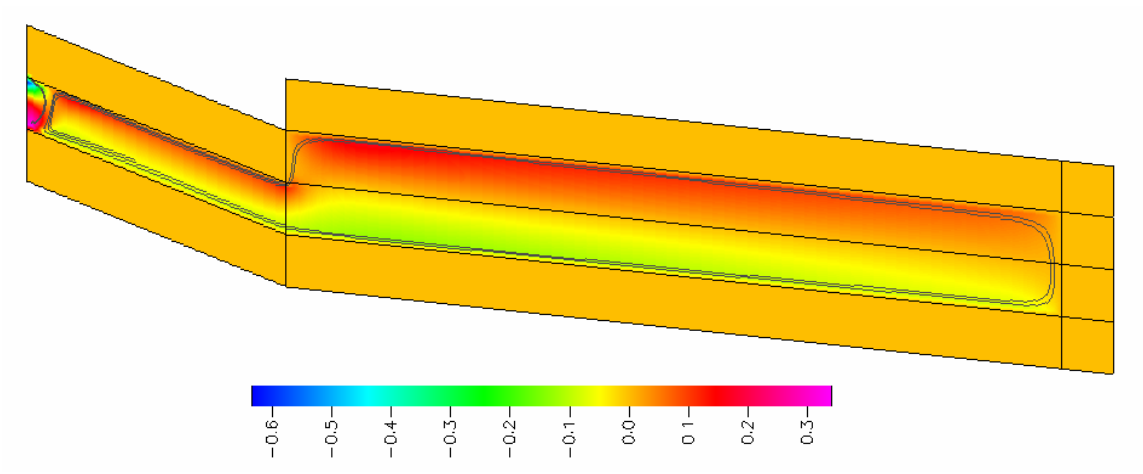


Figure 66. U (x-direction air velocity, m/s) Profile for Case 6c (Small-diameter, Inclined Culvert).

Since bats commonly hang from the roof or back, we graphed the temperature profiles at y = 6 m in Figure 67 for various closure scenarios. The temperature profile from the model of the pre-closure mine is shown in blue. The profile begins at the roof ( y = 6 m) of pre-closure portal (x = 0 m) where the surface temperature is 279 K (42.5 °F). Temperature falls to 278.2 K (41.1 °F) along the first 0.3 m of the roof line because this area is the first cell where air is flowing out of the mine along the roof. From this point, temperature rises to 279.6 K (40.2 °F) at x = 1.9m in the area between the first and second cells and drops to 278.9 K (42.4 °F) at the beginning of the second cell (x = 3.2 m). From there the temperature rises gradually to 280.9 K (46.0 °F) at x = 27.2 m approaching the intersection of the roof and the face at x = 30 m. Then there is a sharp rise through the face and into the rock until the profile reaches the temperature (283 K, 49.7 °F) set for the rock mass (2 m into the rock at x = 32 m). The scenario where a culvert which has the same diameter (4 m) and slope (6 ° ) as the mine is added shows a temperature profile (the green line) that is similar in shape, but begins at the post-closure portal (at x = -10 m). The profile for the 2-m diameter culvert, shown in red, is the same shape in the pre-closure mine area (from x = 3 m to x = 32 m); however temperature values are warmer by approximately 1 K (~2 °F). The shape of the profile is very different in the culvert area (from x = -10 m to x = 0 m) because the y = 6 datum is in the roof rock above the portal. The temperature profile for the inclined (27 °) culvert case in the pre-closure mine area (from x = 3 m to x = 32 m) is similar to that of the 6 ° culvert case. The shape of the profile in the culvert area is different, however, because the y = 6 m datum crosses from the floor of the culvert at the portal, into the roof rock, and then falls along the pre-closure mine roof.

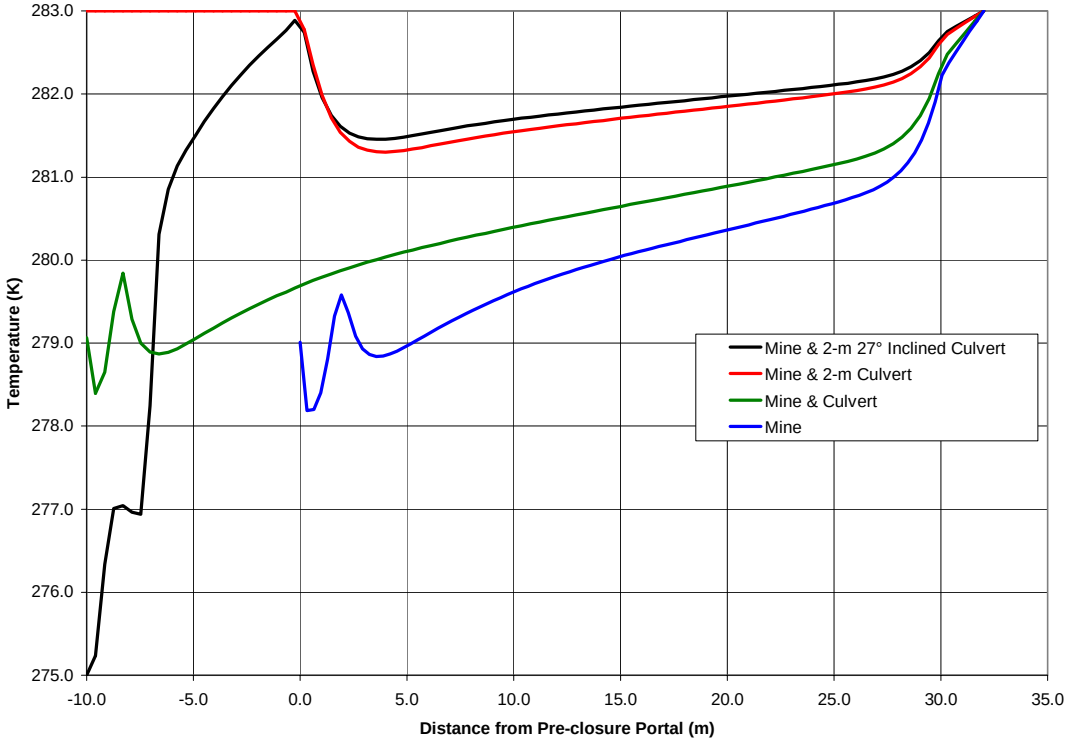


Figure 67. Comparison of Temperature Profiles Along the Mine Roof (y = 6 m) in Various Closure Scenarios.

Figure 68 compares temperature profiles for the various closure scenarios along the center of the mine (y = 4 m)

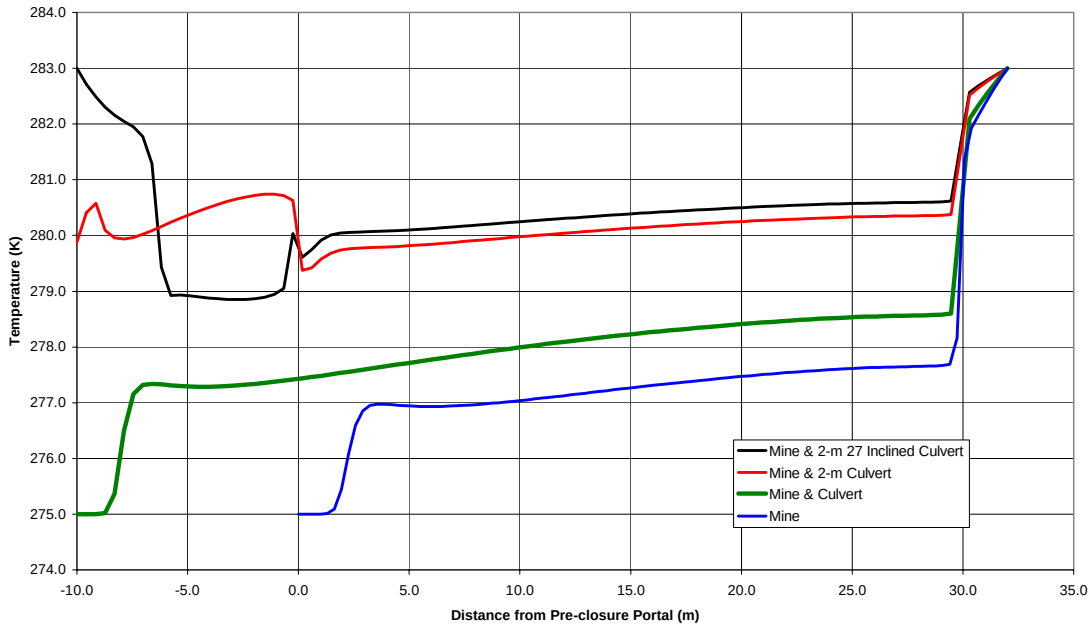


Figure 68. Comparison of Temperature Profiles Along the Center of the Mine (y = 4 m) in Various Closure Scenarios.

Figure 62 showed that U (x-direction air velocity) profile shape and magnitude did not vary when a 4-m diameter culvert was added to the mine model. Figure 69 shows the effect on U of reducing the culvert diameter to 2m. The 2-m U profile was graphed at y = 3 m and y = 4 m since y = 3 m is the center of the culvert and should be used for the culvert area (the first 10 m of the plot where x = -10 m to 0 m) and y = 4 m is the center of the mine and should be used in the mine area (x = 0 m to x = 30 m). At y = 4 m, the U values and the profile shapes for the 2-m culvert (shown in green) and 4-m culvert (shown in red) models are very similar in the mine area. In the culvert area the U profiles along the center (y = 3 m in 2-m culvert shown in dark blue and y = 4 m in the 4-m culvert shown in red) show that reducing the diameter of the culvert shortens the first cell from 1.7 m to 1.3 m and reduces the maximum U magnitudes in positive (0.23 to 0.13 m/s, 45.3 to 25.6 fpm) and negative (-.06 to -.03 m/s, -11.8 to –5.9 fpm) directions.

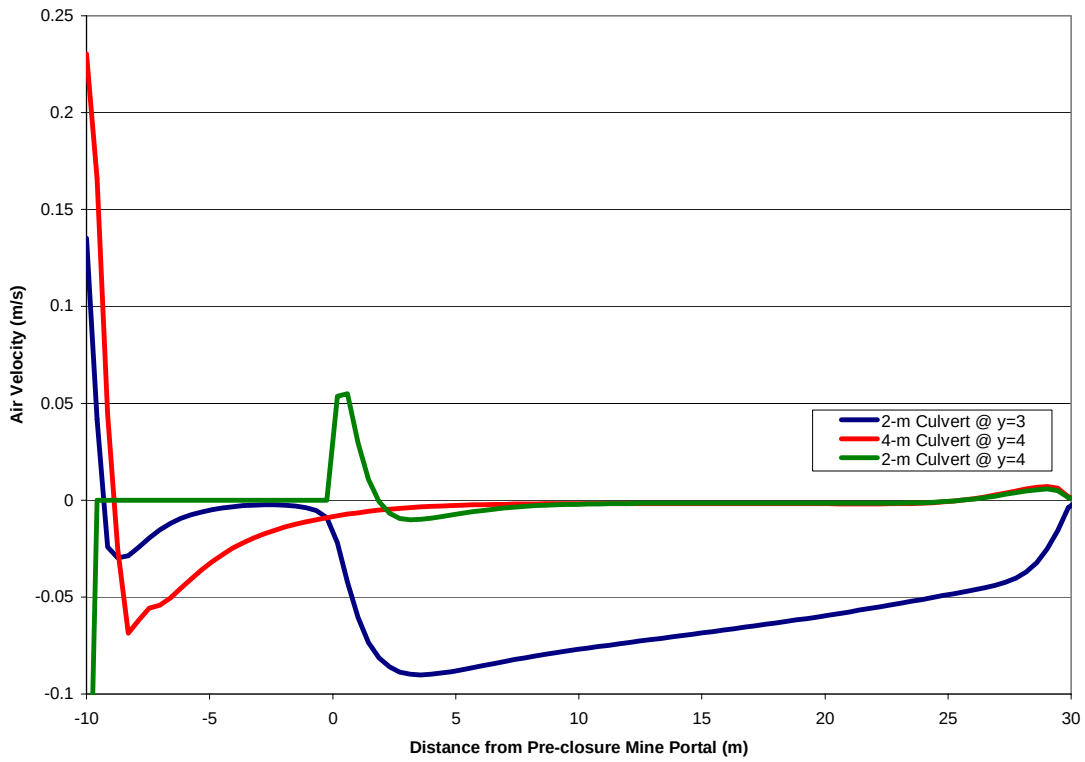


Figure 69. Comparison of U (x- direction air velocity) values for 2-m and 4-m Diameter Culvert Closure Models.

# 6.0 Air Flow

## *6.1 Introduction*

Gross air movement and high-speed flow are usually measured with a pressure or thermal sensor. The sensor may be as simple as a spring-loaded vane that is pushed aside by the flow. More accurate sensors use pitot tubes and diaphragm pressure transducers or hot wires that are cooled by the flow. The lower velocity limit for reasonably priced commercial devices is about 1 fps (60 fpm). We evaluated several low-flow transducers and found them to be very expensive (~$5,000 each) or too delicate for a mine application. Therefore, Dr. Grover developed a relatively inexpensive ultrasonic transducer that transmits and receives sound waves in opposite directions and determines the difference in transit time. A sound wave that is traveling in the direction of the airflow will move faster than a wave that is traveling against the flow.

Ultrasonic devices are inexpensive, small, sensitive, and rugged. In still air, distance can be calculated from the time of flight and the velocity of sound in the following equation:

$$L = (C)(T)$$

where:
L= distance between transmitter and receiver (ft),
C = velocity of sound = 1,125 ft/s at 20 $^{o}$C, and
T = time (s).

We set the sensors at a known distance and determined time for the two sound waves traveling in opposite directions:

$$T = L/(C)$$

If air is moving at some velocity, V, the transit time becomes:

$$T = L/( C \pm V )$$

where sign for V depends on the relative directions of flow and sound.

Our sound source and receiver are piezoelectric crystals, resonant at 40 kHz. (We tried to use a higher frequency, 216 kHz, but the crystals were not stable over long periods.) It is possible that the ultrasound signal affects the bats, but we did not research this issue.

The manufacturer supplied the transducers in a mounting that gives good coupling to the air. We aligned the two transducers on a frame, so the spacing between them, L, equaled 15 cm. The speed of sound is about 344 m/sec, so the one-way transit time in still air was:

t = (0.15 m) / (344 m/sec) = 436 μs.

To determine the velocity of the air flow, we measure the phase shift which was related to the difference in transit time, $\Delta t = t_1 - t_2$ between the two transmissions. When the flow is parallel to a line between the source and receiver, Δt was at maximum. For other directions, Δt was proportional to the cosine of the angle between the flow direction and a line between sound receiver and source. We devised a stiff mount and carefully aligned the transducers to obtain the best signal.

Δt can be used to determine air velocity, V:

$$\Delta t = t_1 - t_2 = \frac{L}{C-V} - \frac{L}{C+V} = \frac{L(C+V) - L(C-V)}{(C-V)(C+V)} = \frac{2LV}{C^2 - V^2}$$

Making the assumption that $V^2$ can be neglected in the denominator since it is much smaller than $C^2$ for low flows:

$$\Delta t = 2\ L\ V / C^2, \text{ and}$$

$$V = C^2 \bullet \Delta t / 2L$$

We measured the change in transit time of the wave by a three-step process:

1. Convert the received wave to a digital waveform. A reference digital waveform was available for the transmitted wave. The received wave was amplified and an electronic comparison circuit generated a square wave that changed state at the zero crossings of the signal.

2. Perform an exclusive-or of the received and reference waves. This produced a waveform with an average value proportional to the delay between the received wave and the reference. 0 to 5 v output signal represented a 90 ° phase shift that corresponds to a change in the transit time of 6.25 microseconds ((90/360) / 40kHz = 6.25 μs). Therefore, from the equation for V above, the sensitivity of the transducer is:

$((344\ m/s)^2\ (6.25 \times 10^{-6}\ s))/(\ (2)(0.15\ m)(5\ V) = 0.493$ mps/V or 1.618 fps/V or 97.07 fpm/V.

The waveform diagram in Figure 70 shows the phase shift for 10 fpm. The difference in transit time, Δt, for an air flow speed of 0.05 m/sec (about 10 fpm) is $(2 * 0.15\ m * 0.05\ m/sec) / 344^2\ m/sec = 0.126\ \mu s$.

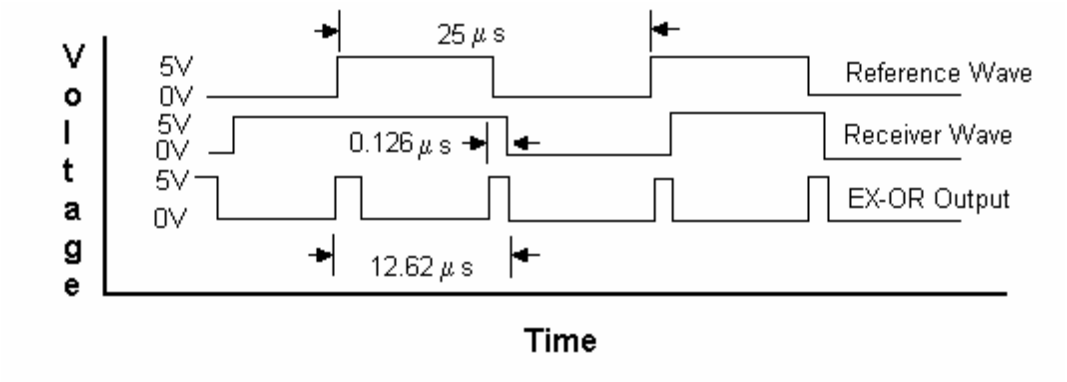


Figure 70. Airflow Transducer Waveform Diagram

3. Use a microcontroller to convert the average value to a digital number and store the number in a non-volatile electronic memory.

The schematic in Figure 71 shows the circuit that drove the sensors. Two relays convert the piezo transducers from source to receiver at 10 Hz.; the receiver becomes the source and the source becomes the receiver. So we transmitted twice for each measurement, first in one direction immediately followed by a transmission in the opposite direction.

Since relays connect each of eight pairs of transducers to the electronics, the electronics are identical for all of the transducer pairs and differences can be reliably ascribed entirely to the transducers. A transistor, coil, and capacitor circuit drives the source transducer with a high-voltage waveform at the system clock frequency. The coil and capacitor are resonant at 40 kHz. The receiver transducer signal is amplified and converted to a logic level waveform by the AC amplifier and comparator circuit. The low-pass filter smoothes the exclusive OR gate's 40-kHz pulse wave output. When the air is flowing, a 10Hz signal appears at the output whose peak-to-peak value is proportional to the air flow speed (0.1 V for 10 fpm).

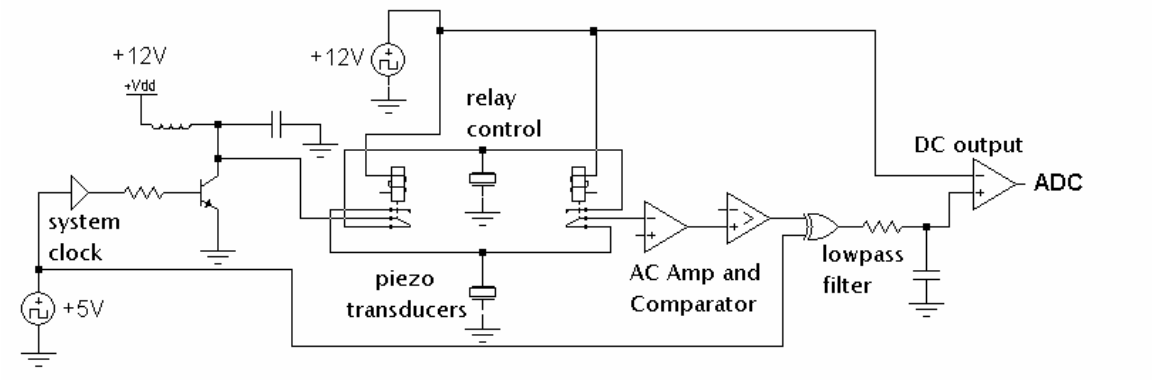


Figure 71. Simplified Circuit Schematic

Dr. Grover designed and purchased a printed circuit board that was mounted in an aluminum chassis along with a 6-V battery and the reference ultrasonic transducer pair (Figure 72). A 25-pin connector provided wiring for the remaining transducers. The chassis was not sealed. We found that relative movement of the transducers was a major error source, so they were mounted on a stiff aluminum sheet metal bracket and secured with silicone.

The circuit boards were assembled without sockets because the MC68HC811 microcontroller can be reprogrammed via the RS232 serial port. The system operates at 5 V, and MAX667 low-dropout power-supply regulators maximized the battery life. A CD4047 oscillator produced the 40 kHz transmitted square wave. A differential amplifier and a LM711 comparator squared up the waveform at the receiver. The clock used a 32768 Hz watch crystal and a CD4022 fourteen stage divider.

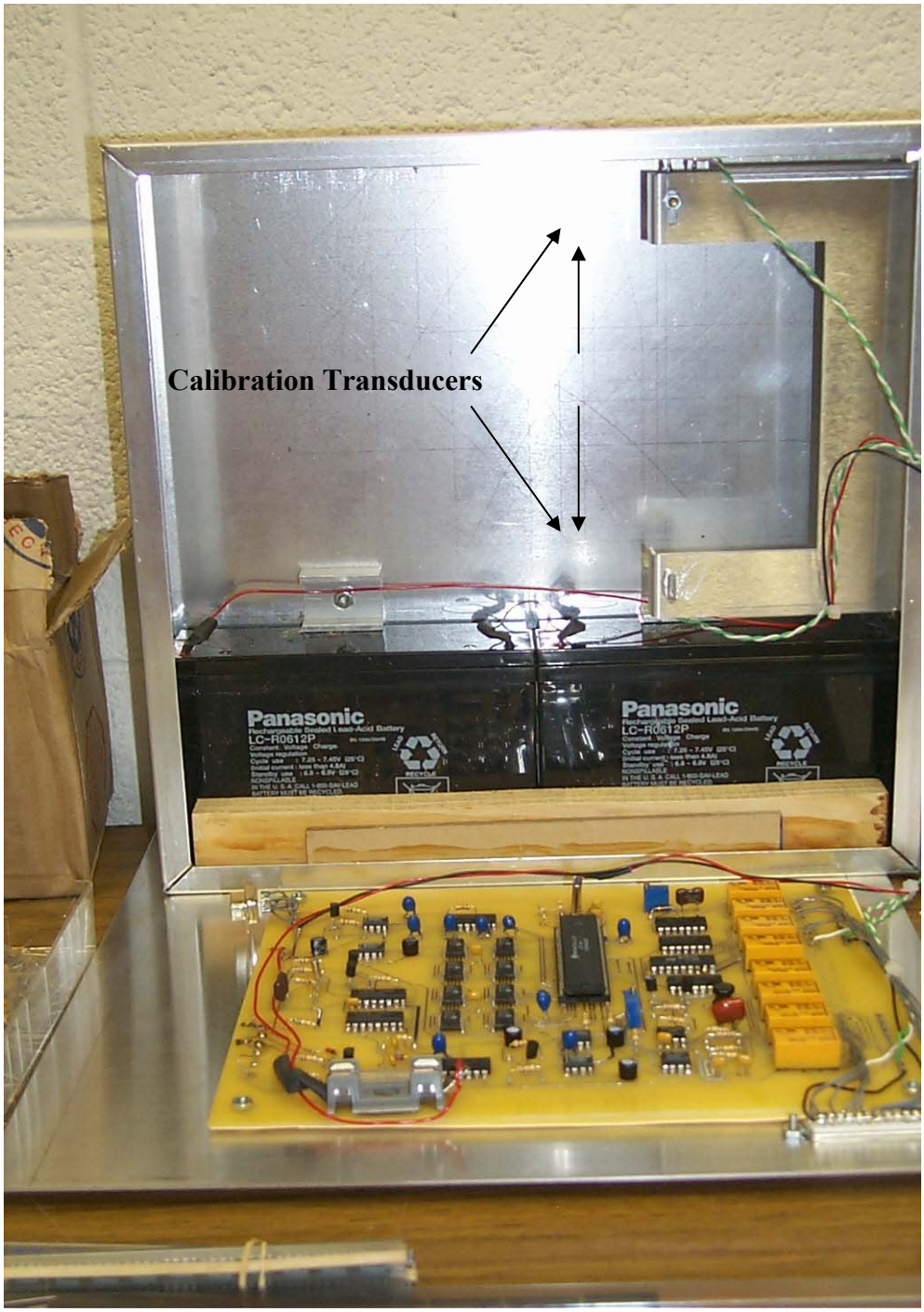


Figure 72. Photograph of Low-flow Transducer Electronics

The design accounted for the fact that the system had to operate under battery power unattended for several months in the mine during the winter when low temperatures reduced battery life and roads were impassable. The microcontroller powered off except when a measurement was being performed. 64K of local non-volatile memory saved the results of 8192 measurements.

The system was designed for automatic transfer to a personal computer. When the system was reset, the microcontroller tested a RS232 (serial port) connector for the presence of a personal computer. If the computer was present, the stored data was uploaded to the PC. If no personal computer was found at reset, the microcontroller executed its measurement sequence and shut down. It was awakened 1024 seconds later by a crystal-controlled clock in the circuit board and the measurement was repeated until the memory was filled. The uploaded data was a byte file that was converted to an ASCII text file.

We suspended the transducer brackets from five-ft high wire fencing as shown in Figure 73. We mounted two sets of transducers at three levels (near the floor, about 2.5 ft higher, and about 5 ft from the floor) by hooking the brackets into the mesh of the fence at the top, bottom and middle, and placed the electronics chassis near the fencing with the connecting cable well above the floor. Despite this precaution, rodents gnawed some cables. In addition, we placed a calibration set inside the box that houses the circuitry and batteries, as shown in Figure 72 for a total of 7 sets, or 14 transducers. One circuit board with two batteries can operate up to 8 sets. The hardware cost for the entire set up is about $300. Later, additional cabling was strung to allow us to upload data from the mine entrance.

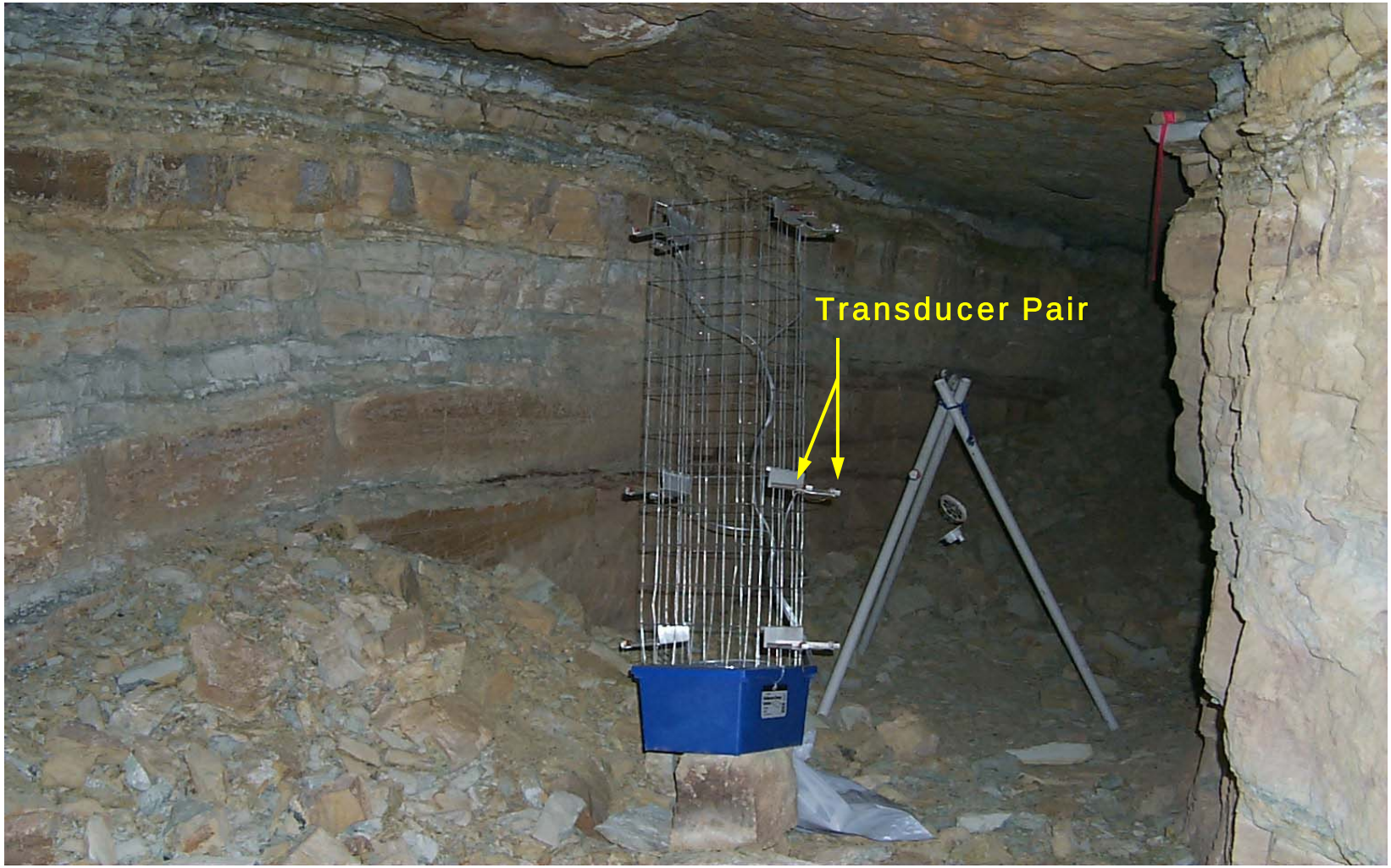


Figure 73. Low-flow Transducer 6 in Mine 31.

## *6.2 Laboratory Tests*

Figure 74 shows an air duct built to simulate the mine convective flows for laboratory testing and calibration. The duct was built from ¼-in. plexiglas with overall dimensions of 2 ft x 2 ft x 4 ft. One end panel was a plywood sheet with cutouts for 4 in. x 4 in. fans. The other end panel was porous rubber foam similar to that used in pillows. The foam allowed air to pass through easily but reduced the effects of air movement in the room. A grid of tape on one side provides a reference for smoke tube tests. Holes were drilled in the plastic sides for mounting the transducers.

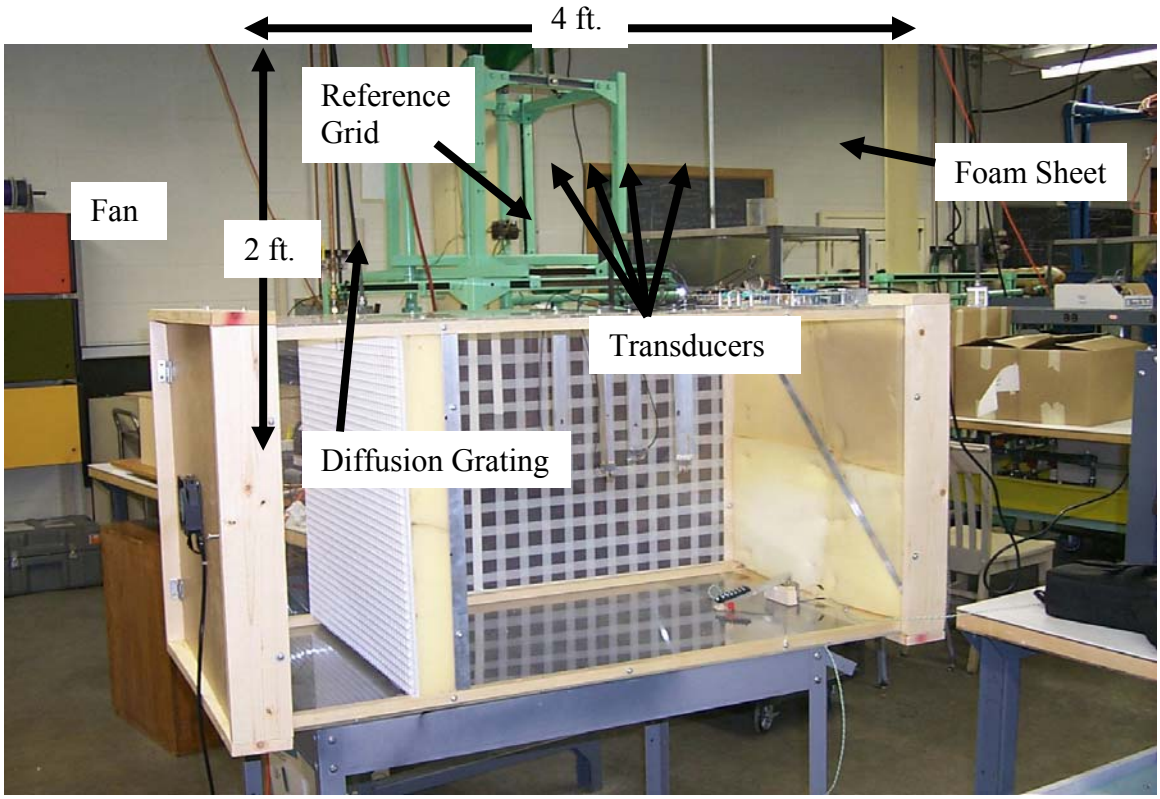


Figure 74. Low-flow Laboratory Apparatus

Airflow was started and stopped by turning the fans on and off. We covered some of the fans and part of the foam to vary the flow rate. The duct was calibrated with smoke tubes

and a stopwatch. The transducer and instrumentation shown in Figure 75 were used to compare smoke-tube and ultrasonic-sensor results.

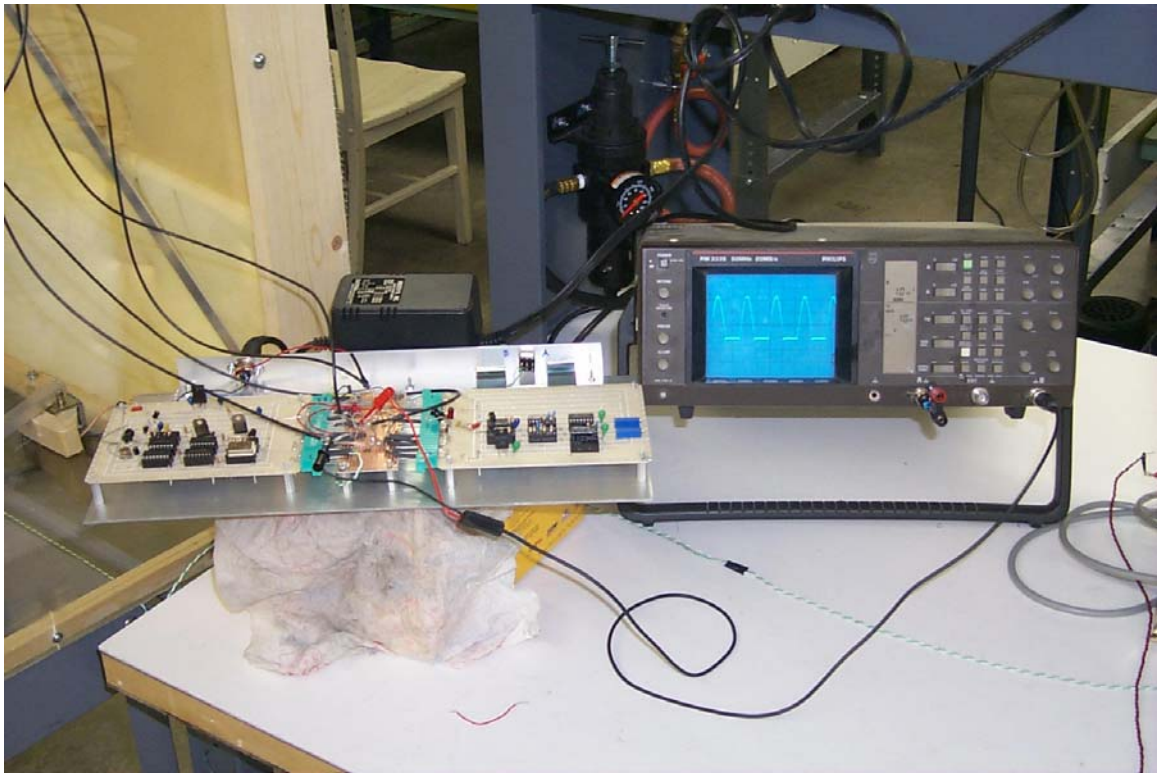

Figure 75. Laboratory Air-duct Test Instrumentation

The airflow sensor got a zero flow calibration at the start of every experiment with the fans off. The results of a 'Wind Tunnel Test' are shown in Figure 76. For this experiment, the fans were off at the start and turned on at 200 s. There are two sensors, A and B, with opposite orientations and their output responds with the opposite sign to the increase in airflow. They have different zero offsets, so each data set was corrected accordingly. We plotted the results with corresponding opposite signs to show that the two sensors have roughly equal responses to the airflow.

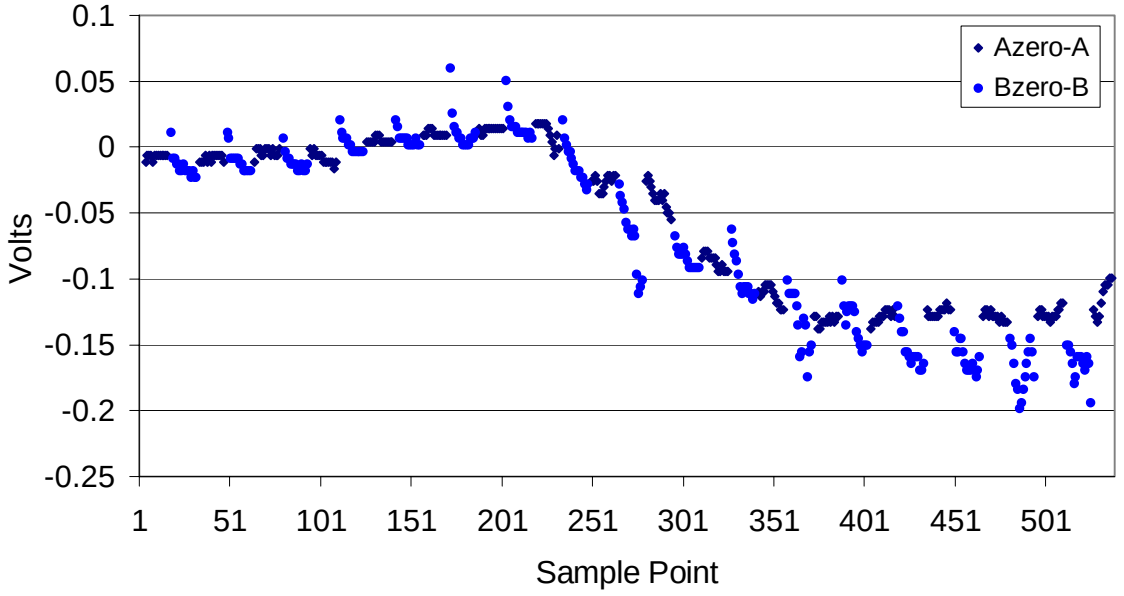


Figure 76. Typical Laboratory Test Results.

The sensors were turned on for 10 seconds and then turned off for 10 seconds in the plotted results. This mimics the actual situation in the mine where we kept the system off for 90% of the time in order to conserve batteries. A careful examination of the data will disclose a 'warm-up' transient as the sensor is turned on. We took a measurement every second to discover the size of the transient. We used the last measurement of the group in our calibration. Our final design allowed a 15 second warm-up for the sensors, to eliminate the effects of this transient warm-up.

Table 11 shows the theoretical and actual values averaged over several tests. The computed values varied over a range of about 2 to 1. The actual values resulted from timing the movement of smoke across the grids on the duct wall. The large range is due to the difficulty of selecting the exact portion of smoke from the tube that represented the average flow. The puff of smoke tended to have large changes in shape and its movement was far from steady and linear. In some cases, the smoke would momentarily reverse its flow direction. We found that this situation closely mimicked the flows in the abandoned mines.

Table 11. Airflow Transducer Output Sensitivity

| Actual Air Flow (fps) | Computed Air Flow (fps) |
|---|---|
| 0.05 | 0.02 |
| 0.1 | 0.07 |
| 0.2 | 0.15 |
| 0.4 | 0.35 |

The sensors' temperature sensitivity is probably the main error contributor with long-term drift the second largest problem. The ultrasonic transducers are mounted in a rubber compound. These materials often have large thermal expansion coefficients and molded-in stresses that relax over time. Panasonic, the ultrasonic transducer manufacturer, describes them as 'temperature stable". Commercial ultrasonic air-speed transducers are normally given a zero calibration each time that they are used.

## *6.3 Prototype Transducer*

We built and depolyed a prototype low-flow transducer in Mine 59 during the September 10, 1999 mine visit (Figure 77 and Figure 78). The transducer was removed in the December 2, 1999 mine visit when the multi-layer transducers were installed.

Figure 77. Prototype Low-flow Transducer in Mine 59 at the Location shown in Figure 78.

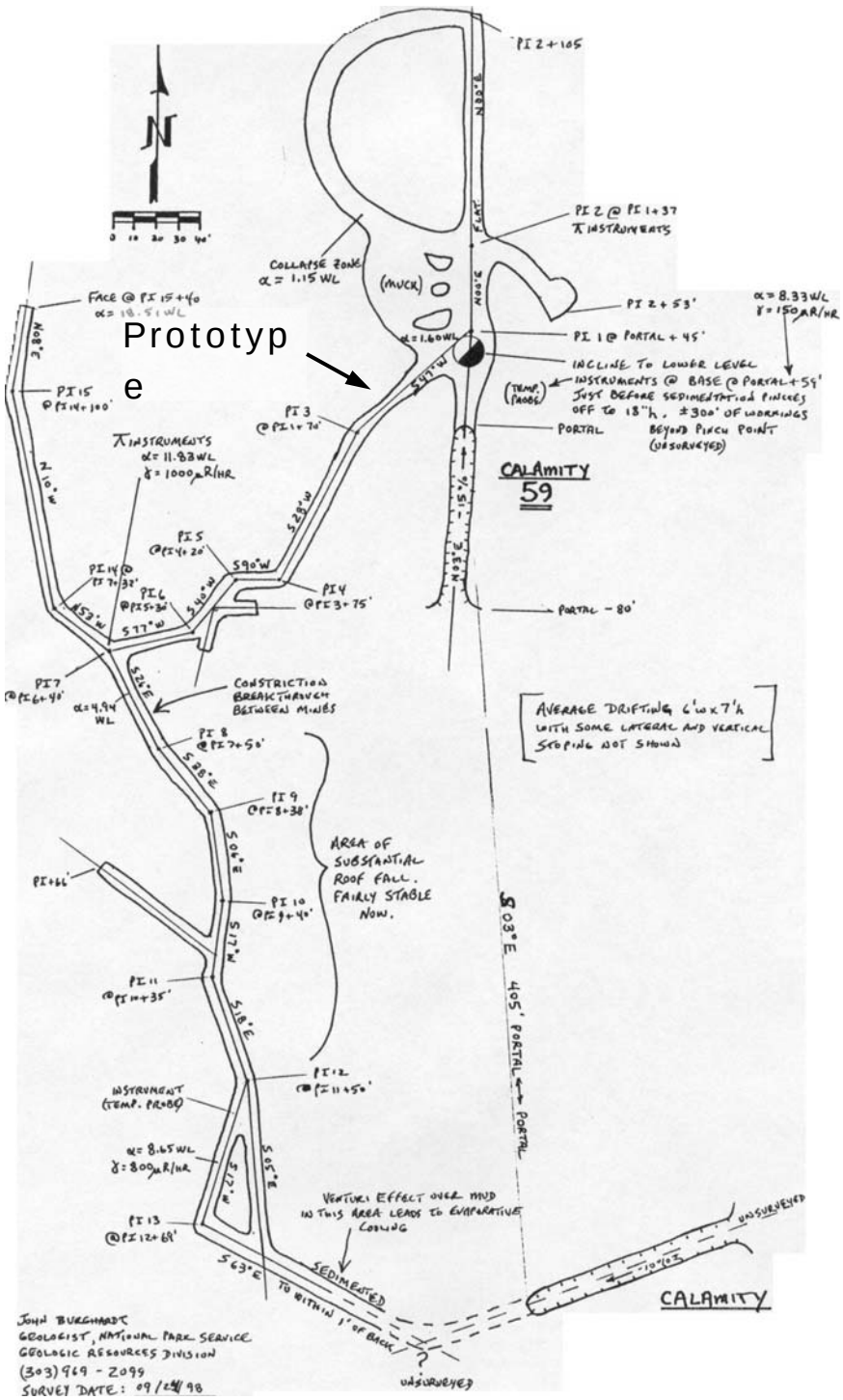


Figure 78. Prototype Low-flow Transducer Location in Mine 59

Table 12 presents example data from the prototype transducer.

Table 12. Example Data from the Low-flow Sensor

| Sample No. | Channel A (V) | Channel B (V) |
|---|---|---|
| 1 | 0.314 | 2.157 |
| 2 | 2.725 | 2.235 |
| 3 | 2.804 | 2.255 |
| 4 | 2.725 | 2.235 |
| 5 | 2.804 | 3.412 |
| 6 | 4.314 | 3.02 |
| 7 | 3.353 | 0.569 |
| 8 | 0.588 | 1.216 |
| 9 | 1.922 | 0.49 |
| 10 | 1.647 | 1.333 |

Figure 79 graphs of the output from both channels. The sampling period, 512s, was used to convert sample number from Table 12 to the date.

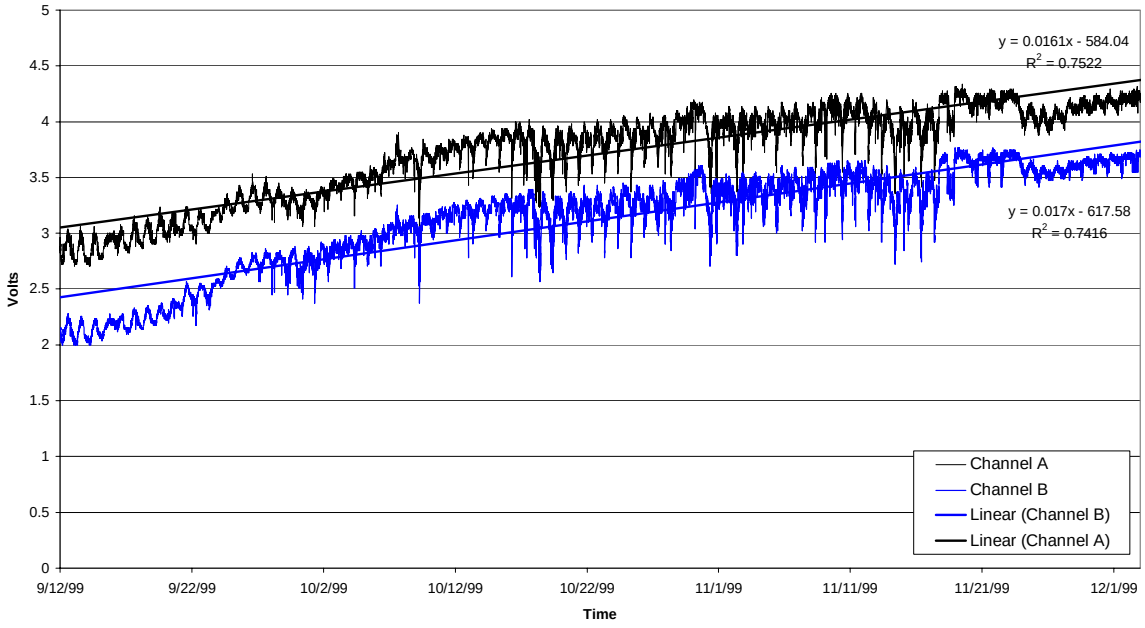


Figure 79. Low-flow Transducer Output

We corrected for drift, converted the values to FPM, and calculated the difference between the opposite-direction transit times. As described in section 6.1, the sensor has two ultrasonic transducer pairs. Each pair contained a transmitter and a receiver. The channel A pair transmited in one direction and the channel B pair transmited in the opposite direction. When the airflow was in the same direction as the transmitted ultrasonic energy, the signal arrived at the receiver sooner. The measurement was made by comparing the phase of the transmitted signal with that of the received signal to determine the amount of shift in the waveform. The voltage data in Table 12 and Figure 79 were proportional to the shift. A 180 ° shift corresponded to a 5 V output. Consequently the output amplitude was proportional to air flow rate: 50 mV = 9.85 fpm.

We assumed that the drift in the data was an artifact of the transducer and was not caused by the airflow in the mine. We corrected it by fitting a line to the data (shown in Figure 79). Next we calculated the discrete values of this line and subtracted them from the transducer data values (Figure 80). This removed the drift so that the data varied about 0 Volts.

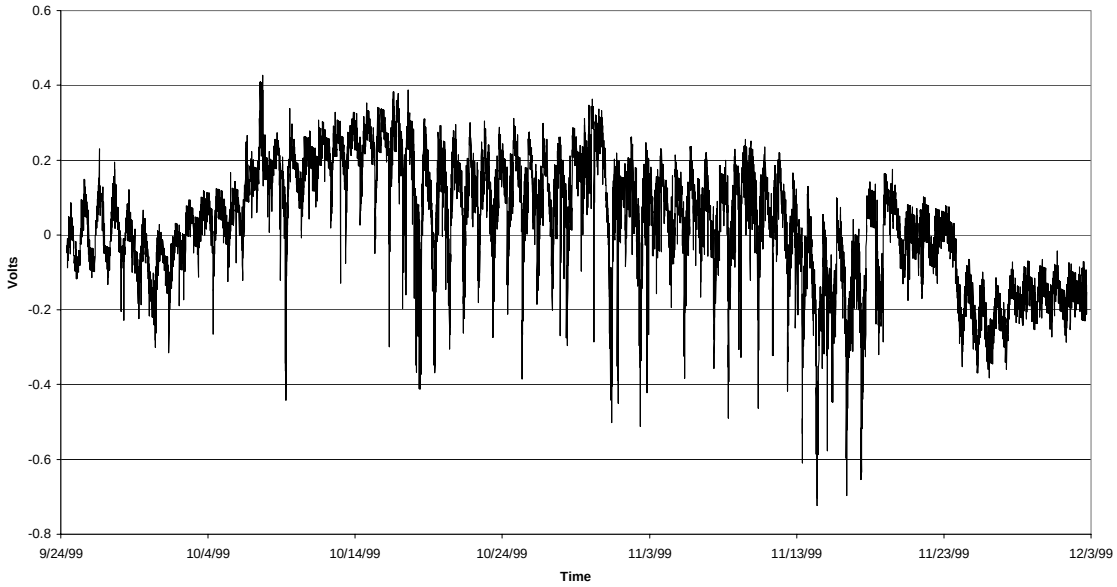


Figure 80. Channel A Output after Removing Drift.

Next, we removed drift from Channel B and subtracted the values from Channel A to determine the difference between the two sensor pairs. The difference doubled the effect since the two sensors measure in opposite directions. For example a flow in the direction of the A transmission decreased the time, causing a negative phase shift. Simultaneously the flow would be opposite the direction of the B transmission which increased the time and produced a positive phase shift. The difference, A – B, produced – A phase shift – B phase shift, essentially doubling the output signal, so we halved the difference.

The differencing operation canceled instrumentation errors like the effect of thermal variations on the instruments. For example, temperature variation might cause an error in the transducer A pair and an equal error in the transducer B pair. The errors subtract to zero. Next, we converted voltage to velocity. The differential measurement result is shown in Figure 81.

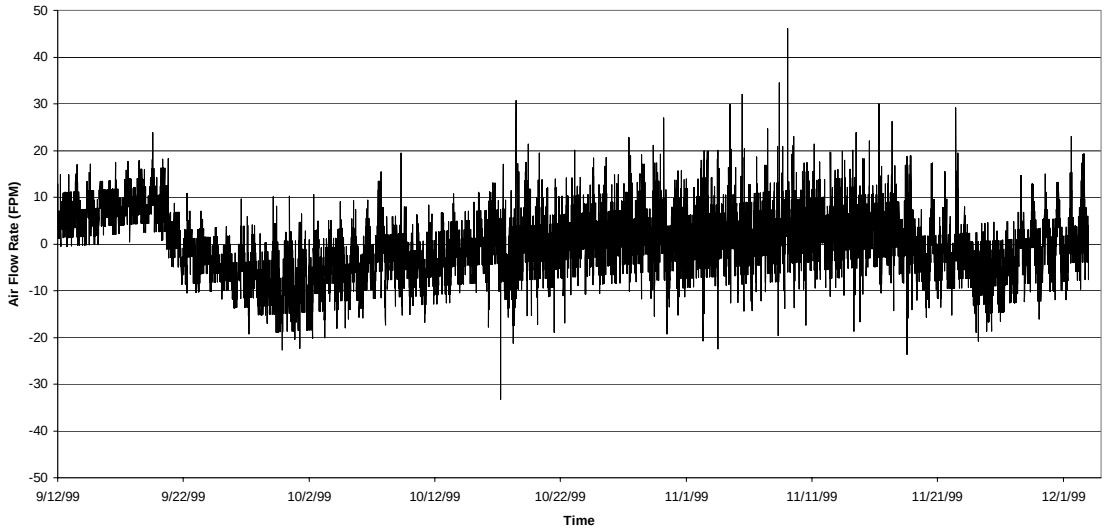


Figure 81. Mine 59 Airflow Rates Measured by the Prototype Low-flow Transducer.

Table 13 gives an example of the worksheet used to develop the Figure 81 graph.

Table 13. Sample Data Analysis Worksheet

| A | B | C | D | E | F | G | H | I | J | K |
|---|---|---|---|---|---|---|---|---|---|---|
| | Date | CH A | CH B | Diff | CH A * N | CH B * N | CH A | CH B | Zeroed | Flow Rate |
| | | Volts | Volts | Volts | | | Zeroed | Zeroed | Diff. | FPM |
| 1 | 9/10/99 | 0.314 | 2.157 | -1.843 | 4537.928 | 31172.96 | -2.72692 | -0.20797 | -2.51895 | -247.865 |
| 2 | 9/10/99 | 2.725 | 2.235 | 0.49 | 39381.7 | 32300.22 | -0.31601 | -0.13007 | -0.18594 | -18.2966 |
| 3 | 9/10/99 | 2.804 | 2.255 | 0.549 | 40523.41 | 32589.26 | -0.23711 | -0.11018 | -0.12693 | -12.49 |
| 4 | 9/10/99 | 2.725 | 2.235 | 0.49 | 39381.7 | 32300.22 | -0.3162 | -0.13028 | -0.18592 | -18.2945 |
| 5 | 9/10/99 | 2.804 | 3.412 | -0.608 | 40523.41 | 49310.22 | -0.2373 | 1.046612 | -1.28391 | -126.337 |
| 6 | 9/10/99 | 4.314 | 3.02 | 1.294 | 62345.93 | 43645.04 | 1.272608 | 0.654507 | 0.618101 | 60.82114 |
| 7 | 9/10/99 | 3.353 | 0.569 | 2.784 | 48457.56 | 8223.188 | 0.311514 | -1.7966 | 2.108111 | 207.4382 |
| 8 | 9/10/99 | 0.588 | 1.216 | -0.628 | 8497.776 | 17573.63 | -2.45358 | -1.1497 | -1.30388 | -128.302 |
| 9 | 9/10/99 | 1.922 | 0.49 | 1.432 | 27776.74 | 7081.48 | -1.11968 | -1.87581 | 0.756132 | 74.40342 |
| 10 | 9/10/99 | 1.647 | 1.333 | 0.314 | 23802.44 | 19264.52 | -1.39477 | -1.03291 | -0.36186 | -35.6067 |

The values in the worksheet were developed as follows:

Column A: Sample Number from Air Flow Transducer Output
Column B: Initial Date & Time + 512/3600/24 (formatted as date and time)
Column C: Channel-A Voltage Amplitude from Airflow Transducer Output
Column D: Channel-B Voltage Amplitude from Airflow Transducer Output
Column E: Difference = Channel-A Voltage Output – Channel-B Voltage Output
Column F: Channel-A Voltage Output * Total Number of Samples
Column G: Channel-B Voltage Output * Total Number of Samples
Column H: Drift Removed from Channel A: (Channel-A Output * N - (1.3659 * Sample Number + 43946))/14452; where 1.3659 = slope from linear regression, 43936 = linear regression intercept, & 14452 = Total Number of Samples
Column I: Drift Removed from Channel B: (Channel-B Output * N - (1.5171 * Sample Number + 34177))/14452; where 1.5171 = slope from linear regression, 34177 = linear regression intercept, & 14452 = Total Number of Samples
Column J: Difference (Column H – Column I)
Column K: Airflow in FPM: (9.84/0.050 * Difference)/2; where 9.84 FPM /0.028 V = transducer sensitivity & 2 = correction from doubling flow with differencing process.

Figure 82 is a portion of the Figure 81 data at a scale that shows cyclic patterns and digitizing resolution.

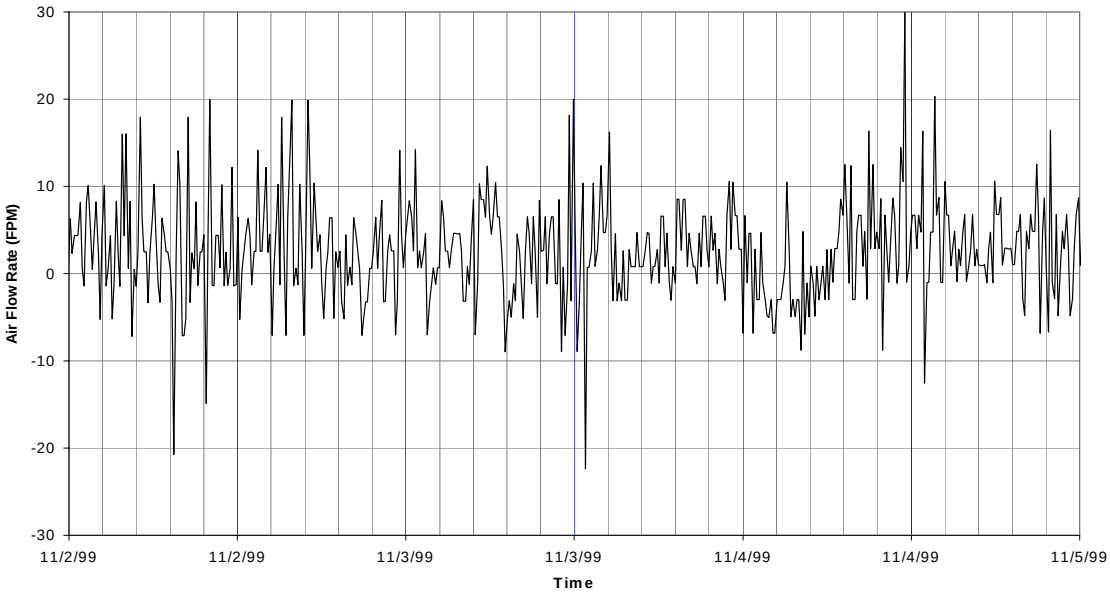


Figure 82. Prototype Transducer Airflow Rate Measurements 11/2/99 – 11/5/99.

## 6.4 In-mine Measurements

Gas flow measurements for slowly moving material often use a tracer such as smoke to mark a portion of the flow and follow the tracer's movement for several seconds. We used a commercial 'smoke tube' to gain an appreciation of the characteristics of slow airflow during the September 9, 2000 mine visit (Table 14).

Table 14. Smoke Tube Measurements

| Mine 31 | | | Mine 65 | | Mine 59 | | | | | |
|---|---|---|---|---|---|---|---|---|---|---|
| | Air Station 1 | | Air Station 3 | | Air Station 0 | | | | Station 0 + 30 ft | |
| | Back | | Floor | | Mid | | Back | | Back | |
| | (s) | (FPM) | (s) | (FPM) | (s) | (FPM) | (s) | (FPM) | (s) | (FPM) |
| | -9.0 | -20.0 | 13.0 | 13.8 | 6.0 | 50.0 | 21.0 | 14.3 | 14.0 | 21.4 |
| | -9.0 | -20.0 | 16.0 | 11.3 | 8.0 | 37.5 | -14.0 | -21.4 | -10.0 | -30.0 |
| | -7.0 | -25.7 | 16.0 | 11.3 | 8.0 | 37.5 | | | 10.0 | 30.0 |
| | -6.0 | -30.0 | | | | | | | 16.0 | 18.8 |
| | | | | | | | | | -8.0 | -37.5 |
| | | | | | | | | | | |
| Mean | | -23.9 | | 12.1 | | 41.7 | | -3.6 | | 0.5 |
| Std Dev | | 4.9 | | 1.5 | | 7.2 | | 25.3 | | 31.7 |
| Range | | 10.0 | | 2.6 | | 12.5 | | 35.7 | | 67.5 |
| Minimum | | -30.0 | | 11.3 | | 37.5 | | -21.4 | | -37.5 |
| Maximum | | -20.0 | | 13.8 | | 50.0 | | 14.3 | | 30.0 |
| | | | | | | | | | | |
| Dist = | 3 | ft. | 3 | ft. | 5 | ft. | | | | |

Observations of the smoke showed that the flow is highly turbulent with vortex formation and circular air movement. Diffusion was evident with the smoke trail quickly becoming invisible as the smoke dispersed. Therefore, we expected highly variable data from the airflow transducers, and in the range of 0 - 50 fpm moving into and out of the mine.

We built seven transducer systems to deploy in the mines 31, 59 and 65 at the locations shown in Figure 11, Figure 15, and Figure 21 respectively (Table 15).

Table 15. Distance from Portal to Airflow Transducer

| Mine | Transducer No. | Distance to Portal | Lower Transducer | Middle Transducer | Upper Transducer |
|---|---|---|---|---|---|
| 31 | 1 | 20 | | | Figure 84 |
| | 6 | 76 | | Figure 85 | Figure 86 |
| 59 | 0 | 60 | | | |
| | 2 | 82 | Figure 87 | Figure 88 | |
| | 4 | 700 | | | Figure 89 |
| 65 | 3 | 10 | | | |
| | 5 | 135 | | | |

In addition to the different distances from the portal, the airflow environment had several variations for the six sensors. Mine 31 had a very large entrance, nearly twice the area of the other mines. Mine 59 and 31 had multiple branches and were fairly level. Mine 59 drifts connected two openings. Mine 65 was more inclined and might be expected to have greater natural convection effects.

The air-flow measurements began on December 2, 1999 and the systems were recovered and data downloaded in May 10, 2000. We recovered data from most of the units for about one month. This was only half of the data memory. A software error caused the system to stop data collection prematurely, and rodents damaged the transducer cables to several of the transducer systems as shown in Figure 83. The data is graphed in Figure 84 through Figure 89 for the functional systems.

The transducer data showed high variability with flows switching directions frequently as expected from the smoke tube tests. Most of the data was within the 0 to 0.2 fps (0 – 12 fpm) range with a small number of readings reaching 0.4 fps (24 fps). This compared with smoke tube measurements of 10 – 50 fpm, and model predictions of about 12 fpm. Rodents damaged the air flow sensor in the prototype location, so exact comparison of pre- and post closure velocities was not possible, but general comparison with ranges of measurements with other transducers did not show a significant difference. For example transducer 4 in mine 59, in the same air stream as the prototype transducer, measured velocities mostly in the 0-1 fpm range with maximum values around 20 fpm a few days after closure.

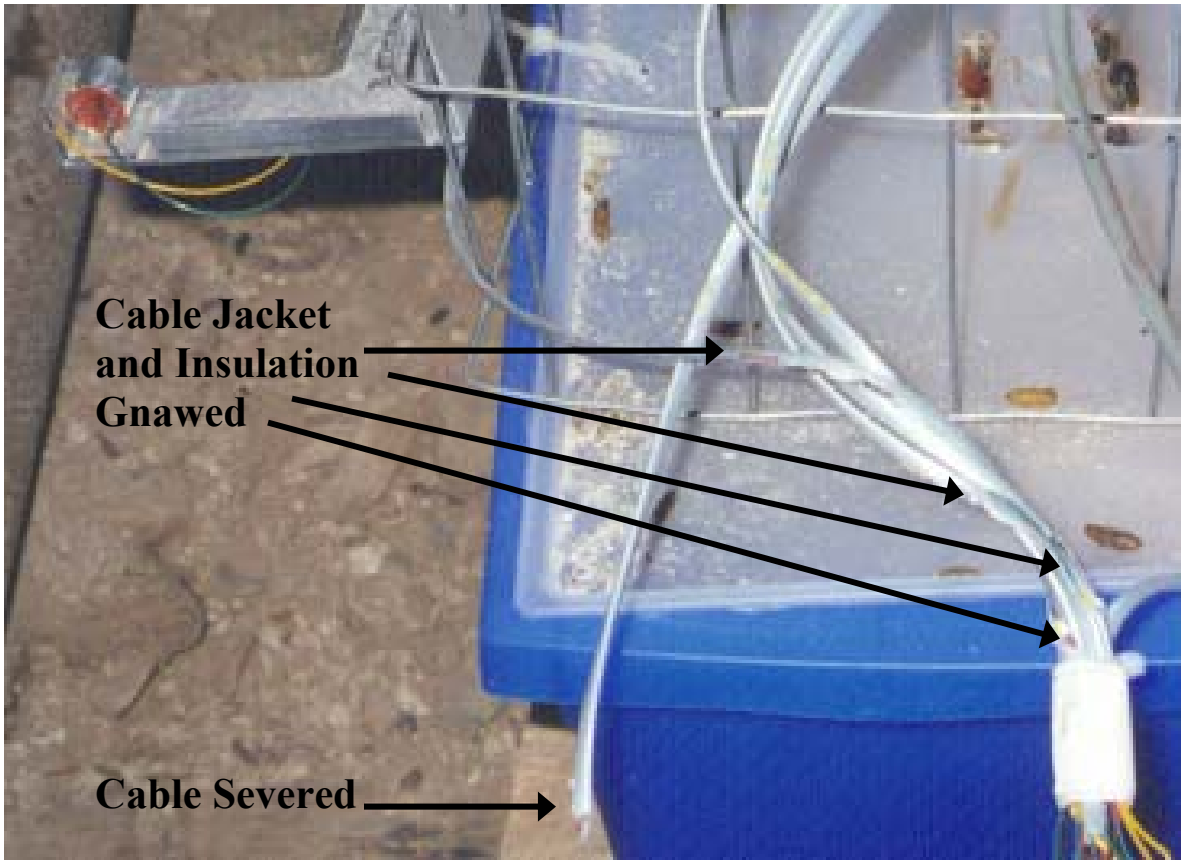


Figure 83. Rodent Damage to Airflow Transducer Cables

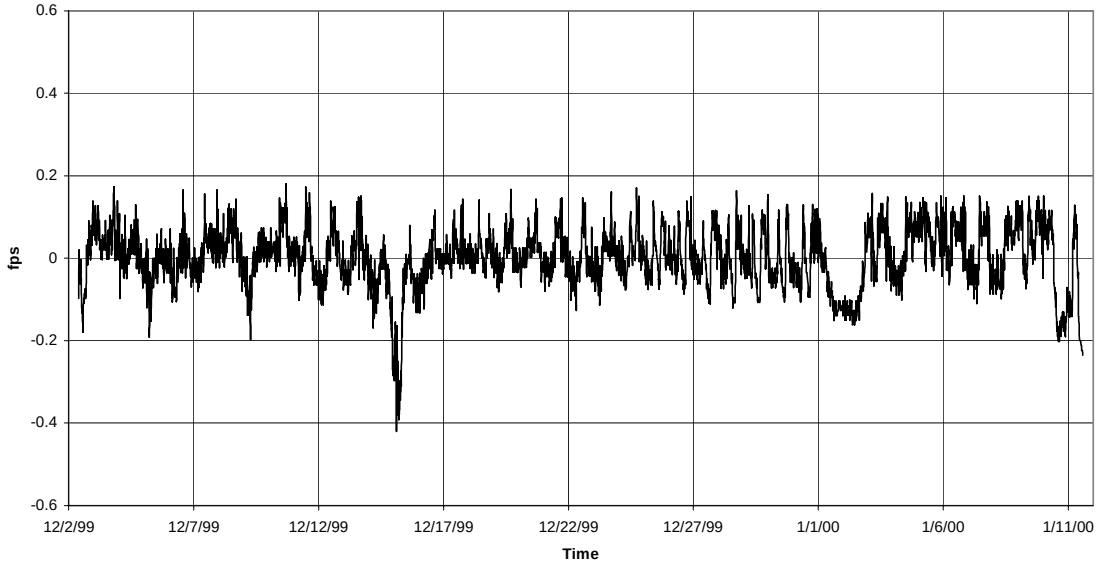


Figure 84. Mine 31, Airflow Transducer 1, Upper Flow

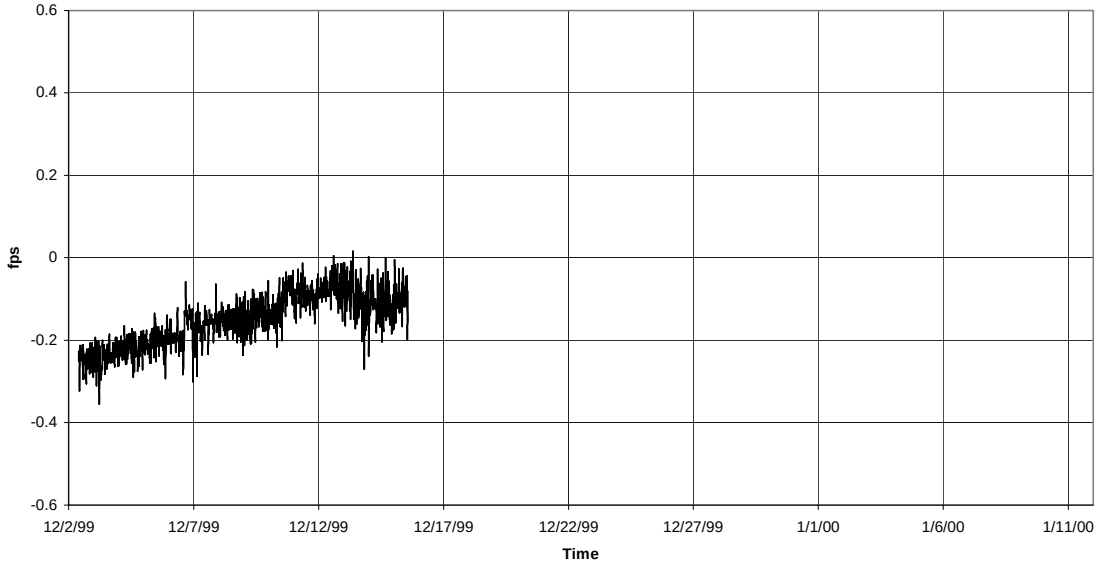


Figure 85. Mine 31, Airflow Transducer 6, Middle Flow

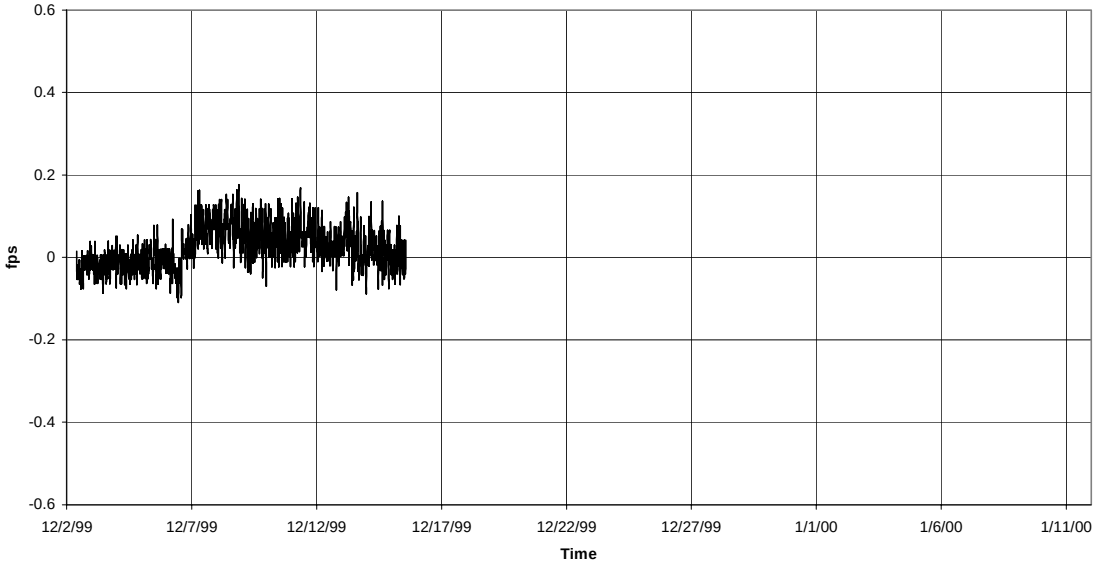


Figure 86. Mine 31, Airflow Transducer 6, Upper Flow

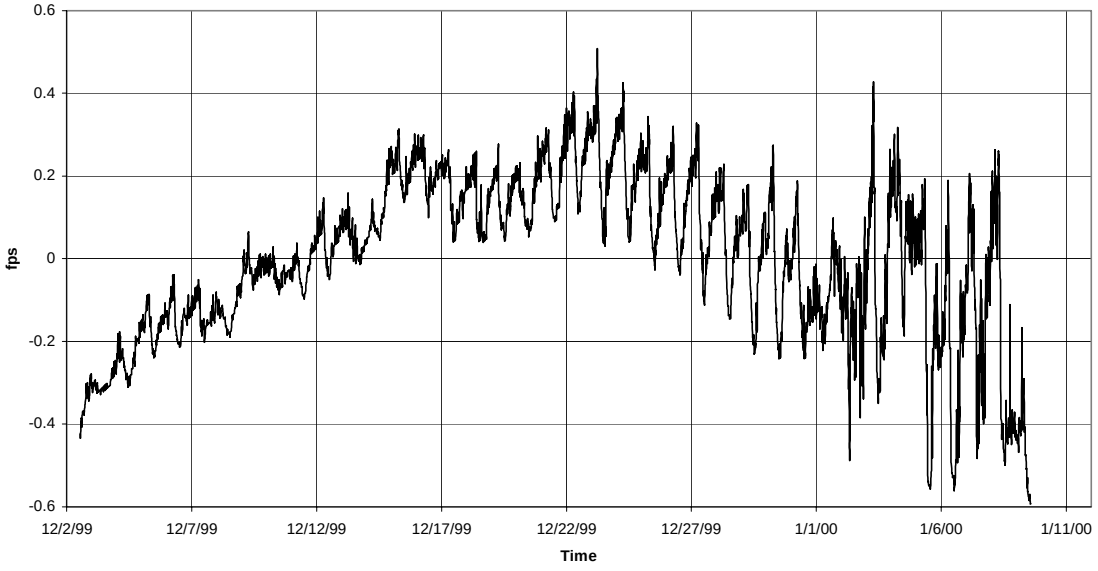


Figure 87. Mine 59, Airflow Transducer 2, Lower Flow

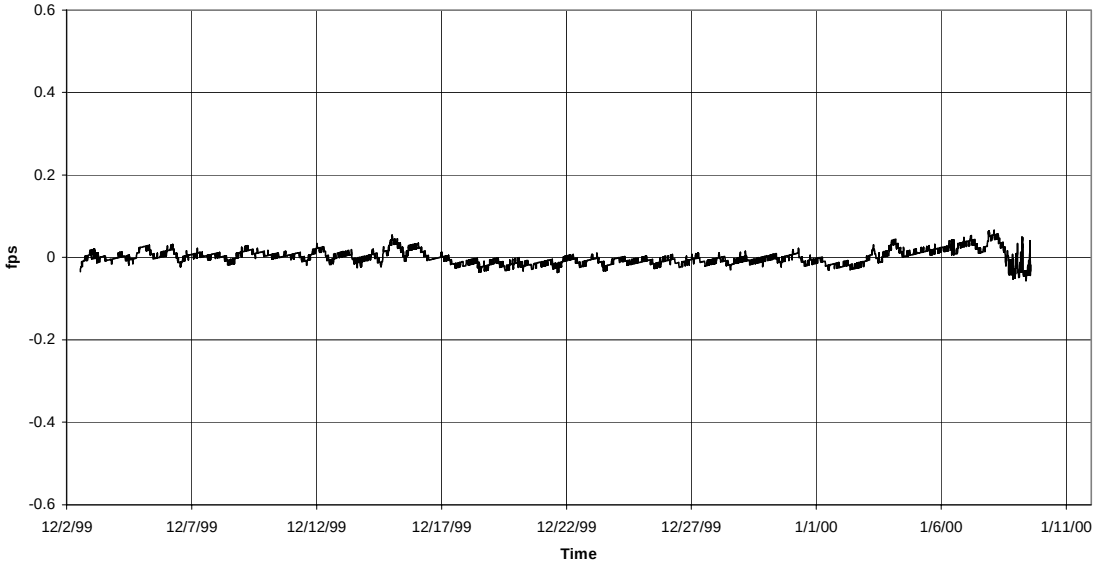


Figure 88. Mine 59, Airflow Transducer 2, Middle Flow

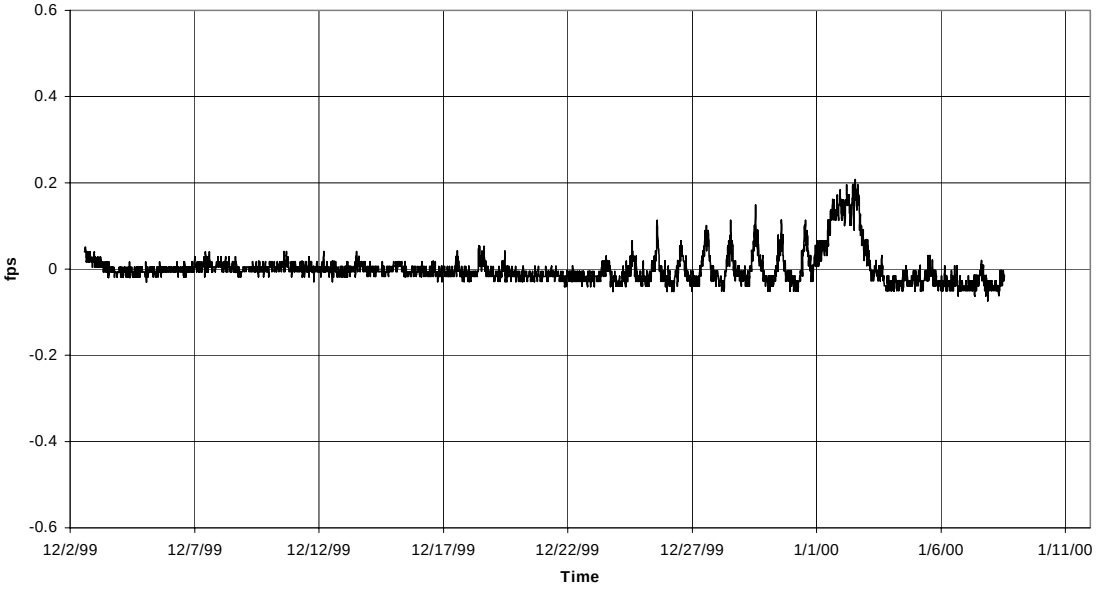


Figure 89. Mine 59, Airflow Transducer 4, Upper Flow

# 7.0 Radiation

## *7.1 Working Level and Gamma Measurements*

Radiation emanates from the radioactive ores in the Morrison Formation that were extracted from the study mines (Burghardt, 1996). Alpha radiation results when a radioactive atom decays by releasing two neutrons and two protons (an alpha particle). The atom's atomic mass drops by four, and it becomes an offspring of the original atom. Radon gas is the direct offspring of radium that decays to Radium A, B, C, and C′ which attach to dust particles or droplets. These particles can be inhaled and may be trapped in the lungs where the associate radio nuclides continue to decay, emitting high-energy alpha particles that may cause lung cancer.

Working Levels are a unit of measurement for alpha radiation. A working level is a concentration of radon daughters that will deliver $1.3 \times 10^5$ MeV of alpha energy per liter of air. At equilibrium 1WL = 100 pCi/l.

John Burghardt measured radiation in the three mines studied during the initial mapping and safety inspection visit on 9-20-98. His results were handwritten on the maps in Section 4. Burghardt loaned the NPS Instant Working Level Meter and Gamma Meter for radiation measurements during the 12-2-99 mine visit. Time for other activities restricted the 12-2-99 measurements to Mine 59. Figure 90 and Figure 91 compare the pre- and post-closure measurements. Most of the measurements made on 12/2/99 (blue font) are lower than those made on 9/24/98. We believe this is caused by the difference in airflow between the two measurement dates. The third week in September daytime surface air temperature was higher than the daytime air temperature in the mine, so there was very little convective airflow. However the December measurements were made when surface air temperature had fallen below the mine temperature for some time, causing increased airflows. Generally, higher airflow reduces working level measurements (Burghardt, 1996); however, Figure 90 shows two locations where the working levels were higher on 12/2/99: at the entrance to the winze and in the connecting drift to the other portal.

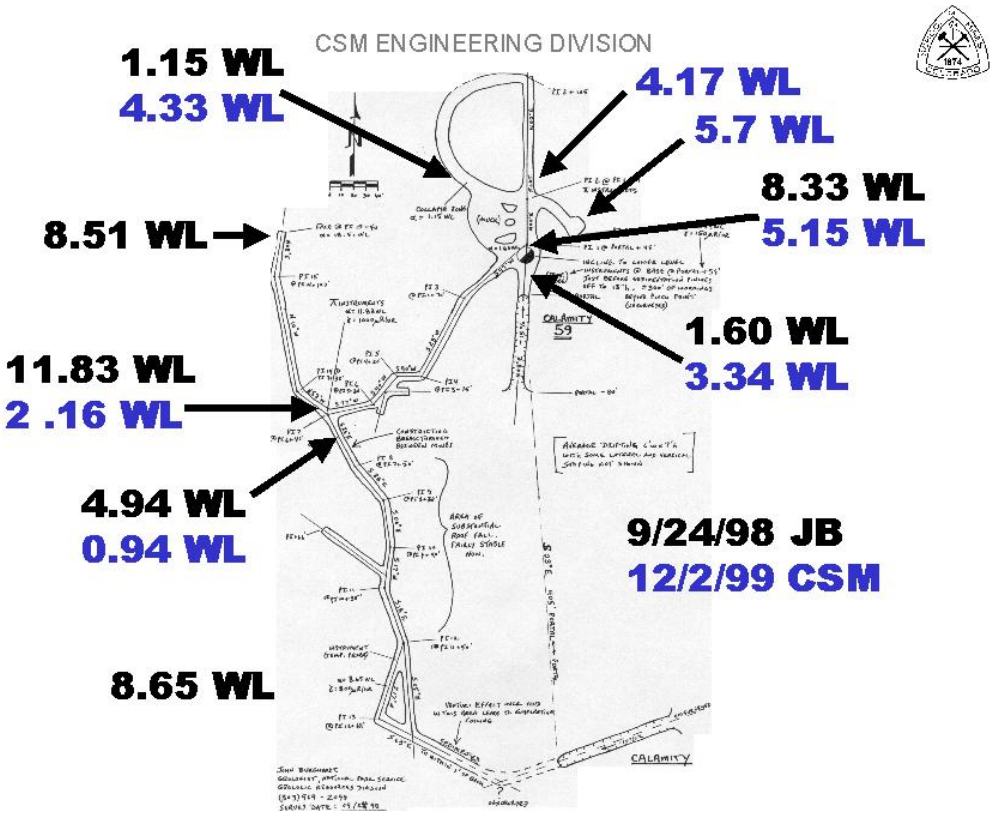


Figure 90. Instant Working Level Measurements in Mine 59

Since gamma is not affected by air flow, the readings for the two different times should be very similar if they are taken exactly in the same location. Even though we were not aware of Burghardt's exact measurement locations, the values are very similar. One measurement is exactly the same but the one at the entrance to the winze was slightly higher on 12/2/99 (Figure 91).

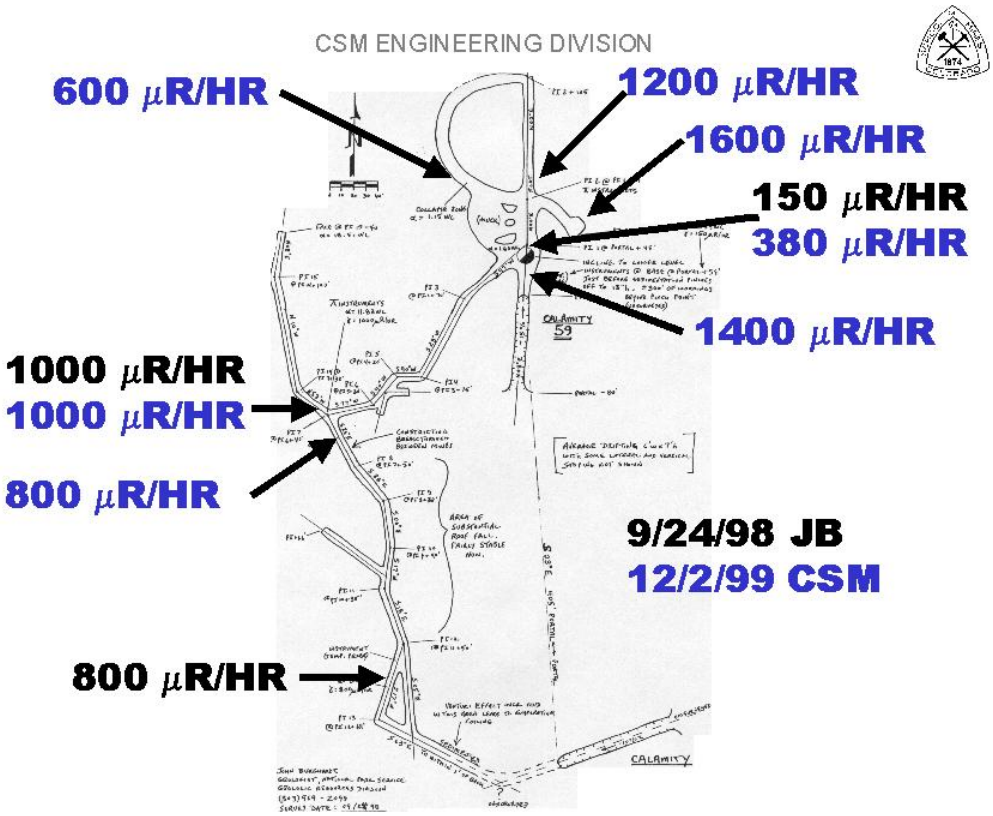


Figure 91. Gamma radiation measurements in Mine 59

## *7.2 Dosimeters and Alpha Cups*

Dosimeters measure combined radiation exposure from x-ray, beta, and gamma radiation through a thin layer of aluminum oxide. We obtained dosimeters from Landauer, Inc whose dosimeters contain aluminum oxide that is stimulated with a laser light causing it to become luminescent in proportion to the amount of radiation exposure (Figure 92).

The dosimeter's exposure range is 1 mrem to 1,000 rem for x and gamma radiation and 10 mrem to 1,000 rem for energetic beta. Dose equivalents arising from exposures to x or gamma rays will have a deep, eye and shallow value (Table 16). Depending on the energy of the x- or gamma rays, these values may or may not be equal. Beta exposures are only reported as a shallow dose equivalent.

Deep dose equivalent applies to external whole-body exposure and is the dose equivalent at a tissue depth of 1 cm (1,000 mg/cm$^2$). Eye dose equivalent applies to the external exposure of the lens of the eye and is taken as the dose equivalent at a tissue depth of 0.3 cm (300 mg/cm$^2$). Shallow dose equivalent applies to the external exposure of the skin or an extremity, and is taken as the dose equivalent at a tissue depth of 0.007 cm (7 mg/cm$^2$) averaged over an area of one square centimeter.

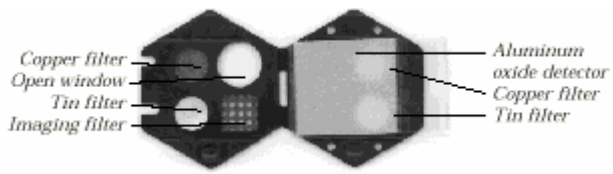


Figure 92. Dosimeter Internal Components (courtesy of Landauer, Inc.)

We deployed dosimeters at the instrument stations similar to Figure 93 on the dates listed in Table 16. Instrument station locations were shown in Figure 11, Figure 15, and Figure 21 for mines 31, 59, and 65 respectively. We retrieved the dosimeters on 12/2/99 and returned them to Landauer, Inc. for analysis (Table 16).

Table 16. Dosimeter Deployment

| Location | Date | Serial Number | Measurement | | |
|---|---|---|---|---|---|
| | | | Deep DDE | Eye LDE | Shallow SDE |
| 59-2 | 9/24/98 | 0318409AG | 9712 | 10246 | 10751 |
| 59-1 | " | 0318410AN | 7764 | 8169 | 8565 |
| 65-3 | " | 0318408AH | 2263 | 2440 | 2578 |
| 31-1 | " | 0318407AI | 319 | 336 | 352 |
| control | | 0318406A | 186 | 186 | 192 |

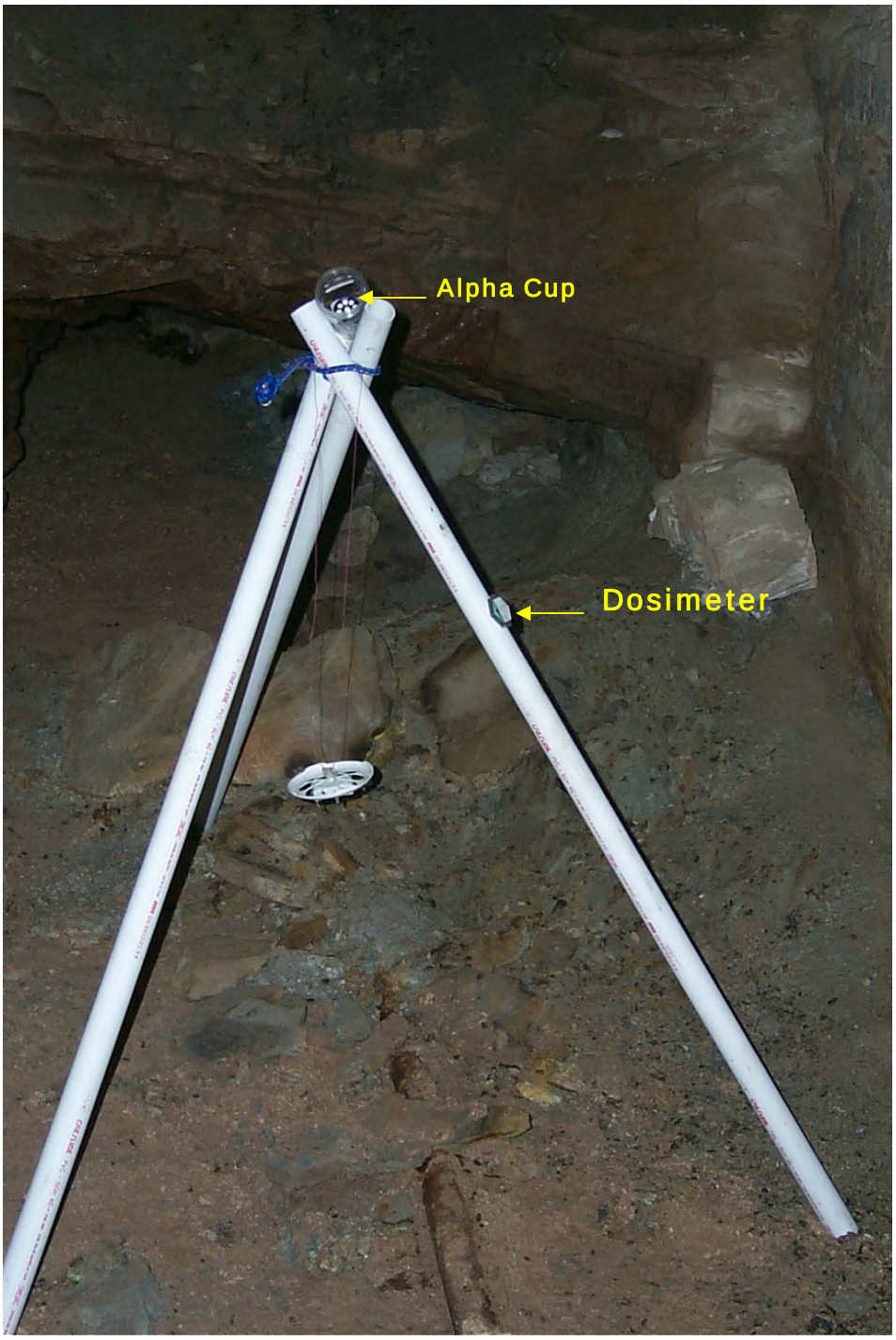


Figure 93. Dosimeter and Alpha Cup at Typical Instrument Station

We deployed alpha cups along with the dosimeters. We collected them on 12/2/99 and returned them to Lindauer for analysis. All alpha cup data exceeded the maximum 140,000 PCi/L capabilities of the Landauer measurement apparatus.

## *7.3 Radiation Effect on Bats*

Our project raised concerns that the level of radiation in the study mines could affect bats. As a result, Kirk Navo organized a meeting at the Colorado Division of Wildlife offices on 3/2/99 to discuss the issue further. A summary of the meeting follows:

> Doug Halford summarized information from an earlier study. It suggested that bats may be affected by radiation doses from habitation in abandoned uranium mines, but a more thorough study is necessary. His preliminary study suggests that the doses from inhaling radon are fairly insignificant; however, his radon dose conversion factors are based on humans. He believes that the doses resulting from external exposure are much more significant. Bats can give doses to other bats by licking the dust off of each other. Radon Daughters radioactive atoms that emit gamma and alpha emission once ingested. There is concern that radiation will have an affect on fetuses young bats in maternity roosts since cells are most vulnerable during development. Cells will repair themselves from a small dose, but continual doses to bats in mines may cause permanent damage.
>
> Radiation studies have been conducted with rats, but bats have a higher metabolism and longer life span. Further study should incorporate mine usage by individual bats over a long period of time to match health problems with exposure levels. It is very difficult to study individuals. To gather the necessary data, bats could be banded, or transmitters could be epoxied to their backs. The problem is that the epoxy lasts 90 days. Grooming will also remove the transmitters from their backs. If an individual history was known, a sample of the bat tissue could be taken and chromosome studies could be done. These studies are expensive. Also, without killing the bat it is difficult to determine age. To perform an adequate study, a control population is necessary composed of bats similar in all respects except that one uses uranium mines for habitat. Locating such a population is difficult. The goals of a long-term study might be to observe population increase/decrease, observe and record skin effects, and measure maternity rates. The study would have to measure other effects on the population like pesticides. It is important to realize that human disturbance may cause the bats to abandon the roost.
>
> A long-term study is necessary to answer the questions, but by the time this study is done, all the bat gates might be in place. A long-term study would be expensive and there are limited funds available to support bat habitat. Bat surveys are a higher priority use for current funds, and additional funding sources would have to be sought to support a radiation study. An interim measure might be taken such as not gating mines where alpha radiation levels are found to exceed 10WL.

# 8.0 Analysis

## *8.1 Closure Effect on Temperature using a Data Window Method*

Two variables could have caused differences between pre- and post closure microclimates: surface climate and the culvert-gate closure, so we had to separate closure effects from surface climate effects. Consequently, we attempted to located short periods where the surface climate was approximately the same before and after closure. It was impossible to find periods where the surface climate was exactly the same, but we found periods where the surface climate was similar.

Finding similar surface climates before and after closure was complicated because we had to match both surface temperature and humidity. When humid air enters the mine, the dew point rises. If it climbs above the mine temperature, condensation occurs, which cools the air. The surface logger reported much higher humidity throughout most of the measurement period before closure, than after closure (Figure 31). Figure 94 shows a period of high humidity in the surface climate and the resulting high dew-point measurements at logger 59-2.

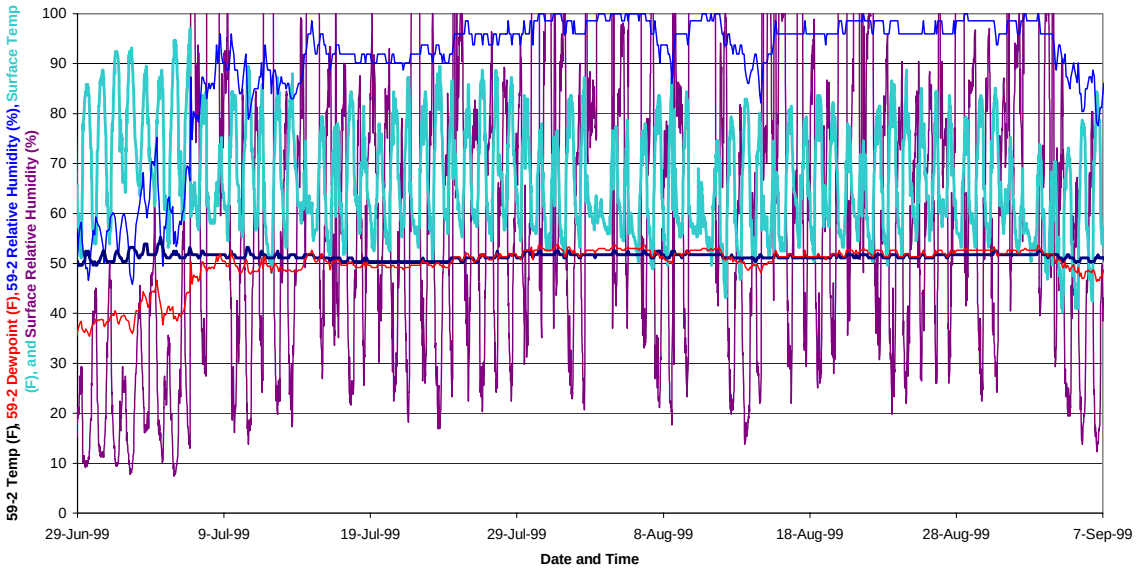


Figure 94. High-humidity Surface Climate Cause High Dew Points in the Microclimate.

Mine humidity and dew point can also be affected by ground water flow. Our mines were not very deep and were relatively dry. Mine 65 had standing water at the outset of the investigation that dried up during the measurement period.

Statistical representation of the surface climate data showed the period from 6/24/99 at 11:50 to 7/5/99 at 11:50 had similar humidity and temperature values as some of the post closure data (Table 17 and Figure 95).

Table 17. Statistical Representation of Climate Measurements in Pre- and Post Closure Data Windows

| Logger and Data Window | Temperature | | | | Relative Humidity | | | |
|---|---|---|---|---|---|---|---|---|
| | Avg | Min | Max | Var | Avg | Min | Max | Var |
| 59-5 Pre-closure | 74.07 | 48.96 | 93.21 | 142.13 | 22.30 | 5.30 | 67.70 | 172.98 |
| 59-5 Post-closure | 74.08 | 48.96 | 97.82 | 201.98 | 19.58 | 2.40 | 63.60 | 210.21 |
| 31-1 Pre-closure | 49.17 | 47.53 | 50.38 | 0.56 | 78.72 | 65.70 | 86.80 | 21.57 |
| 31-1 Post-closure | 52.61 | 51.79 | 53.19 | 0.17 | 92.15 | 87.30 | 95.40 | 2.18 |
| 31-2 Pre-closure | 59.72 | 53.19 | 66.28 | 10.77 | 39.82 | 17.40 | 67.00 | 135.38 |
| 31-2 Post-closure | 53.35 | 51.79 | 53.89 | 0.23 | 86.76 | 64.50 | 90.50 | 10.30 |
| 59-0 Pre-closure | N/A | N/A | N/A | N/A | N/A | N/A | N/A | N/A |
| 59-0 Post-closure | 45.98 | 44.65 | 46.82 | 0.25 | 92.85 | 89.80 | 95.80 | 1.48 |
| 59-1 Pre-closure | 47.46 | 46.82 | 47.53 | 0.05 | 74.26 | 69.30 | 77.90 | 3.58 |
| 59-1 Post-closure | 48.90 | 48.25 | 48.96 | 0.04 | 80.70 | 75.10 | 84.30 | 4.67 |
| 59-2 Pre-closure | 51.30 | 48.96 | 55.28 | 1.83 | 56.54 | 34.80 | 75.20 | 58.92 |
| 59-2 Post-closure | 50.88 | 50.38 | 51.79 | 0.21 | 64.13 | 50.40 | 84.30 | 58.53 |
| 59-3 Pre-closure | 48.89 | 47.53 | 50.38 | 0.35 | 63.27 | 43.30 | 82.20 | 53.54 |
| 59-3 Post-closure | 49.70 | 49.67 | 50.38 | 0.02 | 75.29 | 64.50 | 88.40 | 25.74 |
| 59-4 Pre-closure | 46.97 | 46.80 | 47.60 | 0.11 | N/A | N/A | N/A | N/A |
| 59-4 Post-closure | 48.79 | 48.30 | 49.00 | 0.10 | N/A | N/A | N/A | N/A |
| 65-1 Post-closure | 44.76 | 44.70 | 45.40 | 0.04 | N/A | N/A | N/A | N/A |
| 65-2 Pre-closure | 44.25 | 43.92 | 45.38 | 0.14 | 91.11 | 80.60 | 97.80 | 18.09 |
| 65-2 Post-closure | 46.12 | 45.38 | 46.82 | 0.03 | 103.12 | 102.70 | 103.30 | 0.02 |
| 65-3 Pre-closure | 44.06 | 43.19 | 44.65 | 0.26 | 99.99 | 98.40 | 100.00 | 0.02 |
| 65-3 Post-closure | 44.65 | 44.65 | 44.65 | 0.00 | 100.00 | 100.00 | 100.00 | 0.00 |

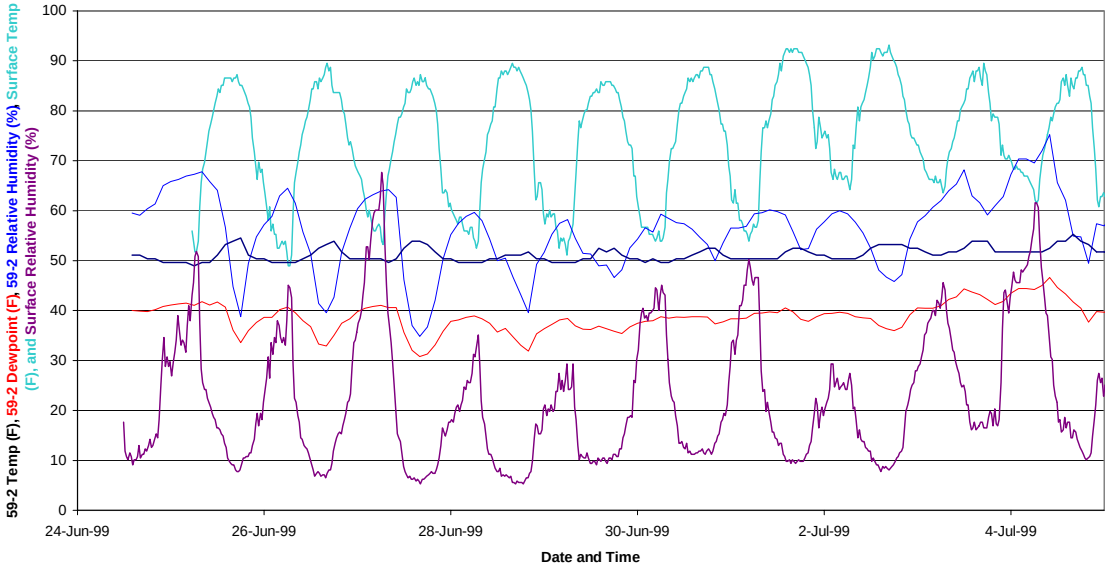


Figure 95. 59-5 and 59-2 Logger Measurements Over the Pre-closure Data Window

The pre-closure data window contains 660 lines, or data points. We calculated average, maximum, minimum, and variance for all possible windows of this size in the post closure data and compared pre- and post-closure statistics to find the best match. The best match between loggers 59-5 and 59-2 occurred from 7/17/00 at 12:52 to 7/28/00 at 11:50 ( Figure 96).

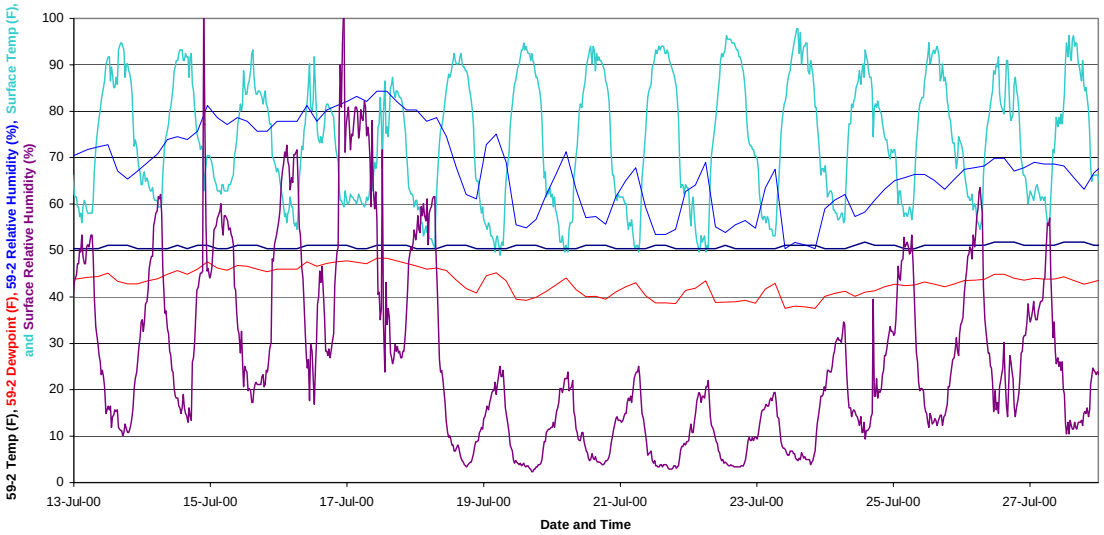


Figure 96. 59-5 and 59-2 Logger Measurements in the Post-closure Window.

The match isn't perfect, but the values are relatively close (Table 17). The post-closure data is slightly more variable, has a slightly higher maximum temperature, lower average humidity, and lower minimum humidity (Figure 97).

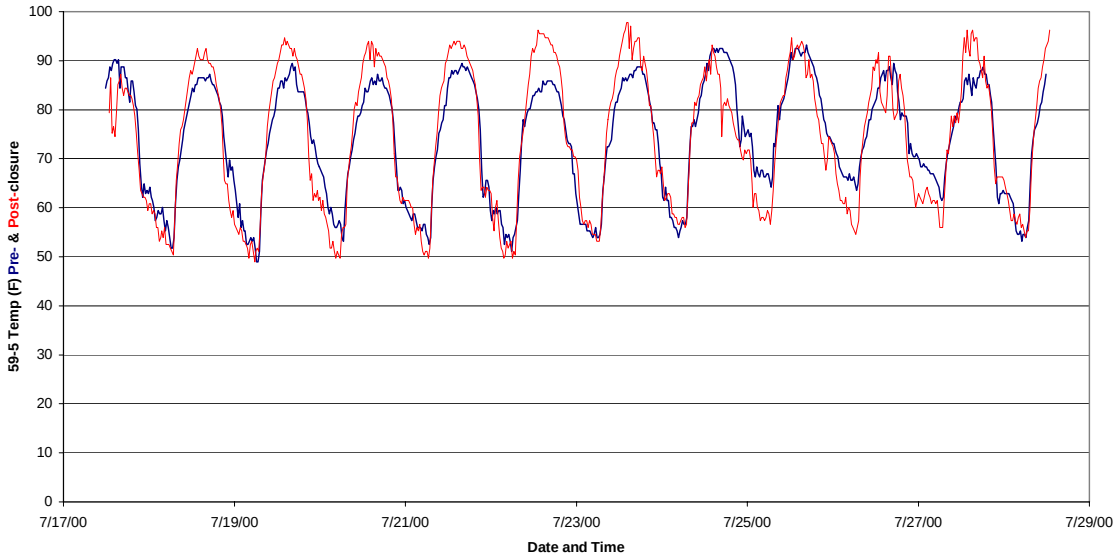


Figure 97. Surface (Logger 59-5) Temperature Measurements in the Pre- versus Post-closure Data Widows.

We shifted the pre-closure dates to match the post-closure dates to facilitate plotting both windows on the same graph (Figure 97 through Figure 107). Graphs include surface climate data from logger 59-5 for comparison with mine measurements where appropriate.

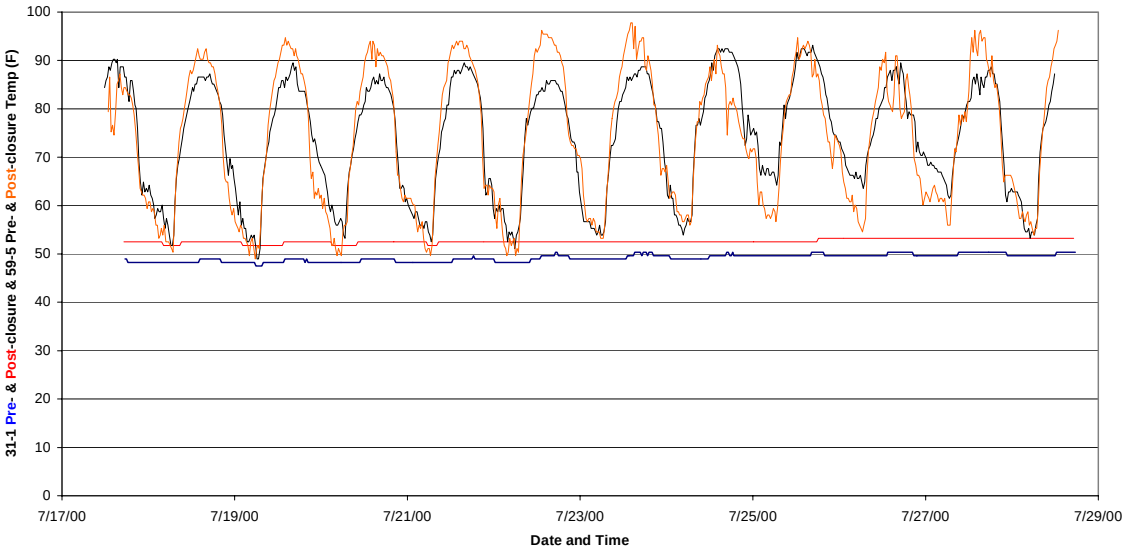


Figure 98. Logger 31-1 and 59-5 Temperature Measurements in the Pre- Versus Post-closure Data Windows.

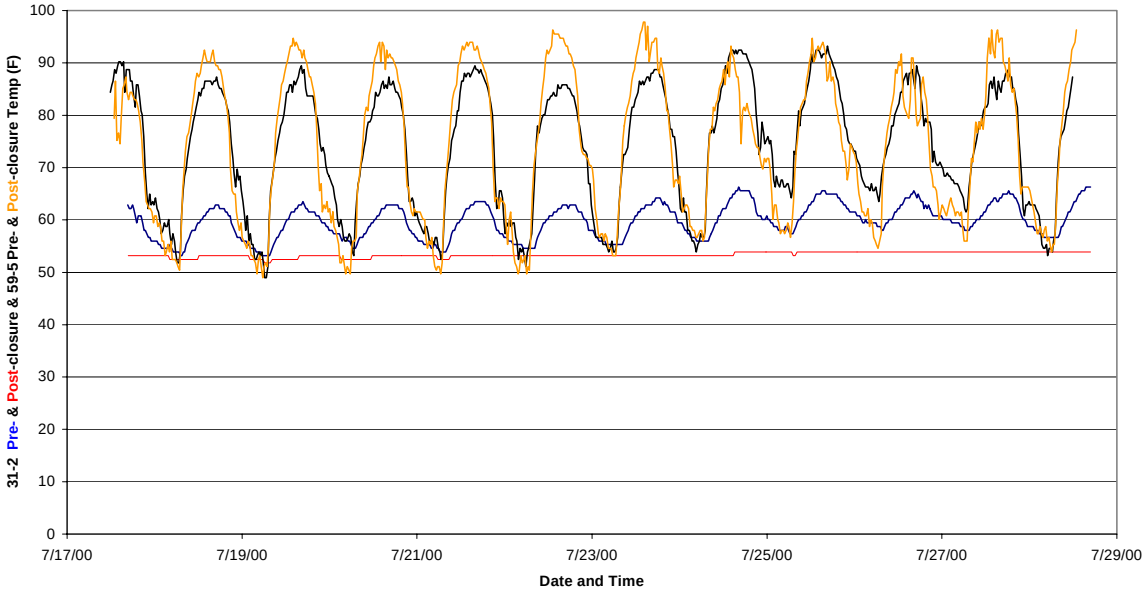


Figure 99. Logger 31-2 and 59-5 Temperature Measurements in the Pre- Versus Post-closure Data Windows.

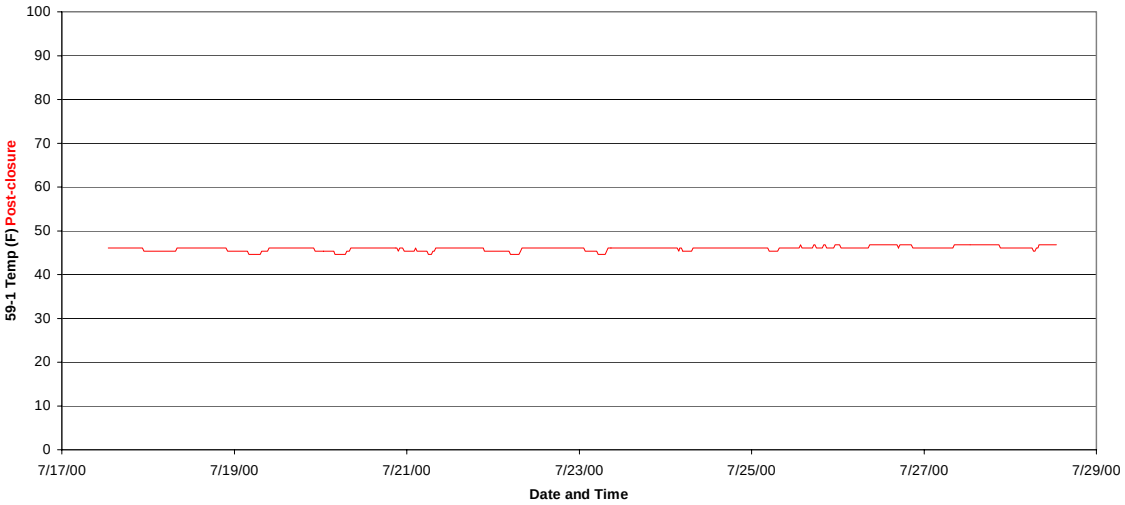


Figure 100. Logger 59-0 Temperature Measurements in the Post-closure Data Window.

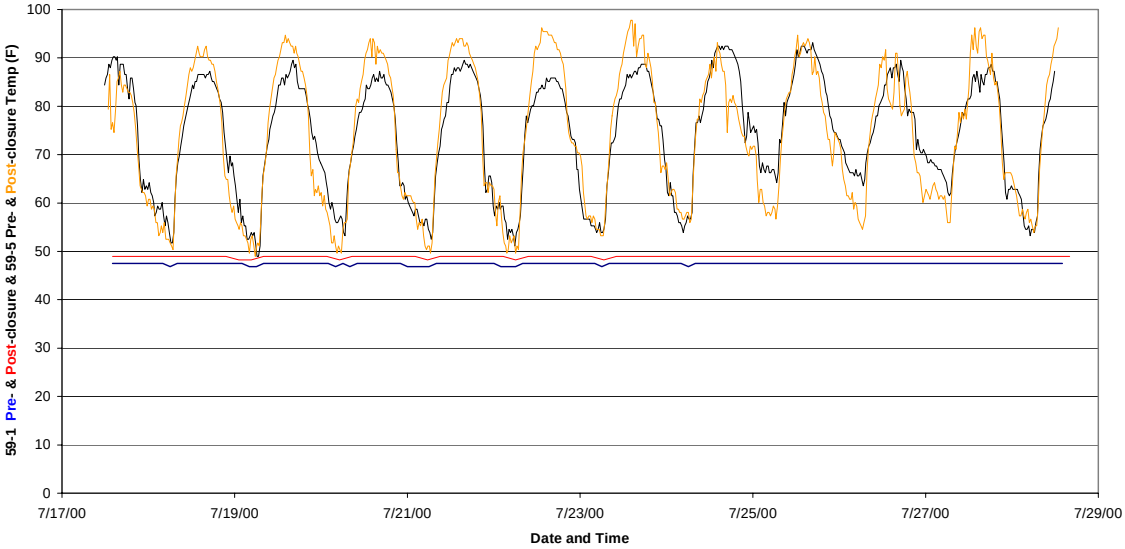


Figure 101. Loggers 59-1 and 59-5 Temperature Measurements in the Pre- Versus Post-closure Data Windows.

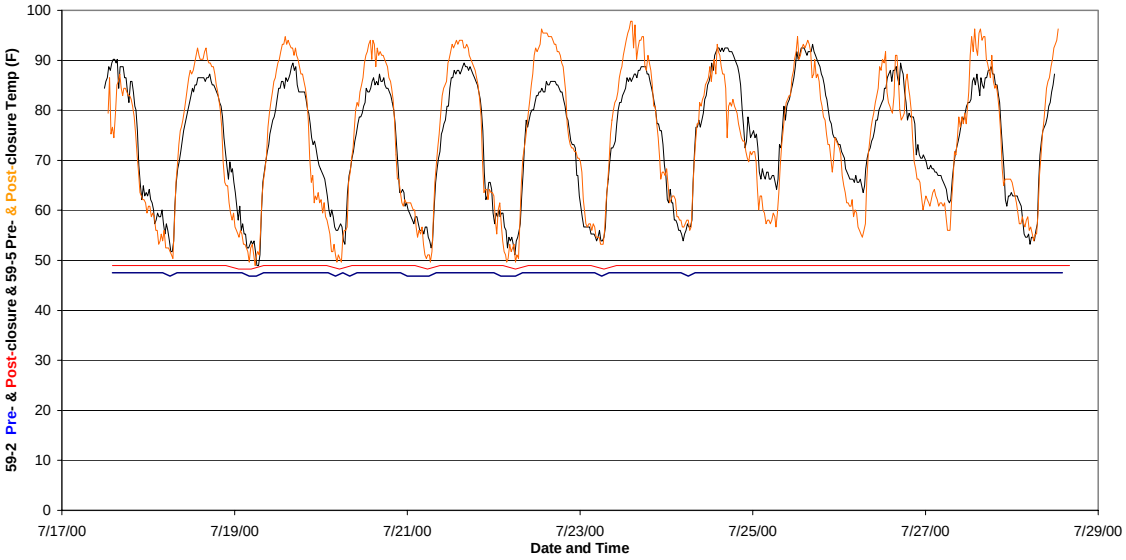


Figure 102. Logger 59-2 and 59-5 Temperature Measurements in the Pre- Versus Post-closure Data Windows.

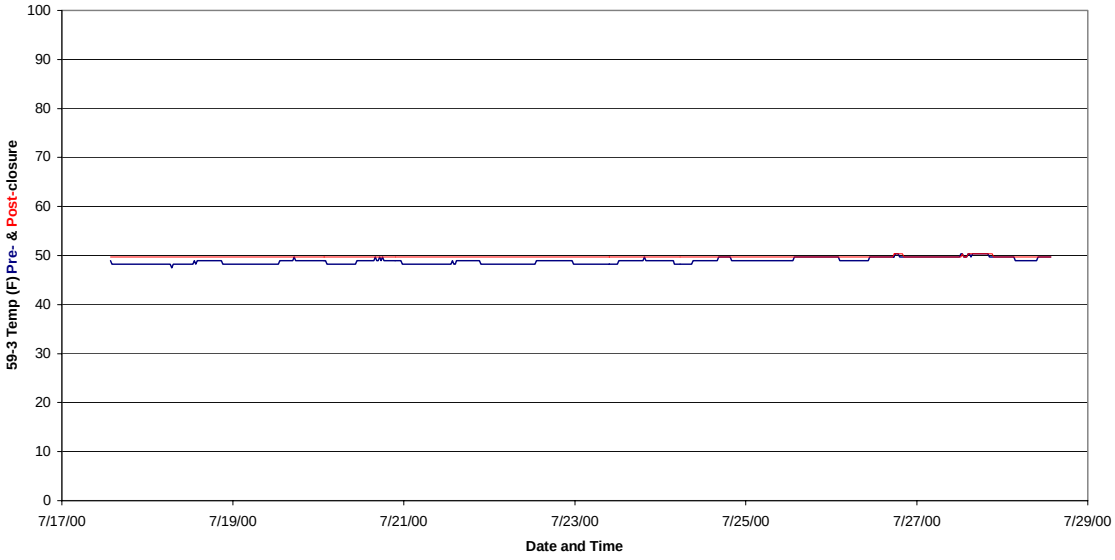


Figure 103. Logger 59-3 Temperature Measurements in the Post-closure Data Window.

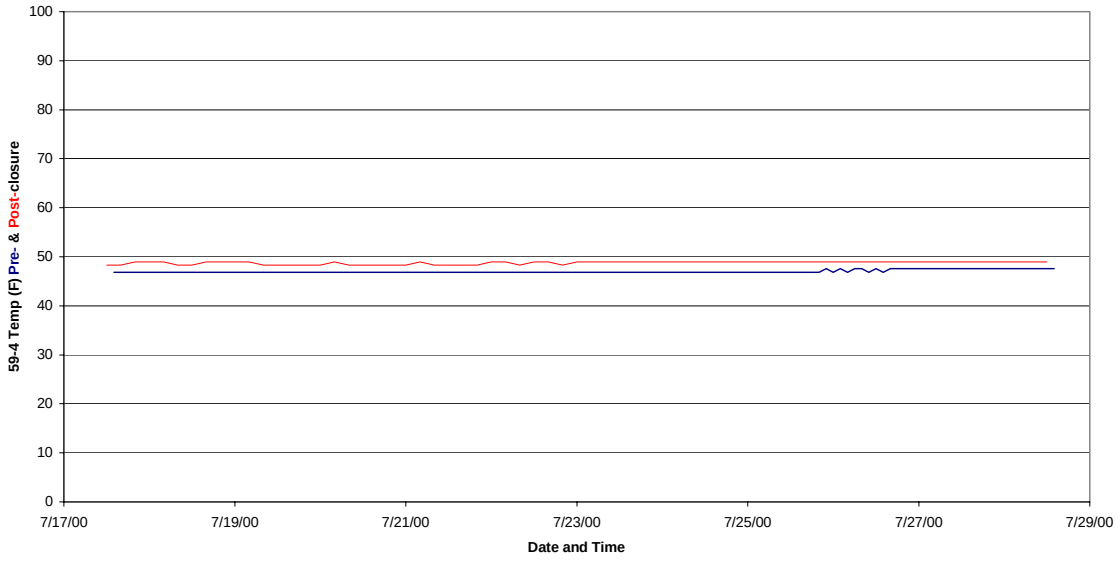


Figure 104. Logger 59-4 Temperature Measurements in the Pre- Versus Post-closure Data Windows.

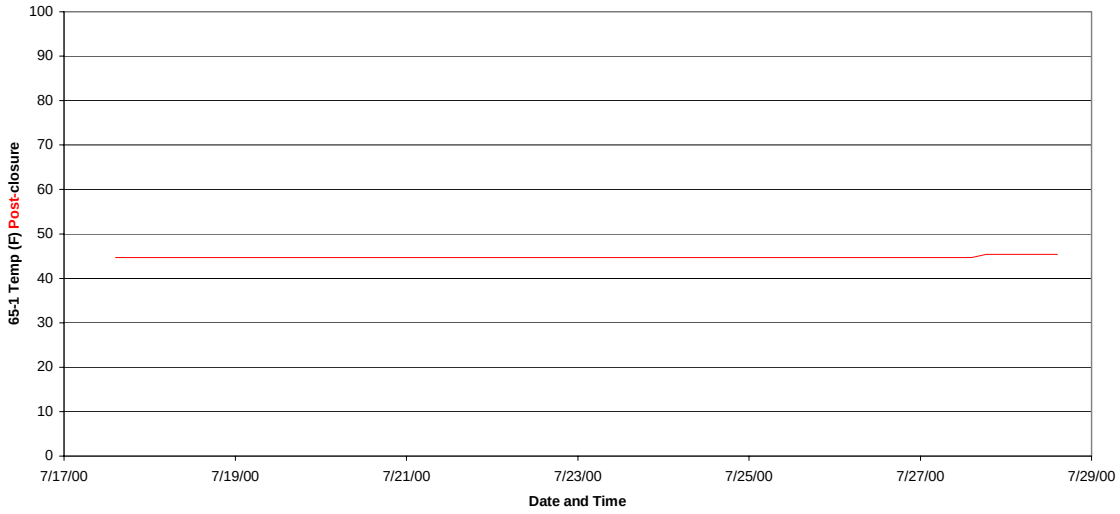


Figure 105. Logger 65-1 Temperature Measurements in the Post-closure Data Window.

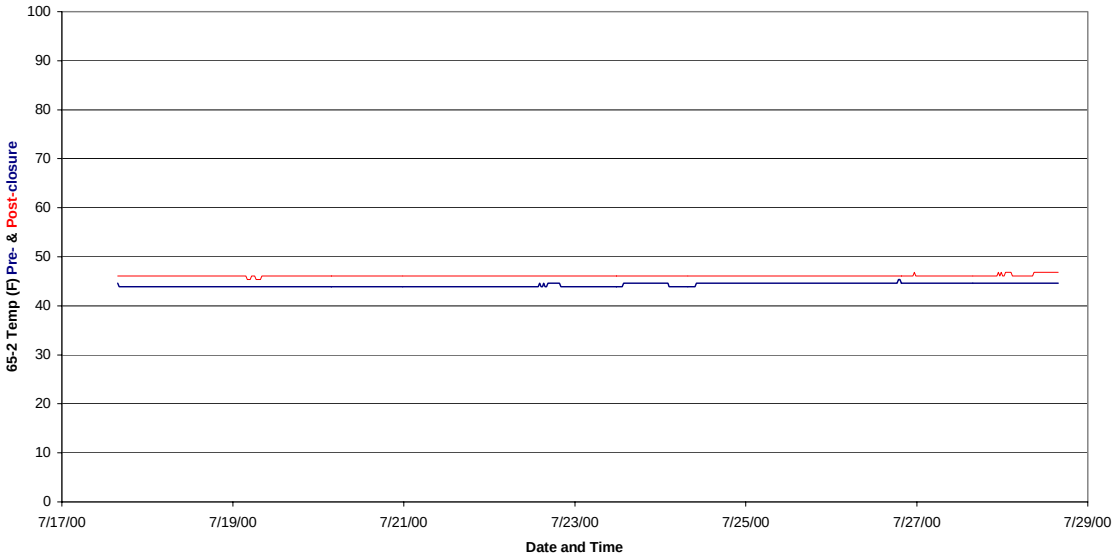


Figure 106. Logger 65-2 Temperature Measurements in the Pre- Versus Post-closure Data Windows.

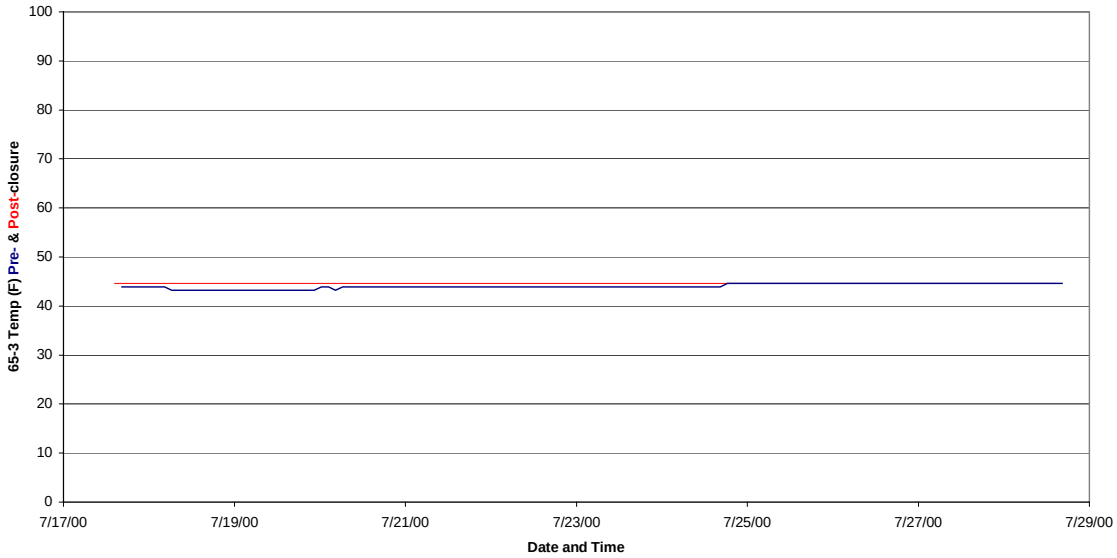


Figure 107. Logger 65-3 Temperature Measurements in the Pre- Versus Post-closure Data Windows.

Mean temperature increased by 0.59 to 3.44 ºF after closure for all loggers except 31-2 and 59-2 (Table 18). The 59-2 and 65-3 differentials might be explained by logger measurement error, but the other differences fall outside of the error range. Therefore something else caused slightly warmer temperatures after closure at most measurement locations. A reason for higher mine temperatures is that surface weather established a higher temperature at the outset of the post-closure data window. Figure 98 through Figure 107 show that the post closure temperature (in red) is at a higher temperature than the pre-closure temperature at the beginning dates of the data window, and the temperatures grow closer over the period of the window. Data from the Grand Junction Weather Station confirms that the 2000 surface temperatures (June 2000 Tavg = 73.0 ºF and July 2000 Tavg = 80.1 ºF) were higher in the 1.5 month period before the data window than the 1999 temperatures (May 1999 Tavg = 58.6 ºF and June 1999 Tavg = 70.5 ºF). During July, air movement in the decline mines is minimal, so the mines were heavily affected by pre data-window conditions. The difference in pre data-window surface climate probably caused the difference between pre- and post-closure mine temperatures, and the difference was most likely not a result of the closure. Nevertheless, warmer temperatures in July could be beneficial for bat maternity roosts.

Closure reduced variance at every logger (Figure 98 through Figure 107). Table 18 summarizes variance values and shows that temperature variances decreased after closure even though surface variance increased. Variance decreased exponentially with increasing distance from the portal (Figure 108).

Table 18. Difference in Temperature Mean and Variance Between Pre – and Post-closure Data Segments for Each Logger.

| Logger | Distance from Portal | Pre – Post Closure Tmean (F) | Logger Accuracy (F) | Pre - Post Tvar |
|---|---|---|---|---|
| 59-5 | 0 | -0.01 | ±0.7 | -59.85 |
| 31-1 | 91 | -3.44 | ±0.7 | 0.39 |
| 31-2 | 36 | 6.37 | ±0.7 | 10.54 |
| 59-1 | 280 | -1.44 | ±0.7 | 0.01 |
| 59-2 | 82 | 0.42 | ±0.7 | 1.62 |
| 59-3 | 132 | -0.81 | ±0.7 | 0.33 |
| 59-4 | 59 | -1.82 | ±1.27 | 0.01 |
| 65-2 | 57 | -1.87 | ±0.7 | 0.11 |
| 65-3 | 135 | -0.59 | ±0.7 | 0.26 |

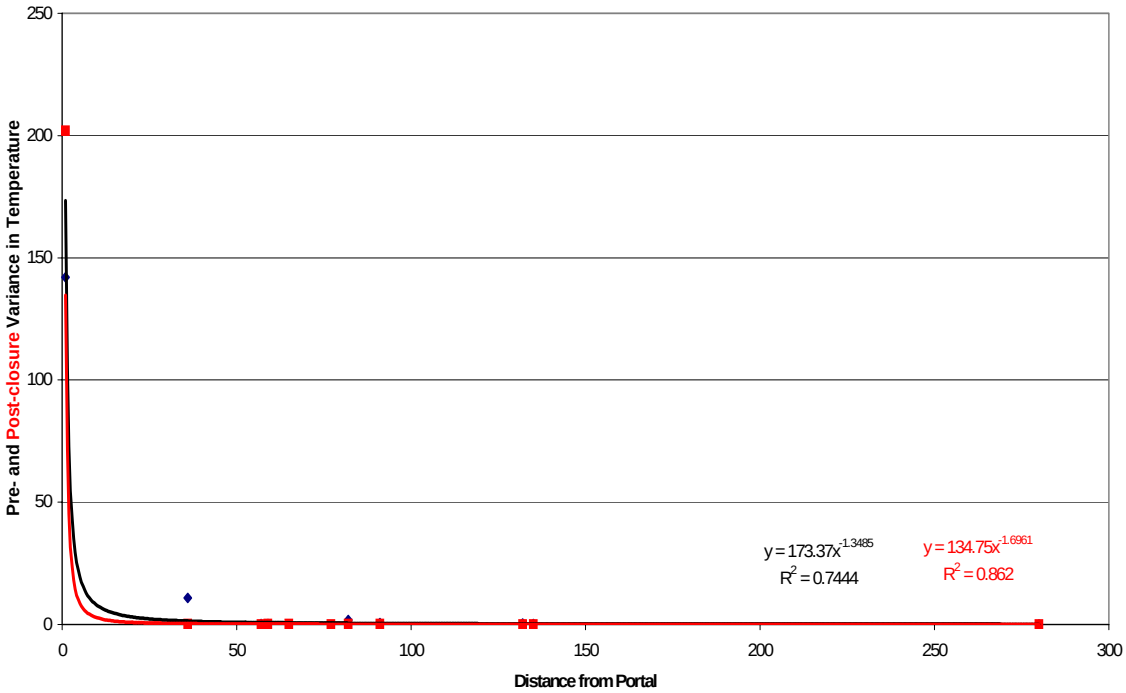


Figure 108. Pre- and Post Closure Variance in Temperature vs. Distance from the Portal

Logger 31-2 is located 36 ft from the pre-closure portal, placing it in the higher variability area. The culvert addition to Mine 31 essentially moved the portal 10 ft further away (see Table 1), putting the logger 46 ft from the portal after closure, which dramatically reduced variation (Table 18 and Figure 99). So the culvert moved logger 31-2 out of the first convection cell predicted by the model.

Since surface temperature is warmer than mine temperature during these data windows the air is affected more by conduction from the surrounding rock than by convection from the surface except close to the portal (Figure 109). Close to the portal, surface air convection has a greater influence than conduction from the surrounding rock indicating higher velocity airflow in this region. Therefore, the data supports the two-cell model predicted by the CFD software.

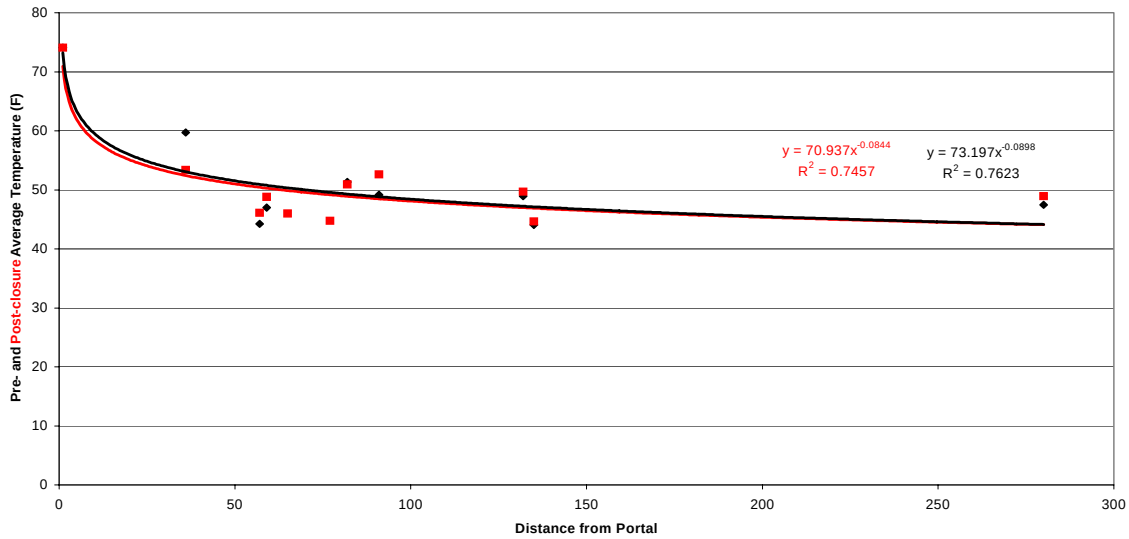


Figure 109. Pre- and Post Closure Mean Temperature vs. Distance from the Portal during Summer Data Windows

The culvert-gate closures did not change the temperatures at locations deeper than 50 ft from the portal (Figure 108 and Figure 109). The culvert and bat-gate closure slightly changed the temperature mean and variation close to the portal. As previously discussed, the literature suggests that bats might be sensitive to these small changes, especially if the temperature change occurs near either extreme of the bat's desirable temperature range (Tuttle and Taylor, 1994). If the small changes in temperature and variation in temperature are unacceptable to bats, they could move a few feet to experience the same temperature range and variation after closure as they did pre-closure. Or, simply put, the addition of a culvert and bat gate made the mine a little longer. The range of

temperatures and the variation in temperatures are the same before and after closure, but a particular temperature, or particular variation in temperature will occur in a different location. Therefore a bat can probably find a desirable temperature and variation in temperature within the mine; it just might be in a slightly different location after closure.

## *8.2 Phase Shift*

Time elapsed between a surface climate change and the corresponding effect on the mine microclimate (Figure 110 and Figure 111). Attenuation is caused by both the rock mass and the delayed reaction to the cyclic nature of the surface temperature. For example, the mine may not react completely to a surface temperature rise before the surface temperature trends downward. At times of the year when natural convection is strongest, less time is required for the mine microclimate to adjust to surface climate changes.

A different amount of time may elapse between rising and falling points (Figure 110 and Figure 112). Sampling rate introduces error into this measurement. The time between samples for 59-5 is 24 m whereas the time between samples for 59-2 is 2 h.

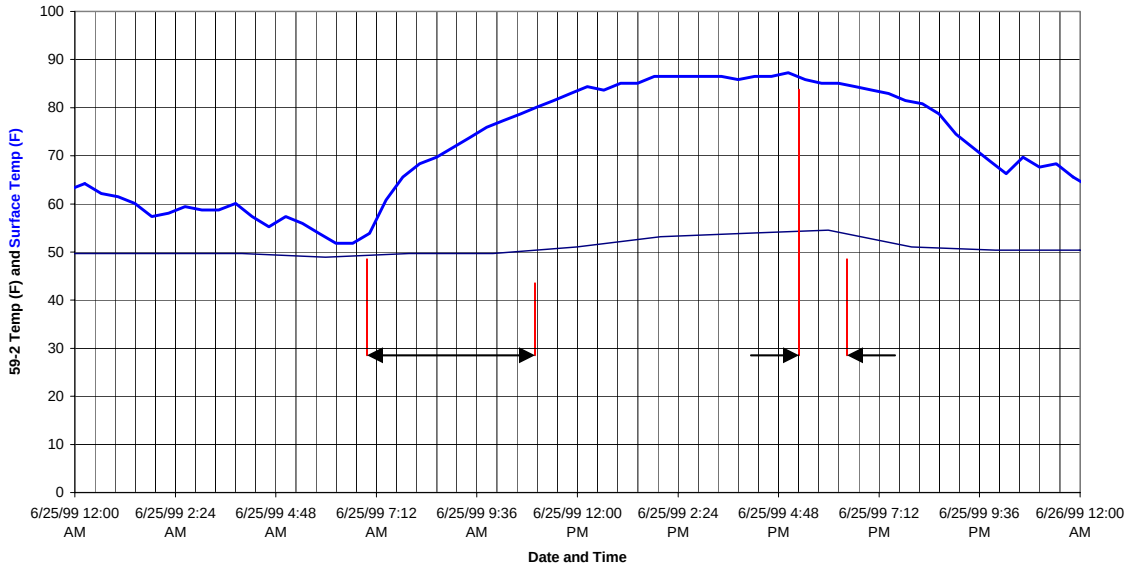


Figure 110. Phase Shift Between a Surface Climate Change and the Corresponding Effect in Mine Microclimate Measured at Logger 59-2 on June 25, 1999.

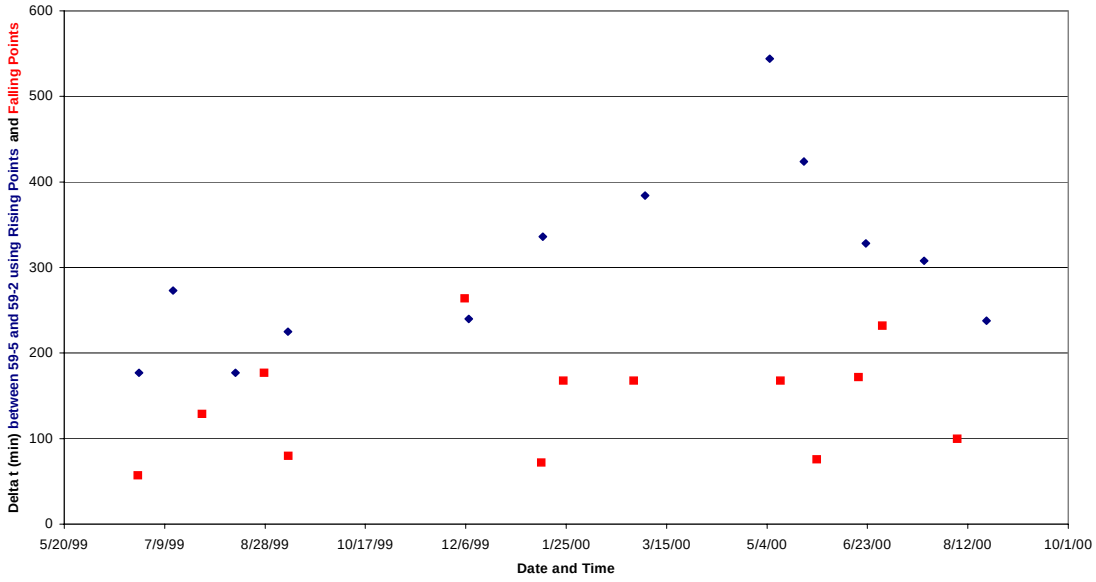


Figure 111. Phase Shift between 59-5 and 59-2 over the Study Period Measured between Falling Points and Rising Points.

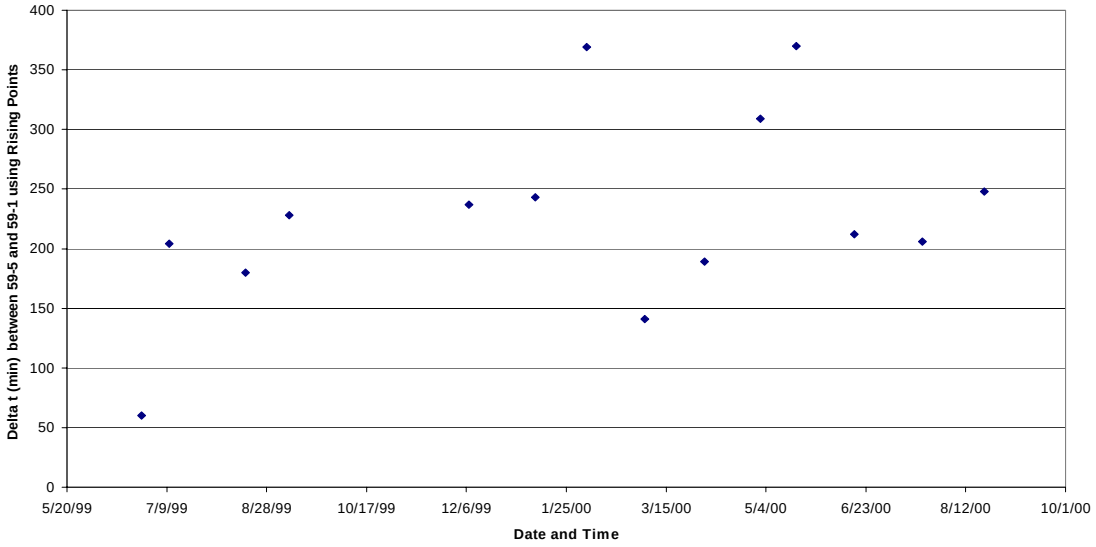


Figure 112. Phase Shift between 59-5 and 59-1 over the Study Period Measured between Rising Points.

We determined the minimum, maximum, and average phase shifts before and after closure between the rising points in the mine and surface loggers for the four data streams with visible responses (Table 19). With the exception of logger 31-1, the phase shift was longer after closure.

Table 19. Comparison of Pre- and Post-closure Phase Shifts.

| Logger | Pre/Post Closure Sampling Interval (min) | Pre-closure Shift (min) | | | Post-closure Shift (min) | | |
|---|---|---|---|---|---|---|---|
| | | Min | Max | Average | Min | Max | Average |
| 31-1 | 24/30 | 247 | 559 | 385 | 86 | 700 | 337 |
| 31-2 | 24/30 | 27 | 75 | 47 | 57 | 501 | 220 |
| 59-1 | 120/210 | 36 | 180 | 79 | 50 | 194 | 115 |
| 59-2 | 120/210 | 153 | 201 | 172 | 184 | 310 | 273 |

Phase shift increases with distance from the portal with the exception of logger 59-1 (Table 20). 59-1 is located in a drift close to a connecting airway between two portals, so the discrepancy is understandable.

Table 20. Distance to Portal vs. Phase Shift

| Logger | Distance to Nearest Portal (ft) | Ave. Shift (min) | |
|---|---|---|---|
| | | pre | post |
| 31-2 | 36 | 47 | 220 |
| 59-2 | 82 | 172 | 273 |
| 31-1 | 91 | 385 | 337 |
| 59-1 | 280 | 79 | 115 |

## *8.3 Gain and Phase Shift for Logger 59-2*

Another way to separate the effects of closure from surface climate is to compare gain before and after closure versus 30-day running-average surface temperature. Gain is the ratio of mine temperature to surface temperature after the mine temperature is shifted forward to match the phase of the surface cycle.

The analysis is based on typical, introductory electrical engineering analysis of cyclic waveforms. Measurements of surface and mine temperatures cycle with a 24-hour period; however maximum and minimum amplitudes and shape are not constant. We developed representations of the temperature cycles of the three waveforms: surface temperature, pre-closure mine temperature, and post-closure mine temperature. First we represented the surface temperature function:

$$T(t)_{surf} = T_{surfmax}\ f(t)$$

where $T(t)_{surf}$ is the temperature (ºF) on the surface at a particular time, t (min), $T_{surfmax}$ is the maximum value of surface temperature during a daily cycle, and f(t) is a function of time varying between 0 and 1, similar to a sin θ function.

We considered the above function to be similar to a forcing function. The surface climate is the forcing function and it enters the mine where it is changed by convection and conduction into the microclimate. The output of the process (convection and conduction) acting on the forcing function (the surface climate) is measured at certain points, which are the logger locations. The process altered the forcing function by attenuating it with a gain and delaying it with a phase shift:

$$T(t)_{pre} = G_{pre} T_{surfmax}\ f(t+\Phi_{pre})$$

$$T(t)_{post} = G_{post} T_{surfmax}\ f(t+\Phi_{post})$$

Where $G_{pre}$ is the pre-closure gain, Φ is the pre-closure phase shift, $G_{post}$ is the post-closure gain and $\Phi_{post}$ is the post-closure phase shift.

Even though this approach is straight forward, developing values for G is not easy for a large data set of non-uniform cycles. If the data set were small, the following process could be used:

1. Inspect a cycle waveform like Figure 110 to identify a phase-shifted mine data point that corresponds to a related point on surface data. Perhaps the easiest data points to identify are peaks, valleys, or a standard temperature crossing.
2. Calculate gain at the point. For example, from Figure 106, the peak temperature of logger 59-2 on June 25, 1999 was 54.58 ºF recorded at 17:59. The peak temperature of logger 59-5 (the surface logger) was 87.28 ºF recorded at 17:02.

Therefore the phase shift was 57 min (17:59 – 17:02) and the gain is 0.63 (54.58/87.28).

3. Repeat the process for all the data in the study to determine all phase shifts and gains.
4. Calculate the 59-5 data 30-day running average.
5. Plot gain vs. the 59-5 running average for pre-closure and post-closure data sets.

However, the data set is large, so the above process needed to be automated. This required programming a peak identification algorithm into a spreadsheet program. As shown, a cycle can have several peaks, but the algorithm must report only the maximum value each day to precisely measure the phase shift and to precisely match daily maxima for the gain calculation (Figure 113). Smoothing the data with a running average removes many local maxima and minima. The amount of smoothing depends on the number of data points in the running average. The surface data is more variable than the mine data, and required a 10-point average as opposed to a three-point average for mine data. The running average effectively smoothed the data and "removed" all but the maximum peaks (Figure 114). The next step was to identify the time of each peak by computing the derivative ($dT/dt \cong \Delta T/\Delta t$ or slope) of the data over three points. It is common to identify local maxima and minima where derivatives equal zero, but we did not use that technique because our data had several, long, zero slope zones. Therefore, our technique defined "falling points" from a sharp peak or from a high plateau by selecting the points in time when the derivative changed from a positive to a negative value. Next, the gain was computed from the corresponding daily maxima in surface and mine temperatures (Figure 115 and Figure 116).

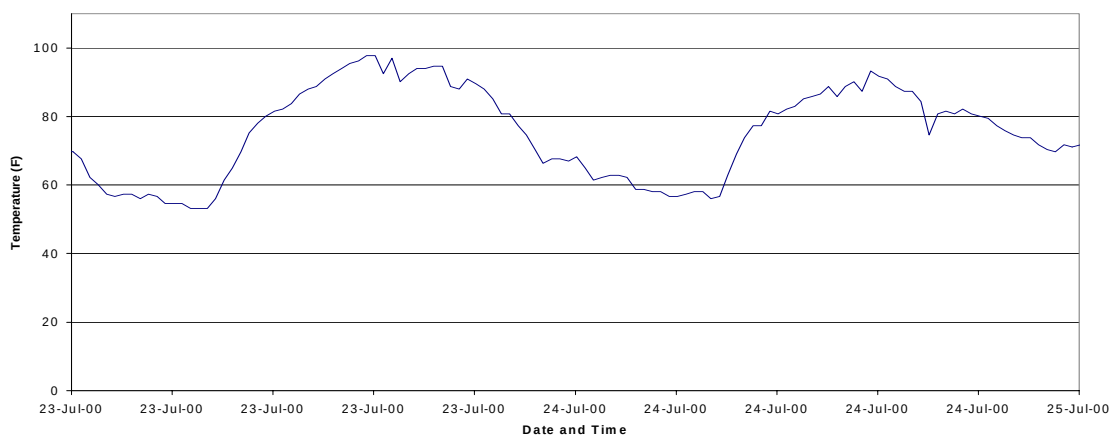


Figure 113. Typical Surface Temperature Cycle.

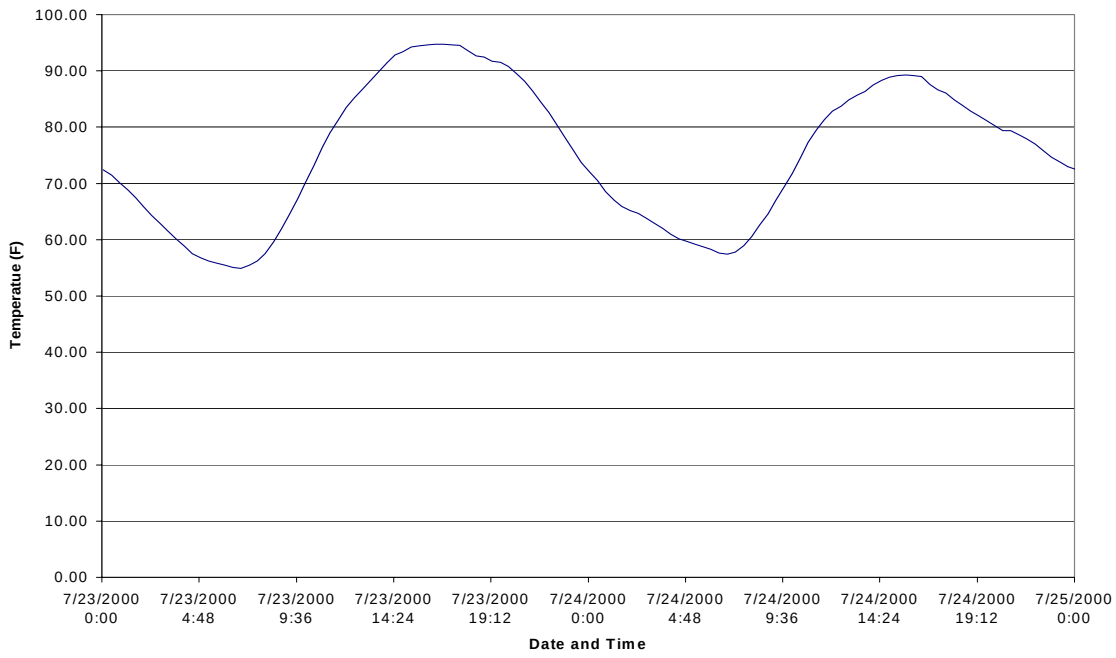


Figure 114. 10-point Running-average Surface Temperature Data

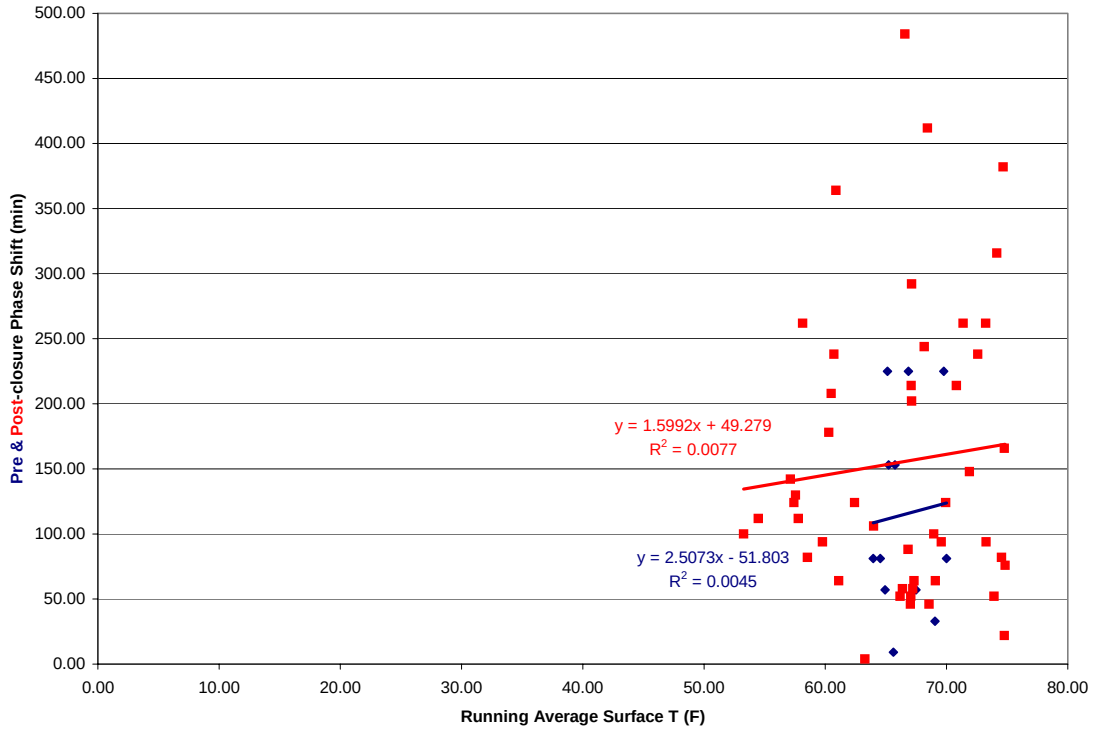


Figure 115. Logger 59-2 Pre- and Post-closure Phase Shift Versus 30-day Running-average Surface T.

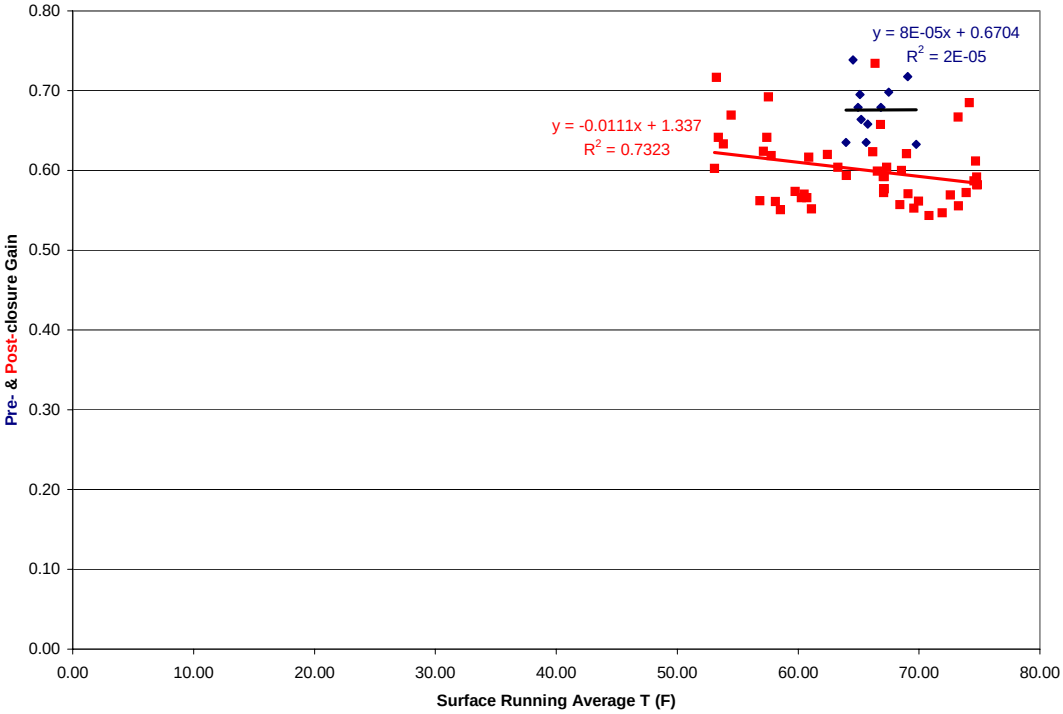


Figure 116. Logger 59-2 Pre- and Post-closure Gain Versus 30-day Running-average Surface T.

The data is significantly scattered so the linear fits are poor (Figure 115 and Figure 116). Nevertheless, these approximations show that for a given 30-day running-average surface temperature, phase shifts are longer after closure, and gain is lower. This is consistent with the previous data window analysis, which showed lower variation after closure and longer phase shifts (Table 18 and Table 19). Because there were few peaks in the logger 59-2 data over the winter, the analysis and conclusions are limited to summer months.

# 9.0 Conclusions, and Recommendations

Our project combined predictive models with experimental data. The predictive models can be used in future projects to predict the effects of various remedial actions. We tried several approaches to modeling the small natural convection flows in abandoned underground mines and found that the CFD-ACE software package was effective. We modeled a simple, short, inclined mine, similar to one of the three studied, during the winter when cooler surface air temperatures (275 K, 35.3 °F) should induce convective flow where rock temperatures were approximately equal to the MAST 283 K (49.7 °F). The results predicted two convection cells, one near the portal and the other throughout the remainder of the mine. The interface between the cells moved from 0.75 to 0.9 m from the portal when T between the surface and mine air increased from 3 K (5.4 °F) to 11 K (19.8 °F). The flows in the second cell are extremely low, about 0.05 m/s (0.2 fps or 12 fpm). The model responded to time varying surface temperatures, reporting that the characteristic time for a change in outside temperature to completely make its effect inside the mine is about one hour. The model results attenuate with depth into the mine, similar to measured data. The data shows a temperature fluctuation of about 6 K versus a fluctuation of about twice that for the temperatures outside of the mine. The damping within the actual mines, however, is still more pronounced than that of the simulated mine. This is due to the complexities that are inherent to a real mine that were not included in our simple simulation. The real mines were not perfectly cylindrical, the rock walls were not smooth, drifts turn and bend, drifts changed dimensions, and activities like roof collapses caused abrupt changes in drift perimeters. These complexities could be included if resources become available to support future simulations.

We also modeled the effects of remediation via a backfilled culvert and bat gate. We added a 10-m long 4-m diameter culvert to the simulated mine with the same slope (6°) as the mine. The 10-m long culvert shifted the interface 10 m from the end of the mine; consequently, the microclimate in the first 20 m of the mine remained the same, but it was shifted by 10 m. Next, we investigated the effects of reducing mine closure costs by using a smaller diameter culvert. We reduced the diameter of the culvert by 50% to 2 m. Finally we investigated the effects of installing the culvert at a steeper angle (27°) to shorten its length and further reduce closure costs. Since bats commonly hang from the roof, we graphed the temperature profiles resulting from the models along the roof for various closure scenarios. The scenario where the mine is closed with a culvert, which has the same diameter (4 m) and slope (6 °) as the mine, showed a temperature profile that was similar in shape, but displaced 10 m. The profile for the 2-m diameter culvert was the same shape in the pre-closure mine area; however, temperature values were warmer by approximately 1 K (~2 °F). The temperature profile for the inclined (27 °) culvert case in the pre-closure mine area was similar in shape and magnitude to that of the 6 ° culvert case.

The model also predicted air velocities. The results showed that U (x-direction air velocity) profile shape and magnitude did not vary when a 4-m diameter culvert was

added to the mine model. Reducing the diameter of the culvert shortened the first convection cell from 1.7 m to 1.3 m and reduced the maximum U magnitudes in positive (0.23 to 0.13 m/s, 45.3 to 25.6 fpm) and negative (-.06 to -.03 m/s, -11.8 to –5.9 fpm) directions.

In addition to modeling a simulated mine, we measured the microclimate in the three mines. We desired to measure airflow from natural convection since we believed it to have a major effect on changes in the mine microclimate. However, most instruments for measuring low airflows are expensive, delicate, and can not be left in a mine to record data continuously for several months. Therefore, Dr. Grover developed a transducer based on an acoustic principle where a sound wave that is traveling in the direction of the airflow will move faster than a wave that is traveling against the flow. We built and tested the transducer in the laboratory and in the mine. Then, we mounted two sets of transducers at three levels in seven different locations throughout the three research mines. Consequently, there were two sets near the floor in the mine, two sets about 2.5 ft higher, and two sets about 5 ft from the floor. The hardware cost for each, three-level set-up is about $300. The transducer data showed high variability with flows switching directions frequently. Most of the data was within the 0 to 0.2 fps (0 – 12 fpm) range with a small number of readings reaching 0.4 fps (24 fps). This compared with smoke tube measurements of 10 – 50 fpm, and model predictions of about 12 fpm. Rodents damaged the air-flow transducer that was located in the prototype location, so exact comparison of pre- and post closure velocities was not possible, but general comparison with ranges of measurements with other transducers does not show a significant difference. For example, transducer 4 in mine 59, which should be in the same air stream as the prototype transducer, measured velocities mostly in the 0-1 fpm range with maximum values around 20 fpm a few days after closure.

John Burghardt measured radiation in the three mines studied during the initial mapping and safety inspection visit on 9-20-98. We measured radiation in mine 59 just after closure on 12-2-99 with the same National Park Service Instant Working Level Meter and Gamma Meter. Most of the measurements made on 12/2/99 were lower than those made on 9/24/98. We believe this was caused by the difference in airflow between the two measurement dates. In the third week in September, daytime surface air temperature was higher than the daytime air temperature in the mine, so there was very little convective airflow. However the December measurements were made when surface air temperature had fallen below the mine temperature, causing increased airflows. Generally, higher airflow reduces working level measurements. Gamma radiation measurements between the two inspections were about the same.

Precise comparison of pre- and post closure mine air temperatures was difficult since surface climate was different before and after the culvert and bat gates were installed. Therefore, we found two short periods where the surface climate was approximately the same before and after closure and used those shorter periods for the evaluation. Temperatures rose slightly (by 0.59 to 3.44 ºF) after closure for all loggers except 31-2 and 59-2. The rise was larger than instrument error in all but two loggers. Therefore something else caused slightly warmer temperatures after closure at most measurement

locations. A reason for higher mine temperatures is that surface weather created a higher temperature at the outset of the post-closure data window. During July, air movement in the decline mines was minimal, so the mines were heavily affected by pre data-window conditions. Therefore we concluded that the difference in pre data-window surface climate probably caused the difference between pre- and post-closure mine temperatures, and the difference was not a result of the closure. Nevertheless, the literature suggested that warmer temperatures in July could be beneficial for bat maternity roosts. (Tuttle and Taylor, 1994)

Temperature variances decreased after closure even though surface variance was higher. The data showed higher variance within 50 ft of the portal and very low variances in the rest of the mine. Only logger 31-2 is located within 50 ft of the portal. The culvert addition to Mine 31 essentially moved the portal 10 ft further away from logger 31-2, putting the logger 46 ft from the portal after closure. Therefore logger 31-2 had a more dramatic reduction in variance than other loggers that were already more than 50 ft away from the portal. This data supports the two-cell prediction by the model.
The data and the power curves in Figure 108 and Figure 109 show that if bats are sensitive to the small changes in temperature and variation in temperature, they could move a few feet toward the portal to experience the same temperature after closure as they did pre-closure. Or, simply put, the addition of a culvert and bat gate makes the mine a little longer. The range of temperatures and the variation in temperatures are the same before and after closure, but a particular temperature, or particular variation in temperature will occur in a different location. Therefore a bat can probably find a desirable temperature and variation in temperature within the mine; it just might be in a slightly different location after closure. Using the summer data window analysis as an example, the bat would have to move a small distance toward the portal.

Time elapses between a surface climate change and the corresponding effect in the mine microclimate. Attenuation is caused by both the rock mass and the delayed reaction to the cyclic nature of the surface temperature. In addition, the mine may not react to a surface climate change completely before the surface climate changes again. At times of the year when natural convection is strongest, less time is required for the mine microclimate to adjust to surface climate changes. We measured the phase shifts between peaks and valleys in the surface and mine data. Pre-closure shifts varied from 47 to 172 min and post closure shifts varied from 115 to 273 min for the loggers that recorded longer phase shifts after closure. Data showed that the phase shift increased with distance from the portal, with the exception of logger 59-1. 59-1 was located in a drift close to a connecting airway between two portals, so the discrepancy is understandable. The model predicted 1-hr shifts within 30m of the portal.

We developed another method to separate the surface climate changes from closure effects - comparing phase shift and gain, pre- and post-closure, based on their relationship with 30-day running-average surface temperature. This analysis showed that for a given 30-day running-average surface temperature, phase shifts were longer after closure, and gain was lower, consistent with the previous data window analysis. Because

there were few peaks in the logger 59-2 data over the winter, the analysis and conclusions applied only to summer months (Figure 28).

If the temperature is already on the edge of the tolerable range for bats, a small shift is significant. Tuttle reports on a Tennessee cave where a 2°F variation caused a 67% reduction in one species of bat and an 87% reduction in another because the January air temperature was already 52F, near the upper limit of temperatures tolerated by hibernating bats in that region. Bat surveys in our study area suggested that microclimate changes reduced bat use of the abandoned uranium mines that we studied. "At this point, pending evidence from the School of Mines study, we would have to believe that culvert gate designs, installed in portals associated with large trench features, and smaller diameter than the original portals, are changing the internal conditions and having an effect on bat use of such sites." (Navo and Ingersoll, 2001) However, our data showed only small temperature changes and the changes increased temperatures in the summer maternity roost season, so even though small, they should have been beneficial. Therefore, we recommend that bat surveys continue and that other causes of bat use decline be investigated through the surveys. We also recommend continued microclimate monitoring and modeling to accompany the bat surveys. However, it is possible that the frequent visits by researchers and the instrumentation installed in the mines affected the acceptability of the sites for bat habitat. Therefore, we recommend that the bat surveys continue now that researchers and instrumentation are gone. We recommend that new mines be identified for additional instrumentation.

The importance of small temperature variation to bats indicates that high-resolution temperature transducers be used in any further monitoring projects. In addition, high sampling rates are necessary when measuring the time elapsed (phase shift) between surface climate changes and the effect on the mine microclimate. In addition, remote communications are necessary thereby reducing the number of trips into the mine to reduce disturbance for bats and hazards to researchers. Armored cables should be used to reduce rodent damage.

# 10.0 Acknowledgements

Many people contributed to this project. Their contributions are listed below:

Bruce Fowler monitored the project progress for the BLM and participated in all of the mine trips.

Rob Robinson developed the initial scope for the project.

Dr. Tom Grover specified, maintained, and installed the instrumentation for the project including designing, developing, and installing the low-flow sensors and the communications system. He participated in most of the mine trips. Mr. Lee Johnson assisted Dr. Grover with the wind tunnel laboratory calibration of the low-flow sensor.

Dr. J. P. Delplanque supervised to computational fluid dynamics modeling work.

Mr. Joe Dodds analyzed humidity data and developed the computational fluid dynamics model. Section 6 is a modification of his master of engineering report.

John Burghardt, a National Park Service geologist, surveyed the three mines, assessed their safety for the researchers during the first site visit and subsequently drew the mine maps. Mr Burghardt also loaned the NPS working level meter to us.

Mr. Bill Zuckermandel, Mr. Toby Padilla, and Mr. Kurrin Barrett worked on the initial stages of the computer model.

A group of undergraduate students in the CSM Engineering Division senior design course (Tiffany McGowen, Brad Reiner, and Carlvin Umali) did initial work on data analysis and modeling.

Henry Foust, a former graduate student at CSM, currently a graduate student at Tulane, installed an initial set of instruments and wrote the initial proposal.

# 11.0 References


Altringham, J. D. 1996. Bat biology and behavior. Oxford University Press. New York, NY, 262 p.

Armstrong, David M. et al. 1995. Bats of Colorado: shadows in the night. Colorado Division of Wildlife, 29p.

BLM's Abandoned mine lands program, [Home page of the Bureau of Land Management], [Online}. (May, 23, 2001—last update). Available: http://www.blm.gov/aml/, [Viewed September 17, 2001].

Burghardt, J. E. Bat-compatible closures of abandoned underground mines in the national park system, [Home page of the National Park Service]. [Online]. (May 17, 2001 – last update). Available: http://www2.nature.nps.gov/grd/distland/amlreports/batgate.pdf, [Viewed September 17, 2001].

Burghardt, J. E. 1996. Effective management of radiological hazards at abandoned radioactive mine and mill sites [Home page of the National Park Service]. [Online]. (May 17, 2001 – last update). Available: http://www2.nature.nps.gov/grd/distland/amlreports/radpaper.pdf, [Viewed September 17, 2001].

CFD Research Corporation [Home page of the CFD Research Corporation], [Online]. Available: http://www.cfdrc.com/, [Viewed September 19, 2001.]

Cleaning up abandoned mines: a western partnership, [Home page of the Western Governors Association], [Online]. (November 11, 1999—last update), Available: http://www.westgov.org/wga/publicat/miningre.pdf, [Viewed September 17, 2001].

Colorado Climate Center [Home page of the Colorado State University], [Online]. (December 18, 2000 – last update). Available: http://ccc.atmos.colostate.edu/, [Viewed September 17, 2001.]

Dodds, J. A., 2001. Microclimate modeling of bat habitat in abandoned mines, Master of Engineering Report T-5513. Colorado School of Mines, Golden, CO, 61p.

Harvey, J.M., J.S. Altenbach, T. L. Best. 1999. Bats of the United States, Arkansas Game and Fish Commission, 64 p.

Herder, M. 2000. Monitoring the effectiveness of bat compatible mine gates. BLM-NARSC Resource Notes No. 18, 4pg.

Landauer, Inc. [Home page of the Landauer Corporation], [Online]. Available: http://www.landauerinc.com/, [Viewed September 17, 2001.]

Meier, L. J. Garcia. 2000. Importance of mines for bat conservation. Pages 17-28 in Vories and Throgmorton (eds), Proceedings of Bat Conservation and Mining: A Technical Forum. St. Louis. OSM, Alton IL.

National Park Service, Disturbed Land Restoration, [Home page of the National Park Service]. [Online]. (May 17, 2001 – last update). Available: http://www2.nature.nps.gov/grd/distland/amlindex.htm, [Viewed September 17, 2001].

Navo, K. W. and T. Ingersoll. 2001. Colorado bats/inactive mines project, 2000 project summary. unpublished report by the Colorado Division of Wildlife, Denver, CO.

Navo, K. W. 1994. Guidelines for the survey of caves and abandoned mines for bats in Colorado. Colorado Division of Wildlife, Denver, CO.

National Weather Service -- Central Region, [Home Page of the National Weather Service], [Online]. (September 24, 2001 – last update), Available: http://www.crh.noaa.gov/, [Viewed September 24, 2001]

Onset Computer Corporation, [Home page of the Onset Computer Corporation], [Online]. (September 2001—last update), Available: http://www.onsetcomp.com/, [Viewed September 17, 2001].

Pierson, E. D. 1998. Tall trees, deep holes and scarred landscapes: conservation biology of North American bats. in T. H. Kunz (ed.). Bat biology and conservation. Smithsonian Institution Press, pp 309-325.

Raschen, R. 2000. Abandoned mine land hazard awareness: what is BLM doing to inform the public?, BLM-NSTC Resource Note 22, 3p.

Sherwin, R. E. et al. 1993. Methods for determining local mine characteristics of importance to bats. Pages 109-114 in Pete (ed) Proceedings of the 1993 national cave management symposium. Carlsbad, NM. Speleobooks.

Tuttle, M. D. 1977. Gating as a means of protecting cave dwelling bats. in Aley, T. and Rhodes D. (eds). Proceedings of the National Cave Management Symposium - 1976, Mountain View, AR, pg 77-82.

Tuttle, M. D. and D. A.R Taylor. 1994. Bats and mines, Bat Conservation International Resource Publication no 3, 50p.

Tuttle, M. D. and D. E. Stevenson. 1978. Variation in the cave environment and its biological implications. In R. Zuber (ed.). Proceedings of the National Cave Management Symposium – 1977, Big Sky, Montana. Pgs 108-121.

U. S. Geological Survey. 1991. Geological map of the gothic quadrangle, Gunnison county, Colorado. U. S. Geological Survey.